

**FABRICATION AND ANALYSIS OF COMPLEX ELECTROSPUN SCAFFOLDS AND
CONSTRUCTS**

by

Nicholas James Amoroso

B.S.E., Case Western Reserve University, 2006

Submitted to the Graduate Faculty of the
Swanson School of Engineering in partial fulfillment
of the requirements for the degree of
Doctor of Philosophy

University of Pittsburgh

2013

UNIVERSITY OF PITTSBURGH
SWANSON SCHOOL OF ENGINEERING

This dissertation was presented

by

Nicholas James Amoroso

It was defended on

January 28, 2013

and approved by

Toby Chapman, PhD
Associate Professor, Department of Chemistry

Michael S. Sacks, PhD
Professor, Department of Bioengineering and W. A. “Tex” Moncrief, Jr. Simulation-Based
Engineering Science Chair
University of Texas at Austin

Sanjeev G. Shroff, PhD
Professor and Gerald McGinnis Chair, Department of Bioengineering

Kimimasa Tobita, MD
Research Assistant Professor, Department of Developmental Biology

William R. Wagner, PhD
Dissertation Director, Professor, Departments of Bioengineering & Chemical Engineering
Director, McGowan Institute for Regenerative Medicine

Copyright © by Nicholas James Amoroso

2013

FABRICATION AND ANALYSIS OF COMPLEX ELECTROSPUN SCAFFOLDS AND CONSTRUCTS

Nicholas James Amoroso, PhD

University of Pittsburgh, 2013

Tissue construct mechanics are of pivotal importance in mechanically active tissues, particularly where the construct must assume a functional role immediately upon implantation and during the remodeling period. While numerous methods exist to generate porous scaffolds for tissue engineering, electrospinning has become increasingly applied as a means of generating microfibrillar scaffolds that provide surface structures roughly comparable in scale to that seen with ECM proteins such as collagen. Simple mechanical relationships have been explored in electrospun scaffolds such as simple fiber alignment to achieve planar anisotropy, however more thorough structure-function characterization has not been pursued to date. Further, the effect of cellular or other component incorporation has not been studied. An understanding of cellular function within scaffolds is critical for the design of seeded tissue constructs. For these reasons, this research aimed to gain an understanding of how structural and compositional modifications to electrospun scaffolds can result in a change in mechanical function and host response. This research question was approached through a series of directed modifications to the electrospinning process designed to alter the microenvironment within the scaffold. These micro-scale changes were related to tissue-level changes in both planar biaxial and flexural mechanical response. This knowledge was used to fabricate cellularized constructs for cardiac right ventricular outflow tract replacement in order to discern the fate and function of implanted cells within electrospun scaffolds. The results from this research can be combined with structural deterministic modeling in order to gain a more complete understanding of the mechanical and biological function of cellularized electrospun constructs and therefore help guide future work in the rational design of engineered tissues.

TABLE OF CONTENTS

NOMENCLATURE.....	XVIII
PREFACE.....	XX
1.0 INTRODUCTION.....	1
1.1 CARDIOVASCULAR DISEASE AND THE TISSUE ENGINEERING PARADIGM.....	1
1.2 BIOMATERIALS FOR TISSUE ENGINEERING	2
1.2.1 Natural Biomaterials	3
1.2.2 Synthetic Biomaterials	3
1.2.3 Biomaterial Processing Techniques	4
1.3 ELECTROSPINNING FOR TISSUE ENGINEERING APPLICATIONS.....	5
1.3.1 Electrospinning Background and Scientific Principles.....	5
1.3.2 Controlling Electrospun Topology.....	10
1.3.3 Modifying Electrospun Constructs for Bioactivity and Cell Infiltration .	11
1.3.4 Mechanically Appropriate Cellularized Electrospun Scaffolds.....	15
1.3.5 Toward the Rational Design of Electrospun Cardiovascular Tissue Engineering Prostheses.....	16
1.4 OBJECTIVES	17

1.4.1	OBJECTIVE #1: Determine the effects of processing conditions and modifications on PEUU microstructure and planar biaxial mechanical response.....	18
1.4.2	OBJECTIVE #2: Evaluate and control the flexural response of electrospun scaffolds.....	18
1.4.3	OBJECTIVE #3: Produce biomimetic electrospun constructs with curvilinear microstructures	19
1.4.4	OBJECTIVE #4: Determine the in vivo behavior and response of heterogeneous microintegrated constructs.....	20
2.0	PROCESSING CONDITIONS AND MODIFICATIONS ON THE MICROSTRUCTURE AND PLANAR BIAxIAL MECHANICAL RESPONSE OF ELECTROSPUN POLY(ESTER URETHANE) UREA.....	21
2.1	INTRODUCTION.....	21
2.2	METHODS	23
2.2.1	Smooth Muscle Cell Culture.....	23
2.2.2	PEUU Synthesis	23
2.2.3	Scaffold Fabrication and Characterization.....	24
2.2.4	Microscopy and Fiber Architecture Characterization.....	25
2.2.5	Mechanical Characterization	26
2.3	RESULTS	27
3.0	MICROSTRUCTURE MANIPULATION TO TUNE BENDING STIFFNESS IN ELECTROSPUN SCAFFOLDS FOR HEART VALVE TISSUE ENGINEERING	37

3.1	INTRODUCTION.....	37
3.2	MATERIALS AND METHODS	39
3.2.1	Scaffold Fabrication	39
3.2.2	Imaging and Structural Analysis	41
3.2.3	Mechanical Testing.....	42
3.2.3.1	Uniaxial Mechanical Testing.....	42
3.2.3.2	Suture Retention Strength.....	42
3.2.3.3	Biaxial Mechanical Testing	42
3.2.3.4	Flexural Mechanical Testing.....	43
3.2.4	Statistical Analyses	44
3.3	RESULTS	45
3.3.1	Effect of Mandrel Translation on Dry PEUU	45
3.3.2	Effect of Secondary Fiber Populations	47
3.4	DISCUSSION	52
3.5	LIMITATIONS AND FUTURE WORK.....	59
3.6	CONCLUSION	60
4.0	BIOMIMETIC ELECTROSPUN TISSUE CONSTRUCTS WITH CURVILINEAR MICROSTRUCTURES	61
4.1	INTRODUCTION.....	61
4.2	MATERIALS AND METHODS	63
4.2.1	Scaffold Fabrication	63
4.2.2	SEM Imaging and Structural Analysis.....	66
4.2.3	Cell Culture	66

4.2.4	Biaxial Mechanical Testing	67
4.2.5	Uniaxial Mechanical Testing	67
4.2.6	Suture Retention Strength	67
4.2.7	Statistical Analyses	70
4.3	RESULTS	70
4.4	DISCUSSION	73
4.5	LIMITATIONS AND FUTURE WORK	76
4.6	CONCLUSIONS	76
5.0	FATE AND FUNCTION OF INTEGRATED CELLS WITHIN ELECTROSPUN ELASTOMERIC CONSTRUCTS IN VIVO	78
5.1	INTRODUCTION	78
5.2	MATERIALS AND METHODS	80
5.2.1	Biaxial Mechanical Testing of the RVOT	80
5.2.2	Scaffold Fabrication	82
5.2.3	Cell Culture	82
5.2.4	RVOT Replacement Procedure	83
5.2.5	Patch Explantation	85
5.2.6	RT-PCR	85
5.2.7	Histology and Immunohistochemistry	86
5.3	RESULTS	86
5.3.1	Biaxial Mechanics of the Native RVOT	86
5.3.2	Postoperative Gross Observations	87
5.3.3	Histology and Immunohistochemistry	88

5.3.3.1	Inflammatory Response and Cell Infiltration	88
5.3.3.2	Endothelialization and Neovascularization	90
5.3.3.3	Residual Cells	91
5.3.4	RT-PCR Results.....	92
5.4	DISCUSSION.....	93
5.5	LIMITATIONS AND FUTURE WORK.....	97
5.6	CONCLUSIONS	98
6.0	CONCLUSIONS.....	99
6.1	STRUCTURAL MODIFICATIONS	100
6.1.1	Fiber Intersections.....	100
6.1.2	Curvilinear fibers	103
6.2	COMPOSITIONAL MODIFICATIONS	104
6.3	CLOSING REMARKS.....	107
APPENDIX A	108
APPENDIX B	109
APPENDIX C	110
APPENDIX D	111
APPENDIX E	112
BIBLIOGRAPHY	113

LIST OF TABLES

Table 1. A selection of important parameters in the electrospinning process and their effect on fiber morphology. Adapted from (45,46,51,52,54–57).....	9
Table 2. Polymer mass fraction in grams within each group.....	27
Table 3. Uniaxial mechanical properties of electrospun scaffolds fabricated on conical and cylindrical mandrels.....	.70

LIST OF FIGURES

- Figure 1 A. A diagram of a simple electrospinning device illustrating the key features. B. An example scanning electron micrograph of electrospun Dacron. Scale bar = 10 μm 6
- Figure 2. A. Schematic of the electrospinning setup. B. SEM micrograph overlaid with skeletonized representation of the construct microstructure. 22
- Figure 3. A. The effect of increased translational speed on dry PEUU biaxial mechanical properties. B. The effect of increasing translational speed on fiber orientation and normalized fiber intersection density. C. The relationship between a fabrication parameter (translational speed, top x-axis), a structural measure (fiber intersection density, bottom x-axis), and mechanical response (strain energy, y-axis). * indicates $p < 0.05$ 28
- Figure 4. A,B. Qualitative depictions of fiber microarchitecture of both dry and wet PEUU scaffolds in descending order according to translational speed, with 0.3 cm/s on the top and 30 cm/s on the bottom. C. Comparison of the mechanical response of dry and wet PEUU across translational speeds. (C indicates the circumferential axis, whereas L indicates longitudinal axis) *indicates $p < 0.05$ 29

Figure 5. Comparison between ‘wet’ and ‘dry’ processed PEUU structural elements across translational speeds. a. Fiber intersection density, b. Fiber orientation index. * indicates $p < 0.05$ 30

Figure 6 High resolution SEM micrographs depicting immediate microenvironment surrounding A. integrated microspheres and B. cells. Scale bar = 5 μ m..... 31

Figure 7. A. The change in biaxial mechanical response resultant from integrated particulates within PEUU fiber matrix. Translational speed during fabrication was 3.0 cm/s. * indicates statistically significant difference from both ‘dry’ and ‘wet’ groups. B. Combining slow translational speed with concurrent cell electrospaying produces a construct with mechanical anisotropy reminiscent of the native porcine pulmonary valve. (plots not significantly different from each other)..... 33

Figure 8. A. Schematic of electrospinning apparatus for two-component scaffolds. PEUU was fed from the same location for every group. The mandrel was rotated and translated along its longitudinal axis at varying speeds. Secondary polymer fibers were introduced through separate nozzles. B. Image of a polymeric specimen loaded in the bending device (scale bar = 1 cm)..... 40

Figure 9. A. SEM micrographs of representative scaffolds from each translated group (Scale bar = 5 microns) and B. the corresponding digitized structure. C. A plot depicting the quantitative relationship between translational speed during fabrication and microstructural elements. D. High magnification morphology of a fiber intersection ... 44

Figure 10. A. The relationship between translational velocity during fabrication (top x axis), fiber intersection density (bottom x axis), and bending modulus (y axis). B. Uniaxial tensile modulus of electrospun scaffolds fabricated under different translational velocities. C. Suture retention strengths of scaffolds fabricated under different translational velocities. 46

Figure 11. A. Fluorescent micrograph qualitatively depicting relative distribution of PEUU fibers (green) to PCL fibers (Red) in a 25/75 volume flow rate ratio construct. Scale bar = 20 microns B. Corresponding SEM micrographs representing each PEUU/PCL construct group. C. Change in fiber intersection density observed between PEUU/PCL ratios. No other differences in microstructural features were observed. Groups with different symbols (*, †, ‡) are significantly different from each other ($p < 0.05$) 48

Figure 12. A. Uniaxial tensile mechanical response of constructs containing increasing quantities of PCL fibers. B. Planar biaxial mechanical properties of PEUU:PCL blended scaffolds Groups with different symbols (‡, †, *) are significantly different from one another ($p < 0.05$)..... 50

Figure 13. Bending modulus of mixed polymer constructs at varying ratios of PEUU:PCL. Red solid reference line indicates the bending modulus of native costal cartilage [123]. Blue dashed reference line indicates the bending modulus of intact septal cartilage[124]. Groups with different symbols (‡, †, \bar{T} , *) are significantly different from one another ($p < 0.05$). 51

Figure 14. A. Representative structural images of PEUU/PEO 75/25 scaffolds as spun (dry), after 1 second (1s), and after 4 hours of soaking in water (4 hr). (Scale bar =10 microns. B. Fluorescent micrographs of PEUU (green)/PEO (red) blended constructs before (above) and after (below) treatment with water. Scale bar = 20 microns) C. Difference in normalized fiber intersection density between as spun 100% PEUU constructs and constructs following removal of PEO fibers *indicates $p < 0.05$ 54

Figure 15. A. Tensile modulus of constructs containing varying quantities of PEO following contact with water. B. Suture retention strength of constructs following PEO fiber removal. C. Biaxial mechanical response of constructs following PEO fiber removal. Groups with different symbols (\ddagger, \dagger) are significantly different from one another. ($p < 0.05$)..... 55

Figure 16. A. Qualitative depiction of constructs originally containing varying amounts of PEO placed in a cantilever position following contact with water. B. Bending modulus of constructs following PEO fiber removal. Reference line indicates the bending modulus of the native pulmonary valve (491kPa) [27]. * indicates $p < 0.05$, all groups are significantly different from one another..... 57

Figure 17 A. Graphical representation of the collagen fibril orientation in the native pulmonary valve (above) and the orientation angle values in each region (below). B. A circle of radius 5.13 cm will have a similar radius of curvature as the fibrils in native valve leaflets. 64

Figure 18 A. Schematic used to fabricate the conical mandrel used to collect fibers. B. The flattened projection of the conical mandrel surface includes a partial circle of radius 5.13 cm. 65

Figure 19 A. Qualitative depiction of fiber alignment over biologically relevant linear distances.	
B. Quantitative analysis of the change in main angle of alignment over linear distance on both conical mandrels evaluated.	69
Figure 20 A. Uniaxial stress strain curves from representative constructs. B. Suture retention strength of constructs evaluated. Reference line indicates suture retention strength clinically used ePTFE vascular graft [26]. * indicates $p < 0.05$	72
Figure 21. A. The morphology of sub-confluent MDSCs cultured on the surface of a scaffold with curvilinear fiber microarchitectures. B. MDSCs proliferated to a confluent layer on the surface of the scaffold. Scale bar = 100 μm	73
Figure 22 The biaxial mechanical response of scaffolds fabricated on conical and cylindrical mandrels in comparison to native pulmonary valve.....	74
Figure 23 A. Schematic of the scaffold fabrication assembly. B. Mechanical response of the rat RVOT under equal biaxial tension, overlaid by the nearest fit of electrospun PEUU....	81
Figure 24 A. Preimplant fluorescent micrograph of PEUU microintegrated with GFP(+) MDSCs. B. Preimplant fluorescent micrograph of PEUU microintegrated sequentially with RAOECs and SMCs. Red = α -SMA, CY3. Green = vWF, Alexa 488. Scale bars = 20 μm . C. Representative image of an MDSC integrated construct at explant following one week.....	83
Figure 25 Representative micrographs of the endocardial surfaces of each explanted construct group at each timepoint. Sections stained with Masson's Trichrome stain. Scale bar = 50 μm	87
Figure 26 Quantification of the bulk cellularity within explanted constructs.	88

Figure 27. A. High magnification micrograph of a Masson's Trichrome stained section of a representative wet PEUU explant at one week. B. Immunofluorescent micrograph of the same section stained for vWF (green), α -SMA (red) and Hoescht (nuclei, blue)..... 89

Figure 28. Masson's Trichrome staining depicting ECM elaboration within the bulk of representative sections from each group at two weeks post implantation. Scale bar = 50 μ m..... 90

Figure 29 Immunofluorescent micrographs of explanted constructs at one week (top) and two week (bottom) timepoints. Red = α -SMA, Green = vWF, Blue = cell nuclei (Hoechst)91

Figure 30 A. Density of neovascular structures within the bulk of explanted scaffolds. * indicates significantly different between other groups at the same timepoint. B. Immunofluorescent micrograph of neovascular structures. Green = vWF, Red = α -SMA. Scale bar = 40 μ m..... 92

Figure 31 A. Residual cells within a primary cell microintegrated scaffold at two weeks. B. Residual cells within an MDSC integrated scaffold at two weeks. Green = GFP, Red = Fluorescent dye, Sections were stained for cell nuclei and GFP signal was amplified. C. Quantification of labeled cell density within the bulk of the scaffolds..... 93

Figure 32. Gene expression in explanted patches at one week post implantation. * indicates $p < 0.05$ compared with healthy RVOT tissue 95

Figure 33. Gene expression in explanted patches at two weeks post implantation. * indicates $p < 0.05$ compared with healthy RVOT tissue..... 96

Figure 34 A. Ultimate tensile strength of dry PEUU under uniaxial load.. Elongation at failure of dry PEUU under uniaxial tensile load. Constructs fabricated at different translational speeds were not significantly different under these measures.110

Figure 35. H&E stained micrographs depicting cellularity in the central region of electrospun PEUU patches in each group at each timepoint. Scale bar = 50 μm 111

Figure 36. Immunofluorescent micrographs depicting the anastomosis with healthy RVOT tissue in each group at two weeks post implantation. Dotted line = PEUU border. Green = vWF, Red = α -SMA, Blue – cell nuclei. Scale bar = 100 μm 112

NOMENCLATURE

α -SMA – α -Smooth muscle actin

λ – Stretch

σ – Cauchy stress

χ – Flory – Huggins interaction parameter

ANOVA – Analysis of variance

BDI – 1,4-dicyanobutane

BMP – Bone morphogenic protein

CD31 – Transmembrane protein commonly used to identify endothelial cells

DMEM – Dulbecco's modified eagle medium

DMSO – Dimethyl sulfoxide

dry PEUU – Electrospun PEUU with no other materials or modifications

ECM – Extracellular matrix

ePTFE – Expanded poly (tetrafluoroethylene)

FBS – Fetal bovine serum

FGF – Fibroblast growth factor

FITC – Fluorescein isothiocyanate

GFP – Green fluorescent protein

H&E – Hematoxylin and eosin stain

HFIP – 1,1,1,3,3,3-hexafluoroisopropanol

I.D. – Inner diameter

MDSC – Muscle derived stem cell

Morphology (of electrospun fibers) – basic characteristics of the individual electrospun fibers
such as diameter, shape, and nanostructures which exist on the fibers

MSC – Mesenchymal stem cell

MT – Masson's trichrome stain

OIW – Weighted orientation index of electrospun fibers

PCL - Polycaprolactone

PCR – Polymerase chain reaction

PEO – poly (ethylene oxide)

PEUU – Poly (ester urethane) urea

PLGA – Poly (lactic-co-glycolic acid)

RAOEC – Rat aortic endothelial cell

RVOT – Right ventricular outflow tract

SEM – Scanning electron microscopy (or microscope)

SMC – Smooth muscle cell

TIPS – Thermally induced phase separation

TGF- β – Transforming growth factor β

Topology (of electrospun fibers) – the pattern of a population of electrospun fibers viewed as a
two-dimensional surface.

VEC – Valvular endothelial cell

VegF – Vascular endothelial growth factor

VIC – Valvular interstitial cell

vWF – von Willebrand factor

wet PEUU – PEUU electrospun concurrently with electrospayed cell culture media

PREFACE

ACKNOWLEDGEMENTS

I would like to take this opportunity to thank my dissertation committee for their advice and assistance in carrying out the research included in this dissertation. I would also like to thank my co-workers for their invaluable help in training and assisting me with this work. Especially Dr. William R. Wagner, Dr. Antonio D'Amore, Christian P. Rivera, Christopher M. Hobson, Dr. Hongbin Jian, Dr. Jianjun Guan, Dr. Johnathan A. Stella, Dr. Keisuke Takanari, Dr. Michael S. Sacks, Dr. Ryotaro Hashizume, and Dr. Yi Hong.

This work was funded by NIH R01 HL-068816 and the McGowan Foundation.

1.0 INTRODUCTION

1.1 CARDIOVASCULAR DISEASE AND THE TISSUE ENGINEERING PARADIGM

Cardiovascular disease is the leading cause of death in the United States(1). In 2008, one in every six deaths was due to coronary heart disease, one in 18 is due to stroke, and one in nine death certificates mentions heart failure(1). Additionally, aortic valve disease is responsible for 25,000 deaths and 95,000 valve procedures each year in the US alone(1). Despite advances in clinical care in recent years, tissue engineering and regenerative medicine hold tremendous potential for improving the duration and quality of life of those suffering from cardiovascular disease and defects.

The tissue engineering paradigm has traditionally required three elements designed to function together in order to form a replacement for a tissue of interest. The first element is a cell source which would take the role of forming the required tissue. These cells could be stem cells, primary cells, or even a mixed population of cells. The second element is a growth or differentiation factor or mechanical training designed to assist the cells in producing the target tissue. Third and finally, a scaffold is required to guide and provide structural support to the cellular components during the repair and regeneration process. The rationale being that seeding the scaffold with a population of cells prior to implantation would provide the body with a strong

starting point for regeneration of healthy tissue without excessive scar formation and loss of function that result from an untreated defect. Some recent strategies have diverged from this paradigm in favor of acellular constructs that rely on autologous cell infiltration upon implantation(2). Such scaffolds have the advantage of storage life and ‘off-the-shelf’ convenience in comparison with cellularized scaffolds which would need to be seeded and cultured with either autologous cells or allogenic cells which would be required to be on hand for this use. On the other hand, cellularized scaffolds may have an advantage in that the necessary building blocks of the engineered tissue – the cells – are already in place at implantation. While the cells are responsible for elaboration of extracellular matrix (ECM) that will eventually replace the tissue of interest, they could not adequately function without attaching to a properly designed scaffold.

1.2 BIOMATERIALS FOR TISSUE ENGINEERING

An ideal tissue engineering construct sufficiently replaces the function of a target tissue during the healing process. Whether that function is structural, mechanical, or chemical, some basic form of this behavior should be preserved. As tissue repair ensues, an ideal tissue engineering construct would controllably transfer the function to the newly formed tissue until the artificial construct is completely eliminated by the body, replaced by a healthy functional organ. For this sequence of events to take place, an appropriate biomaterial should be chosen as the tissue engineering scaffold, keeping in mind that a biomaterial successful in one application may catastrophically fail in another.

1.2.1 Natural Biomaterials

ECM based materials represent one class of biomaterials of interest to the tissue engineering community(3,4). Such materials are purified proteins such as collagen and elastin, or are processed intact as decellularized tissues. These materials have the advantage of being biocompatible and bioactive by nature. Decellularized tissues, in particular, are studied extensively for their ability to elicit constructive inflammation and remodeling in vivo(4). A number of reports have demonstrated successful tissue repair with robust fresh ECM elaboration in a variety of applications(3,5–7). However, these materials are primarily limited by their lack of attractive mechanical behavior during the early stages of the healing process(8,9). Another important concern with decellularized materials is that biologic variability in tissues prior to decellularization necessarily results in variability in either mechanics or bioactivity of the decellularized result(8–10). Further, depending upon the processing method employed, decellularized tissues can be hindered by inconsistent performance in terms of their mechanics and local cytotoxicity due to residual processing agents(11).

1.2.2 Synthetic Biomaterials

Synthetic polymeric materials have the advantage of tunable and robust mechanical response, as well as material characteristics that are as consistent as is possible under controlled laboratory or industrial settings. The primary disadvantage of polymeric biomaterials is their lack of inherent bioactivity, which can potentially result in excessive inflammatory response or pronounced fibrous encapsulation(4). To combat these disadvantages, a class of polymers has been synthesized with the specific purpose of use as biomaterials for tissue engineering (12–20). For

each application of interest, a different set of design parameters exist for optimal polymer characteristics. Some polymers have been designed with biofunctional groups as side chains or surface modifications in order to enhance cell attachment(19,21,22), reduce thrombosis(23,24), or promote differentiation(22). The primary criteria necessary for ideal cardiovascular biomaterials are: 1. mechanical strength and resiliency to withstand repeated mechanical forces, 2: low thrombogenicity to prevent additional cardiovascular complications, 3: adequate support of cells without hindrance of proliferation, and 4: amenability to processing into a scaffold that will satisfy the previous three criteria.

To satisfy these criteria, our group has synthesized a class of polyurethanes based on FDA approved materials and reagents including a poly (ester urethane)urea (PEUU) based on polycaprolactone and 1,4-diisocyanatobutane(12,13,15,25–27). PEUU has been shown in several studies to be biocompatible, mechanically robust, and tolerant to cardiovascular applications(28–30). Further, PEUU is amenable to a wide variety of melt and solvent processing techniques which can impart structural features to the material which can be utilized and provide a host of tunability with respect to mechanics and cell support.

1.2.3 Biomaterial Processing Techniques

For appropriate cellularity, tissue engineering constructs must provide sufficient void fraction for cellular infiltration. Toward this goal, the most popular processing techniques for tissue engineering produce a porous structure from a polymer solution. This can be accomplished by introducing a particulate defect such as a salt to the solution prior to solvent evaporation. The salt can be dissolved away to produce a scaffold with a randomly distributed porous structure and high void volume(31). Pores can also be created in solution using a technique known as

thermally induced phase separation (TIPS). In this procedure, a dilute polymer solution is enclosed in a chamber and rapidly cooled, forcing the polymer out of solution. As this occurs, voids develop which act as pores following solvent removal and drying(28). Each of these porogenic techniques have had success *in vivo* with respect to cellular infiltration and proliferation. TIPS scaffolds, in particular, are of particular interest due to the customizability of the process. TIPS scaffolds have been fabricated with interconnected pores of a variety of sizes(32), shapes(33), and degrees of alignment. The primary disadvantage to this technique, however, is the low tensile moduli and lack of mechanical tunability found in fibrous scaffold processing techniques such as electrospinning(28).

1.3 ELECTROSPINNING FOR TISSUE ENGINEERING APPLICATIONS

1.3.1 Electrospinning Background and Scientific Principles

Electrospinning is a technique which utilizes Coulombic forces in the preparation of ultrathin fibers. This technique was developed over 100 years ago(34), however it has been the subject of increasingly extensive research in recent years due to its ability to create fibers of 50 nm to 10 μm in diameter in comparison to 10 to 100 μm produced by more conventional extrusion techniques(35). Such size scales are of particular interest in the medical field, as they encompass the same order of magnitude of diameters found in native extracellular matrix (ECM), which was hypothesized to be attractive for supporting viable cells. Indeed, many *in vitro* studies have demonstrated that living cells thrive on electrospun fibers(36–41) and may be able to maintain a phenotype more similar to that found *in vivo* when compared with tissue culture polystyrene(42).

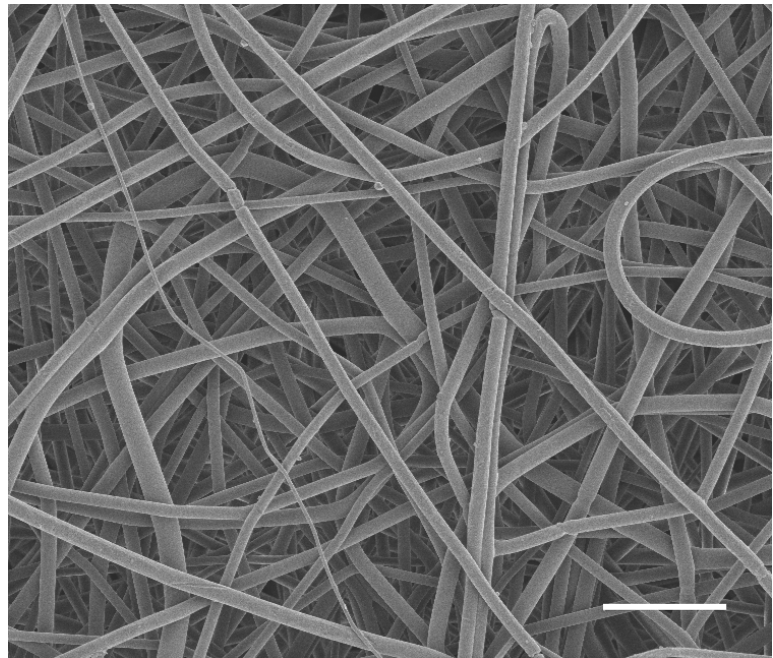
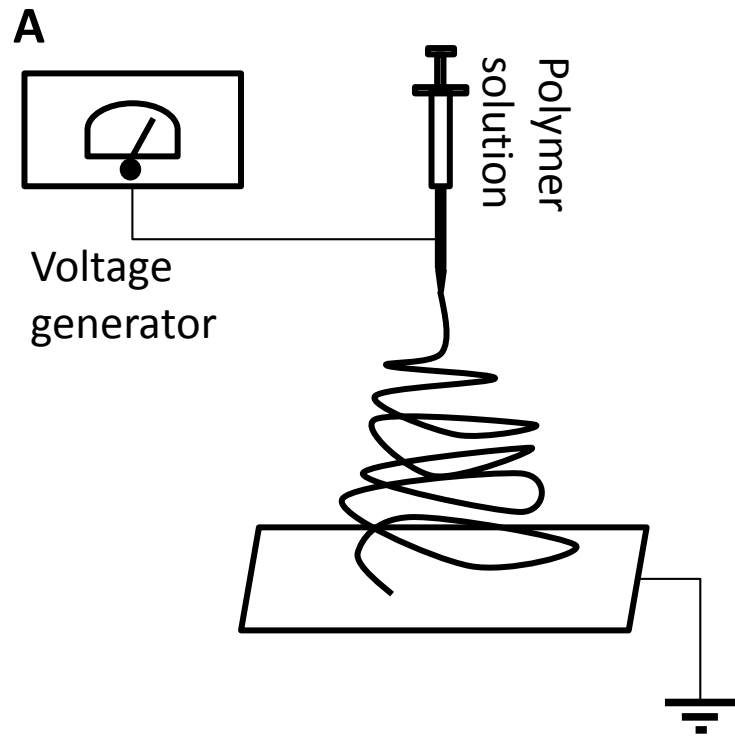


Figure 1 A. A diagram of a simple electrospinning device illustrating the key features. **B.** An example scanning electron micrograph of electrospun Dacron. Scale bar = 10 μm

Therefore electrospun constructs have been researched and marketed for bioreactor and complex 3D culture techniques as well as tissue engineering(15). Electrospinning is further attractive to the medical device industry as it is comparatively low cost with respect to other techniques for nano- to micro-scale material processing and fabrication techniques.

In principle, electrospinning is a simple process brought on by electrostatic forces attracting a polymer solution toward a grounded target; however the number of parameters involved make fully understanding and controlling the process quite complex. At its most basic, electrospinning occurs when an electric field is applied to a viscous polymer fluid in the presence of a grounded or oppositely charged target. **(Figure 1 A)**. A diagram of a simple electrospinning device illustrating the key features. B. An example scanning electron micrograph of electrospun Dacron. Scale bar = 10 μm) The polymer fluid can be a melt(43), however it is more commonly dissolved in a strong, volatile solvent(34). Most commonly, but not necessarily, the polymer solution is fed through a charged capillary. The voltage on the capillary perturbs the fluid at the end nearest the target, drawing it into a cone shape known as a ‘Taylor cone’. When the attractive force on the solution applied by the electrostatic field overcomes the surface tension of the fluid, the fluid begins to escape from the tip of the Taylor cone and travel toward the counterelectrode. If a sufficient number of polymer chain entanglements exist, the escaping fluid forms a stable, complete jet which will deposit solid fibers onto the target(44,45). As the jet travels through the air intramolecular electrostatic repulsions trigger a series of Raleigh instabilities which result in a rapid, chaotic whipping motion. The whipping motion extrudes the jet to such a degree that it is common for fiber diameters upon deposition to be much smaller than the initial size of the jet(46). If chain entanglements are insufficient to form a contiguous jet the fluid can break up into droplets that deposit onto the target counterelectrode. The chaotic nature of fiber motion as they deposit upon the target produces a 2D pattern of indeterminate topology. **(Figure 1 A)** As further fibers deposit on top of the initial layer, a small amount of residual solvent is often present which permits the formation of a bound joint at the intersection between two or more fibers(47). If no changes are made to the processing parameters over time,

the stochastic nature of the process will allow for the formation of a 3D structure in which no two layers are the same, but every layer shares the equivalent structural features on average(48). There have been a number of reports(43,46,49–53) which delve into intricate detail in modeling the physics and kinematics of electrospun fibers, however these are beyond the scope of this dissertation and will not be discussed further.

The morphology of the fibers deposited onto the target is heavily dependent on the qualities of the polymer solution as well as processing parameters and even ambient conditions. Parameters which affect polymer chain interactions within solution are likely responsible for the ability of a solution to be electrospun into intact fibers. These include controllable parameters such as solution concentration and polymer molecular weight as well as properties of the solvent-polymer system such as the Flory-Huggins interaction parameter (χ), a measure of the interaction of the solvent molecules with the polymer chain and the polymer-polymer interactions. In a general sense, polymer chain interactions can be considered to increase the apparent molecular weight of the polymer in solution(54). There is a gradual transition in fiber morphology as apparent molecular weight is increased. Below a critical value, the solution is only capable of electrospay(46). Above this critical value, thin, broken fibers with agglomerates of polymer which appear as ‘beads on a string’ are produced(43). Further increasing the apparent molecular weight allows for the production of intact, beaded fibers(50). When the apparent molecular weight is above a second critical value, fibers produced are bead free, and any further increase in apparent molecular weight will only serve to increase the diameter of the fibers produced(50). Fiber diameter and morphology is also controllable by a number of electrospinning assembly parameters. A summary of these parameters can be found in **Table 1**(44,45,50,51,53–56).

Table 1. A selection of important parameters in the electrospinning process and their effect on fiber morphology. Adapted from (45,46,51,52,54–57)

<i>Parameter</i>	<i>Effect on fiber morphology</i>
<i>Device Design</i>	
Applied voltage	Higher voltage leads to smaller fibers Beading can occur if voltage is excessive
Flow rate	Directly correlated with fiber diameter
Gap distance	Inversely correlated with fiber diameter
Target geometry, motion, modifications	Modifications to the target result in altered topography, but can sometimes affect fiber morphology
<i>Solution Parameters</i>	
Solution concentration/viscosity Flory-Huggins interaction parameter (χ), polymer molecular weight	Concentration/viscosity are directly correlated with fiber diameter. Low chain entanglements result in beaded or broken fibers, whereas high chain entanglement produces clean fibers
Polymer-polymer molecular interactions	Increased interactions result in thicker fibers due to increased apparent molecular weight
Solution conductivity	High conductivity leads to smaller, bead free fibers
Solvent evaporation rate	Less volatile solvents produce fibers that flatten and meld together more than those processed with volatile solvents
Relaxation time	Shorter relaxation times are hypothesized to permit more rapid whipping and therefore smaller fibers
<i>Ambient Parameters</i>	
Relative humidity	Higher relative humidity results in larger fibers
Temperature	Rise in temperature decreases viscosity which works to decrease diameter. It also increases solvent evaporation rate

1.3.2 Controlling Electrospun Topology

As discussed previously, electrospinning in its most basic form produces a chaotic topology of fibers of predictable morphology. A number of modifications have been discussed in the literature with the purpose of producing electrospun constructs with determinate fiber topology(57–65). Some of this work involved complex, small-scale patterning using electrodes with patterns of high conductance or resistance(62,66). Others involved methods of controlling the location of fiber deposition using electrostatic lenses or direct writing(57,67). Still other studies have developed techniques for producing aligned fibers along large scaffolds(60,61,68,69). This can be accomplished by electrospinning onto a rapidly rotating drum. Courtney et al. have demonstrated that by rotating the drum target with a tangential velocity faster than the speed that the fibers accumulate, they can be physically pulled into alignment with the rotation(68). Alternative methods of aligning fibers involve modulating the electric field in order to drive the fibers into alignment. An arrangement of parallel electrodes(60), or an arrangement of knife blade style electrodes which can be used to focus the electric field(70). Aligned fibers are of particular interest in the field of bioengineering, as a number of tissues possess pronounced structural and mechanical anisotropy including peripheral nerve fibers(71), tendon(72), and heart valve leaflets(68). Fabricating scaffolds with high degrees of fiber alignment has been demonstrated to produce scaffolds which possess mechanical anisotropy on the order of magnitude of that seen in vivo(68). Further, cells have been shown to align with electrospun fibers in vitro(73). It has also been demonstrated that cells aligned on such scaffolds can elaborate extracellular matrix in a similar pattern, which would be advantageous for the function of potential engineered tissues(73,74). In conjunction with attempts to control the topology of electrospun scaffolds, various methods have been utilized to

quantify the scaffold microstructure(68,75). Using imaging modalities such as small angle light scattering, optical coherence tomography, and scanning electron microscopy (SEM), structural images have been digitized and quantified through Fast Fourier Transform(75) and customized algorithms which have the capability of automatically detecting fiber diameter and alignment. Recently, our group has developed an image analysis algorithm with the capability of capturing and digitizing the complete structure of fibrous structures from a variety of image types(48). In addition to fiber diameter and alignment, the fiber intersections can be quantified in terms of number, position and density. This permits more complex microstructural manipulation for improved mechanical response and a deeper understanding of force transmission from the macro-scale to the micro-scale.

1.3.3 Modifying Electrospun Constructs for Bioactivity and Cell Infiltration

Recent research has produced a collection of techniques designed to introduce functionality to electrospun constructs(76–79). The high surface area of electrospun scaffolds provides an advantageous platform for drug delivery through diffusion. Bioactive compounds can be introduced directly into the polymer solution in order to produce a consistent distribution of drug throughout the scaffold(80). This can only be accomplished if the drug is soluble in the same solvent as the polymer used for the scaffold. Care must be taken, however, to ensure that any bioactive compounds are not denatured by the volatile organic solvents used in the process. Other techniques have been introduced to prevent interaction between the drug and organic solvents. In 2003, Sun et al. introduced the technique of coaxial electrospinning(79). In this technique, a uniquely designed syringe is designed with an inner chamber that is encircled by a second chamber. These coaxial chambers remain distinct through the end of the needle. When

electrospinning occurs, the fibers form in a bilayer structure in the same manner as the solutions were arranged in the needle as long as materials are chosen properly(79). This technique has been used to fabricate electrospun fibers with two or more immiscible materials, allowing an outer shell to be made of polymer with an aqueous center loaded with drug. In this manner, sensitive bioactive compounds can be protected from harsh organic solvents(81). It is additionally possible for hollow fibers to be made in this manner(79,82).

Further functionality can be introduced to electrospun scaffolds through the introduction of additional polymer sources. When targeted toward a rotating mandrel, each polymer source can produce a separate fiber population comprised of different materials. This permits materials with disparate properties to be combined without being restricted to blending into one fiber population. These fibers can be made to be evenly dispersed among each other(26) or be deposited in a biomimetic pattern in order to instill proper mechanical functionality(83). Additionally, the secondary or tertiary fiber populations can be comprised of extracellular matrix (ECM) proteins(84). These proteins can be purified or in the form of solubilized decellularized ECM materials(85). It has been shown that incorporating such ECM fiber populations into electrospun constructs can impart biological functionality, resulting in increased host response and de novo ECM elaboration in vivo(85).

While many electrospun constructs have been shown to be successful at supporting viable cells on their surface, attempts to cellularize these scaffolds in vitro have met with difficulty in terms of producing uniform cellularity through scaffold thickness. Such attempts involve seeding cells on the external surface of the scaffolds and allowing cells to infiltrate under culture. It has been shown that under static culture, cell infiltration is limited to short distances on the order of several millimeters, however perfusion culture can increase these distances(73,86). The

cause of difficulty with seeding electrospun constructs is the pore size of the scaffolds. Electrospun constructs have been reported to have typical porosity values of approximately 70-80%(87). However the nature of the fabrication technique, particularly when fibers are aligned, leads to tightly packed constructs with pore sizes less than the typical size of a mammalian cell(55). Extrapolating from previous studies(88), it can be hypothesized that cells can be hindered from penetrating deeply into scaffolds with small pores and better results may be achieved if biomaterials for tissue engineering possessed larger pores. For this reason, methods of improving pore size or cellularity in vitro have been extensively researched(55). Pore size can be increased most simply through increasing fiber diameter(40,54,89), however this is potentially at a price of less favorable cellular response(42). Several alternative techniques include introducing a salt to the polymer solution and dissolving it away following fabrication(31), laser ablation(90), mechanical expansion(91) and limited protease digestion(92). Each of these techniques, while successful in increasing pore sizes, involve disruption of intact fibers following fabrication which could result in disrupted construct integrity or mechanics. Baker et al. introduced a technique in which poly (ethylene oxide) (PEO) was electrospun concurrently with polycaprolactone (PCL)(93). Following fabrication, the PEO fibers were dissolved out of the construct leaving only a PCL skeleton. This methodology possessed the advantage of increasing pore size without disrupting the original PCL microstructure. Follow-up studies demonstrated robust cellularity using this technique both in vitro and in vivo(92,94).

One of the distinct advantages of electrospinning is its amenability to modification. Several researchers have developed modalities which produce electrospun scaffolds with fundamentally different fiber topologies in three dimensions in order to produce materials with dramatically lower polymer densities, and possibly encourage ECM elaboration from seeded

cells. Blakeney et al. targeted a jet toward the inner surface of a non-conductive hemispherical dish equipped with an array of electrodes(39). This technique produced a unique electrostatic field within the hemisphere where no region possessed a preferential attraction for the polymer jet, allowing fiber aggregation in mid-air – producing a loose ‘cotton ball-like’ construct, which permitted uniform cell infiltration over 7 days(39). A similar result was achieved by Phipps et al. using a disk shaped collector with protruding needle electrodes(92). Simonet et al also produced a scaffold with a low volume fraction of polymer by cooling the target with CO₂ ice in order to form ice crystals during fabrication which would become void space upon warming(95). This technique was applied to a rabbit calvarial defect model by Schneider et al. using PLGA supplemented with tricalcium phosphate nanoparticles in order to improve bioactivity(96). In this study, the researchers compared the novel material with currently approved Bio-Oss® and PLGA with a similar low packing density. It was found that tricalcium phosphate within the scaffold enhanced bone formation, however the new bone possessed a more spongy structure in comparison to that formed by the current standard-of-care. Longer experimental endpoints would be needed to discern if remodeling into more dense bone would occur, however similar low density structures which have been shown to produce spongy bone were capable of forming dense cortical bone in the presence of an electrospun guiding membrane(97). Further, regenerated bone from a sufficiently porous but higher density electrospun scaffold functionalized with bioactive compounds was found to be highly mineralized and mechanically equivalent to native cortical bone(98). Compiling these reports, it becomes apparent that an interplay likely exists between structure, mechanical support, and chemistry during tissue remodeling and regeneration. For a successful engineered tissue to form, a scaffold of

appropriate structure and mechanical response should be functionalized with bioactive components rationally designed to promote advantageous cellular response.

1.3.4 Mechanically Appropriate Cellularized Electrospun Scaffolds

As discussed previously, structures with appropriate mechanical and structural properties are likely vital in guiding forming tissues toward healthy, site appropriate forms. In this light, ultra-low density electrospun scaffolds would likely be appropriate for loose structures such as spongiosa(96), or non-load bearing structures such as donor-site articular cartilage defects following autologous osteochondral transplant(99). For load bearing applications, such as the cardiovascular system, a more mechanically robust structure is required; however this structure should ideally be capable of providing chemical instruction to the surrounding environment. Therefore, a cellularized thermoplastic elastomer possessing a fibrous structure amenable to cellular proliferation and locomotion would be an attractive biomaterial for cardiovascular tissue engineering prostheses. Toward this end, Stankus et al. developed a technique for rapidly fabricating highly cellularized elastomeric constructs using a combination of electrospinning and cell electrospray. This technique, which the authors named ‘microintegration’ involved electrospraying living cells onto a rotating mandrel concurrently with and in a perpendicular orientation to PEUU electrospinning(100). It has been demonstrated by multiple groups that a variety of cell types can survive the electrospray process with their phenotypes intact(100–105), and that cells microintegrated within electrospun scaffolds can proliferate in in vitro culture(102,104). Further, microintegrated PEUU constructs have been shown to be mechanically robust with tensile strength, suture retention strength, and vessel burst strength well within safety parameters for implantation as cardiovascular tissue engineering

prostheses(100,102). It can be hypothesized that not only would microintegrated cells be capable of contributing to the regenerated tissue in terms of cellularity and elaborated ECM, but they would also be capable of expressing chemotactic factors to encourage host cell infiltration into the growing matrix. However, to date, the fate and function of these microintegrated cells remain unclear.

1.3.5 Toward the Rational Design of Electrospun Cardiovascular Tissue Engineering

Prostheses

A critical feature in the development of any bioprosthetic device is the engineering process. All materials that comprise the device must be sufficiently biocompatible in that they must not produce a negative reaction *in vivo* and must also withstand or predictably react to any mechanical or chemical forces that it experiences. Understanding the response and function of any device *in vivo* is an extremely time consuming, difficult and expensive process, so much of the early evaluation work is performed in simulated *in vivo* environments. Cell microintegrated scaffolds are uniquely suited for this evaluation as they are fabricated with a dense cell population throughout the thickness of the scaffold. Stella et al. performed a series of studies which utilized cellularized electrospun scaffolds to recapitulate the micro-scale interactions which occur between ECM and cells in native and engineered tissues and evaluate the effect of mechanical deformation on the integrated cells(106,107). The most critical piece of information validated in this work was that deformations in the immediate microenvironment surrounding a cell directly relates to the cellular deformations as observed by the nuclear aspect ratio. Macro-scale deformations do not necessarily translate directly to similar levels of micro-scale deformation due to the sum of individual fiber deformations in the electrospun network(106).

Moreover it was demonstrated that physiologic strains during bioreactor culture were associated with pronounced, robust ECM elaboration(107). These studies highlight the need for microstructural and mechanical evaluation paired with structural deterministic modeling during the device development stage, as well as the importance of proper mechanics in any purported electrospun cardiovascular tissue engineering construct.

1.4 OBJECTIVES

The overall goal of this project was to develop methodologies which could be used to mechanically and compositionally optimize elastomeric electrospun scaffolds for a variety of cardiovascular tissue engineering applications, especially for heart valve leaflets. While a fully cellularized, bioreactor conditioned construct would have distinct advantages in terms of tissue present at the time of implantation, an acellular construct would be attractive from a regulatory and practical perspective for instant ‘off-the-shelf’ use. With this in mind, a series of experiments were designed to study methods of tuning both planar and bending mechanical response of electrospun scaffolds in general. Next a mechanically optimized scaffold was implanted in vivo in order to evaluate the fate and biochemical function of microintegrated cells at early timepoints with the goal of possibly elucidating growth factors that may be responsible for beneficial host response.

1.4.1 OBJECTIVE #1: Determine the effects of processing conditions and modifications on PEUU microstructure and planar biaxial mechanical response

Previous research on evaluating scaffold microarchitecture and relating it to mechanical response and function largely focused on fiber orientation. Recently, our group has developed a unique algorithm that can more completely analyze the structure of these scaffolds beyond simple fiber orientation index. The work outlined in this aim focuses on analyzing the structure of electrospun scaffolds and relating quantifiable micro-scale elements to macro-scale biaxial mechanical properties. Moreover, we intended to study several modifications to the electrospinning process that have been previously introduced but not yet adequately evaluated. The hypothesis was that these modifications would alter the scaffold microstructure in such a way that they change the mechanical response without significantly altering the overall fiber orientation. This work challenged the existing paradigm of the field which suggested that fiber orientation is the only important microstructural measure when dealing with electrospun constructs.

1.4.2 OBJECTIVE #2: Evaluate and control the flexural response of electrospun scaffolds

Biodegradable thermoplastic elastomers are attractive for application in cardiovascular tissue construct development due to their amenability to a wide range of physical property tuning. For heart valve leaflets, while low flexural stiffness is a key design feature, control of this parameter has been largely neglected in the scaffold literature where electrospinning is being utilized. This study evaluated the effect of processing variables and secondary fiber populations on the microstructure, tensile and bending mechanics of electrospun biodegradable polyurethane scaffolds for heart valve tissue engineering. Scaffolds were fabricated from poly(ester

urethane)urea (PEUU) and the deposition mandrel was translated at varying rates in order to modify fiber intersection density. Scaffolds were also fabricated in conjunction with secondary fiber populations either designed for mechanical reinforcement or to be selectively removed following fabrication. It was determined that increasing fiber intersection densities within PEUU scaffolds would be associated with lower bending moduli. Further, constructs fabricated with stiff secondary fiber populations had higher bending moduli whereas constructs with secondary fiber populations which were selectively removed had noticeably lower bending moduli. Insights gained from this work will be directly applicable to the fabrication of soft tissue constructs, specifically in the development of cardiac valve tissue constructs.

1.4.3 OBJECTIVE #3: Produce biomimetic electrospun constructs with curvilinear microstructures

Electrospun scaffolds possessing aligned fiber microstructures have been shown to possess high degrees of mechanical anisotropy, similar to that of native heart valve tissue. However, in mathematical models of the valve leaflet motion of such scaffolds, several regions of localized stress and turbulent blood flow were predicted. Such areas of unnatural force have been associated with increased levels of thrombosis and calcification.

Small angle light scattering of native heart valves demonstrates that collagen fibers change their main angle of orientation along the length of each leaflet. Models of valve function further predict that such curvilinear fiber orientations would be responsible for a reduction of localized high stress zones and therefore should provide a better functional outcome. In the present work, we hypothesized that the direction of fiber alignment in electrospun scaffolds could be controllable based on the geometry of the target mandrel. Following this hypothesis, we

electrospun poly(ester urethane) urea onto a conical mandrel of varying opening angles. Each mandrel was rotated in order to achieve a tangential velocity at the target radius of 9 m/s. This tangential velocity was chosen based on previous studies that demonstrate this value is necessary to create high levels of fiber alignment. This method of scaffold fabrication was capable of producing aligned fibrous constructs where the angle of alignment varied over scaffold length. The radius of curvature of each construct was consistent with that of the mandrel geometry. Further, when the radius of curvature of the electrospun construct was equal to that of the native pulmonary valve, the mechanical anisotropy was also similar to that of the native valve (scaffold anisotropy ratio: 0.161 +/- 0.076 vs. pulmonary valve anisotropy ratio: 0.124 +/- 0.017).

1.4.4 OBJECTIVE #4: Determine the in vivo behavior and response of heterogeneous microintegrated constructs

Our laboratory has pioneered the technique of concurrently electro spraying aqueous fluids (with or without living cells) onto an electrospun scaffold during fabrication(102). Previous works by our laboratory have demonstrated in vivo success with such acellular, wet processed scaffolds(108). It is currently unclear, however, how scaffolds processed with electro sprayed, living cells would function in vivo. Such cellularized constructs could be potentially advantageous as rapidly produced tissues; however it is critical that the fate and behavior of the integrated cells be determined. By incorporating living smooth muscle and endothelial cells into a rat right ventricular outflow tract (RVOT) replacement, it will be possible to evaluate the role (if any) that living integrated cells play in tissue growth and remodeling in vivo.

2.0 PROCESSING CONDITIONS AND MODIFICATIONS ON THE MICROSTRUCTURE AND PLANAR BIAXIAL MECHANICAL RESPONSE OF ELECTROSPUN POLY(ESTER URETHANE) UREA

This work has been adapted from the following previously published manuscript:

Amoroso NJ, D'Amore A, Hong Y, Wagner WR, Sacks MS. Elastomeric electrospun polyurethane scaffolds: The interrelationship between fabrication conditions, fiber topology, and mechanical properties. *Advanced Materials*. 2011;23(1):106-111

2.1 INTRODUCTION

Electrospinning has been gaining increasing popularity in the fabrication of engineered tissue scaffolds due to its ability to produce nano to micro scale fibrous sheets. Many investigators have attempted to apply various degrees of control to this process in order to produce fiber meshes with more predictable patterns. These attempts have largely been limited to controlling fiber alignment and have fallen into two categories: physical manipulation of the fibers by pulling them into alignment using a rapidly spinning mandrel(68-69) or manipulation of the electric field during fabrication(63,65).

To fully quantify the structure of native tissues and engineered fibrous scaffolds, a novel image analysis technique(48) was recently developed to quantify fiber intersections (number, position and density), connectivity distribution, and fiber angle distribution (**Figure 2 B**). This

technique was utilized in conjunction with novel fabrication methods and comprehensive mechanical characterization to advance our understanding of how fiber network topology affects meso-scale mechanical properties of electrospun scaffolds. Specifically, two previously unevaluated fabrication modalities were utilized to induce controlled alterations in fiber network topology: (1) variation of collecting mandrel translation speed, and (2) concurrent electrospaying of cell culture medium with or without cells or rigid particulates to emulate the maximum possible micro-inclusion stiffness.

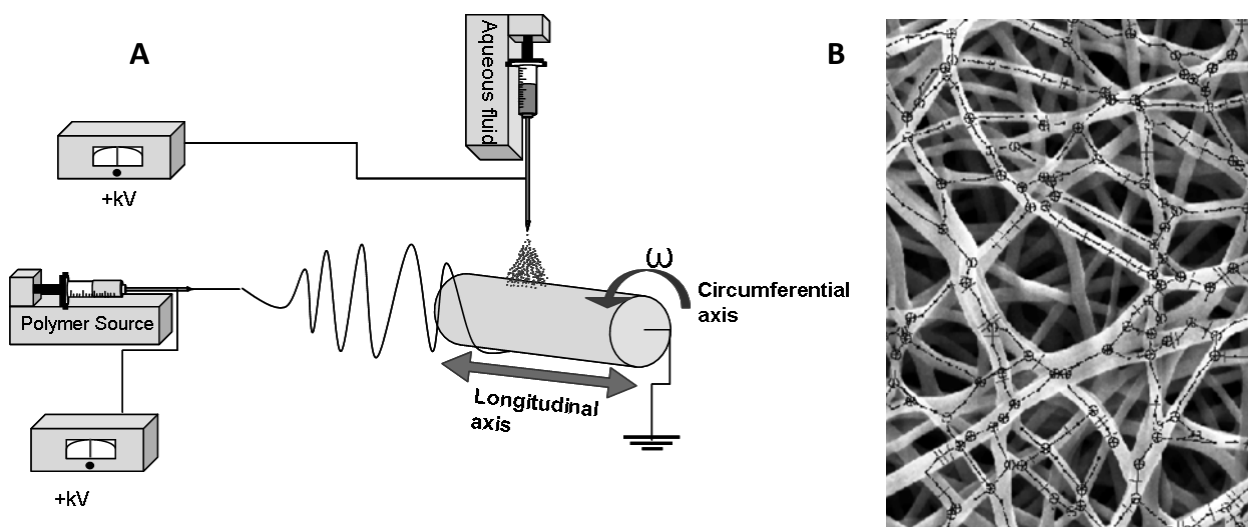


Figure 2. **A.** Schematic of the electrospinning setup. **B.** SEM micrograph overlaid with skeletonized representation of the construct microstructure.

The experimental setup adopted in the current study was similar to that described previously(102,108). Briefly, a solution of poly(ester urethane urea) (PEUU) was fed by syringe pump through a charged capillary located horizontally from a grounded mandrel (**Figure 2 A**). The mandrel was rotated at 266 rpm (~ 8 cm/s tangential velocity) and translated along its rotational axis at 0.3, 1.5, 3 or 30 cm/s. PEUU was electrospun dry (with no further modifications to the process) or “wet” by concurrently electrospaying cell culture medium onto the target from a perpendicular orientation to the polymer stream above the mandrel. The effect

of cell and particulate inclusion into the fiber scaffold matrix was studied by electrospaying the same medium containing a suspension of a known concentration of either vascular smooth muscle cells or polystyrene microspheres into the cell culture medium. Cells were electrospayed at concentrations of 2 and 6 million/mL, and microspheres were electrospayed at 7 million/mL. Scaffolds were evaluated using biaxial mechanical testing in conjunction with structural analysis using a custom algorithm(48).

2.2 METHODS

2.2.1 Smooth Muscle Cell Culture

Vascular smooth muscle cells, chosen for their utility in cardiovascular applications, were isolated from Lewis rat aortas and were expanded on tissue culture polystyrene culture flasks using Dulbecco's modified Eagle medium (DMEM) (Lonza) supplemented with 10% fetal bovine serum and 1% penicillin-streptomycin.

2.2.2 PEUU Synthesis

Polycaprolactone diol (PCL diol, MW = 2000 kDa, Sigma) was dried under vacuum at 50°C for 24 hours to remove any residual water. 1,4-diisocyanatobutane (BDI, Fluka) and putrescine were vacuum distilled before use. Tin(II) 2-ethylhexanoate and dimethyl sulfoxide (DMSO, anhydrous) (Sigma) were used as received. Poly(ester urethane) urea (PEUU) was synthesized in a two-step reaction according to the following protocol developed previously(13,102,108). The

stoichiometry of the reaction was 2:1:1 of BDI:PCL diol:putrescene. The first step consisted of a mixture of 15 wt.% solution of BDI in DMSO with a 25-wt% solution of PCL diol in DMSO in the presence of Tin(II) 2-ethylhexanoate. This was heated to 80°C for 3.5 hours under rapid stirring. Following the initial polymerization, the mixture was cooled to room temperature and putrescine was added dropwise to the prepolymer solution under stirring. The flask was closed and the reaction was continued at room temperature for 18 hours following which the polymer was precipitated in distilled water. Unreacted monomer was removed by soaking wet polymer in three changes of isopropanol. PEUU was dried and stored at room temperature.

2.2.3 Scaffold Fabrication and Characterization

A 12%(w/v) solution of PEUU in 1,1,1,3,3,3-hexafluoroisopropanol (Oakwood Products, Inc) was fed at 1.5 mL/h through a stainless steel capillary (inner diameter: 1.2 mm) charged to 11 kV and located 17 cm horizontally from a stainless steel cylindrical mandrel. (**Figure 2 A**) The mandrel was 6 mm in diameter, charged to -4 kV, and rotated at 266 rpm (~8 cm/s tangential velocity). The mandrel was translated upon its rotational axis at 0.3, 1.5, 3 or 30 cm/s. PEUU was electrospun dry (with no further modifications to the process) or “wet” by concurrently electrospaying cell culture medium (fed at 15 mL/hr, charged to 8 kV) onto the target from a perpendicular orientation to the polymer stream 4.5 cm above the mandrel. The effect of cell and particulate inclusion into the fiber scaffold matrix was studied by electrospaying the same medium containing a suspension of a known concentration of either smooth muscle cells or polystyrene microspheres with 10 micron diameter (Invitrogen) into the cell culture medium. Cells were electrospayed at concentrations of 2 and 6 million/mL, and microspheres were electrospayed at 7 million/mL. Concentrations of particulates in the electrospray suspensions

were determined using a Bright-Line hemocytometer (Hausser Scientific) The mass fraction of polymer in each scaffold was determined by first rinsing sections of known dimensions in distilled water five times and allowing them to dry at room temperature in a desiccator over 48 h. Polymer mass fraction was computed by dividing the mass of the electrospun sample by a sample of cast PEUU of identical dimensions.

2.2.4 Microscopy and Fiber Architecture Characterization

After drying over 24 h the scaffold sections were gold sputter coated and imaged with SEM (JEOL JSM6330F). Sets of five images at ~1000x magnification were chosen from each sample. Fiber structural features were quantified from these images using a method previously described(48). Briefly, the outer layer of fibers was isolated using a combination of threshold segmentation followed by morphological procedures of eroding and dilating. Fiber intersections were counted manually, and a modified Delaunay network was generated from these intersection coordinates. The following micro-architectural data were extracted from the generated network (**Figure 2 B**): (1) fiber intersection number, position and density, (2) connectivity distribution, defined as the percentage of fiber intersections vs. number of fibers crossing a fiber intersection, and (3) fiber orientation angle distribution. Fiber intersection density was normalized to fiber diameter. Fiber angle distribution was further described by calculating the fiber orientation index, defined as: the average over all fiber segments of $\cos^2(\theta)$, where θ represents the angle between a fiber segment and the direction of alignment.

2.2.5 Mechanical Characterization

Following fabrication, constructs were incubated in cell culture medium overnight at 37°C. Samples were divided into 10 mm x 10 mm sections for testing. Slices of polypropylene suture (Ethicon) were affixed to each section to form four small markers of ~1 mm in diameter in the central region. Samples were then tested in a physiological saline solution at room temperature using a Lagrangian membrane tension (\mathbf{T}) controlled protocol as previously described(68). Equi-biaxial tension was imposed up to a maximum of 90 N/m to facilitate comparison with previous studies on valvular tissues(68). Data post-processing was completed using a preconditioned free-float reference, and was converted to stresses using measured specimen dimensions. Strain energy was defined as the work done to stretch the sample, calculated using the following formula(109,110):

$$\Psi = \int_1^{\lambda_1} \sigma_{11} d\lambda_1 + \int_1^{\lambda_2} \sigma_{22} d\lambda_2 \quad (1)$$

Where, σ is the Cauchy stress and λ is the stretch defined by the ratio of the current length, l , to the initial unstressed length, L , $\lambda = \frac{l}{L}$. Subscripts 1 and 2 refer to the circumferential and longitudinal directions, respectively.

Unless mentioned otherwise, data are shown as mean +/- standard error. For each group studied, five independent specimens were fabricated separately to define $n=5$ for all statistical analyses. Significance was determined using one way ANOVA with $\alpha=0.05$. Post-hoc testing was performed using the Holm-Bonferroni method.

2.3 RESULTS

No variations in electrospun scaffold processing studied in this work produced significant change in mass fraction of polymer within the constructs (**Table 2**). Increasing the translational speed above 0.3 cm/s while keeping all other variables constant appeared to produce a modest stiffening ($p < 0.001$) of the circumferential axis, perpendicular to the axis of raster (**Figure 3 A**).

Table 2. Polymer mass fraction in grams within each group

POLYMER MASS FRACTION IN EACH SCAFFOLD				
<i>Dry PEUU</i>			<i>Wet PEUU</i>	
Rastering Speed	0.3 cm/s	0.421+/- 0.011	0.3 cm/s	0.433 +/- 0.011
	1.5 cm/s	0.442 +/- 0.034	1.5 cm/s	0.451 +/- 0.014
	3.0 cm/s	0.383 +/- 0.023	3.0 cm/s	0.409 +/- 0.031
	30 cm/s	0.445 +/- 0.017	30 cm/s	0.379 +/- 0.005

Image analysis revealed a pronounced decrease in fiber intersections at translational speeds above 0.3 cm/s ($p < 0.01$) in a pattern reminiscent of the stiffening observed in the circumferential axis of the same constructs.

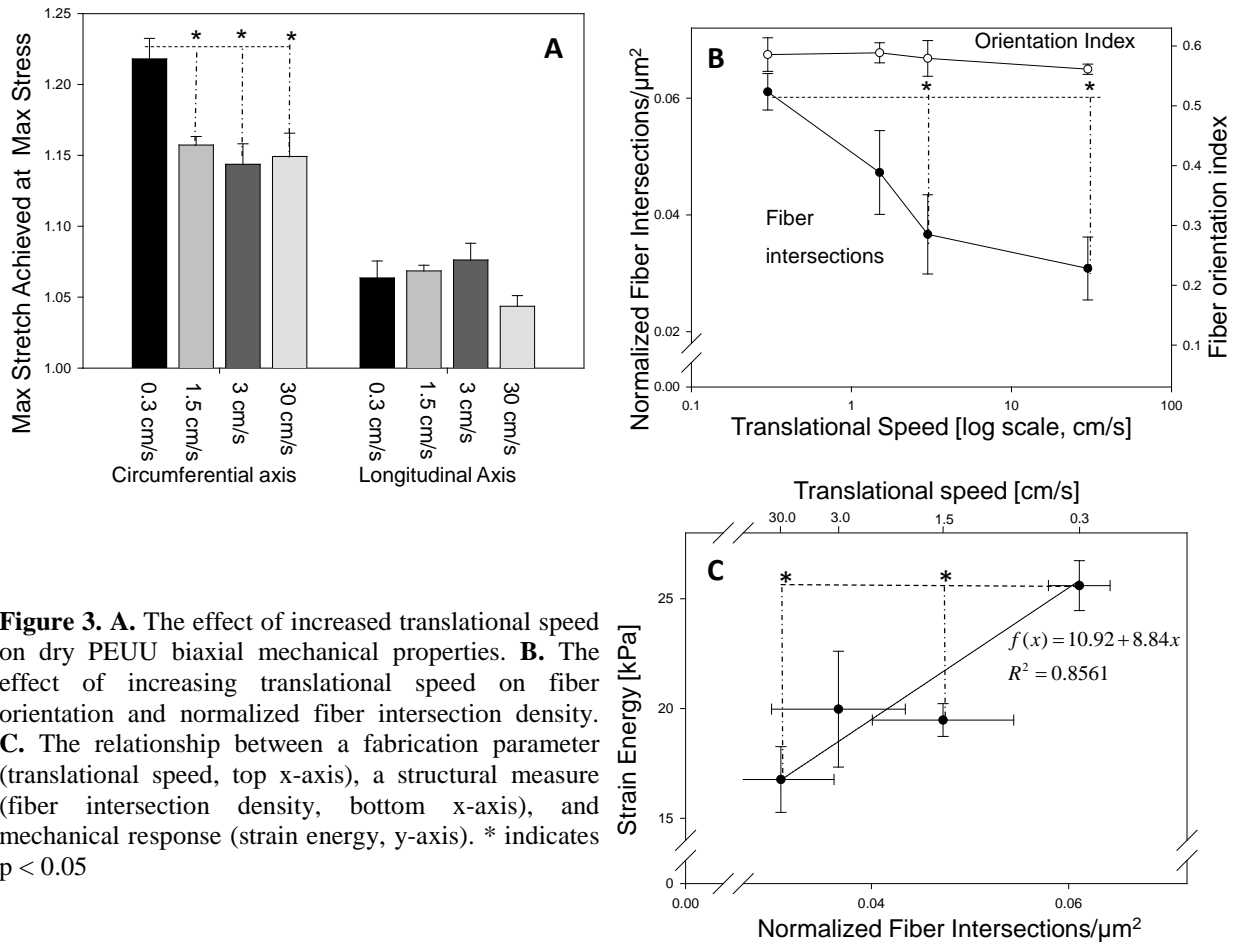


Figure 3. **A.** The effect of increased translational speed on dry PEUU biaxial mechanical properties. **B.** The effect of increasing translational speed on fiber orientation and normalized fiber intersection density. **C.** The relationship between a fabrication parameter (translational speed, top x-axis), a structural measure (fiber intersection density, bottom x-axis), and mechanical response (strain energy, y-axis). * indicates $p < 0.05$

This occurred without any significant change in the fiber orientation index (**Figure 3 B**). Consistently, higher strain energy was observed in specimens processed under lower translational speeds and, consequently, higher fiber intersection densities (**Figure 3 C**). None of the remaining architectural features (fiber angle distribution, connectivity, fiber diameter) identified by the image analysis algorithm demonstrated any recognizable pattern or significant differences between groups. The inclusion of cell culture medium into the construct resulted in a dramatic change in scaffold microarchitecture (**Figure 4 A,B**). Wet PEUU qualitatively appeared

to possess a greater degree of undulation, bundling, and looping that was less common in the ‘dry’ electrospun samples. Unlike dry electrospinning, structural analysis of these scaffolds demonstrated no significant difference in fiber intersection density over the translational speeds studied (**Figure 5** $p = 0.117$, 0.3 to 30 cm/s translated groups). Fiber orientation did not differ significantly from that found in dry PEUU. Faster translational speeds during fabrication were

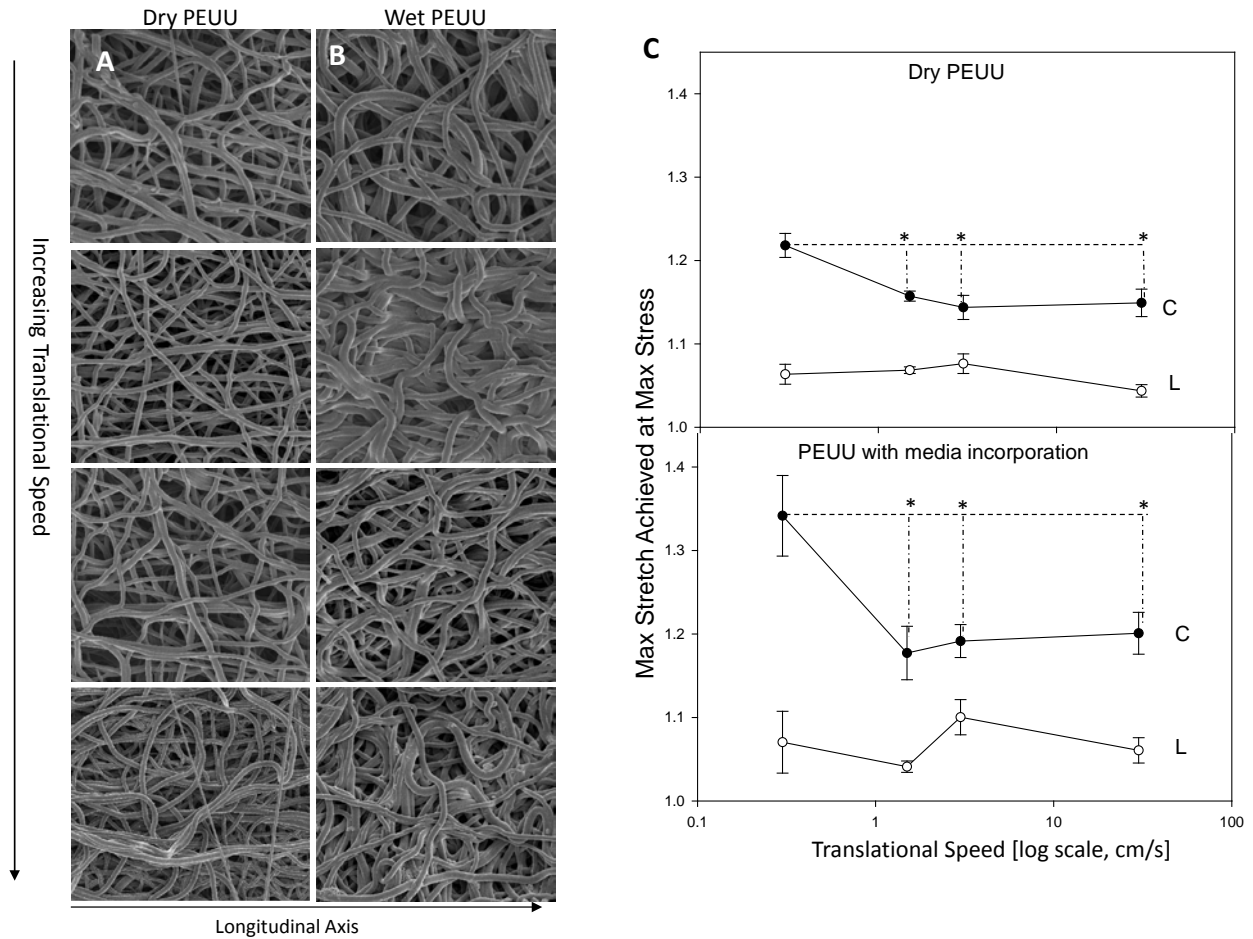


Figure 4. A,B. Qualitative depictions of fiber microarchitecture of both dry and wet PEUU scaffolds in descending order according to translational speed, with 0.3 cm/s on the top and 30 cm/s on the bottom. **C.** Comparison of the mechanical response of dry and wet PEUU across translational speeds. (C indicates the circumferential axis, whereas L indicates longitudinal axis) *indicates $p < 0.05$

associated with pronounced stiffening in the circumferential axis ($p < 0.001$) (**Figure 4 C**). Additionally, strain energies in this group did not differ significantly from those that characterized the dry PEUU groups ($p = 0.382$, **APPENDIX A**). It can also be observed that introduction of culture medium alone only affected the mechanical response of PEUU at the lowest translational speed studied ($p < 0.001$).

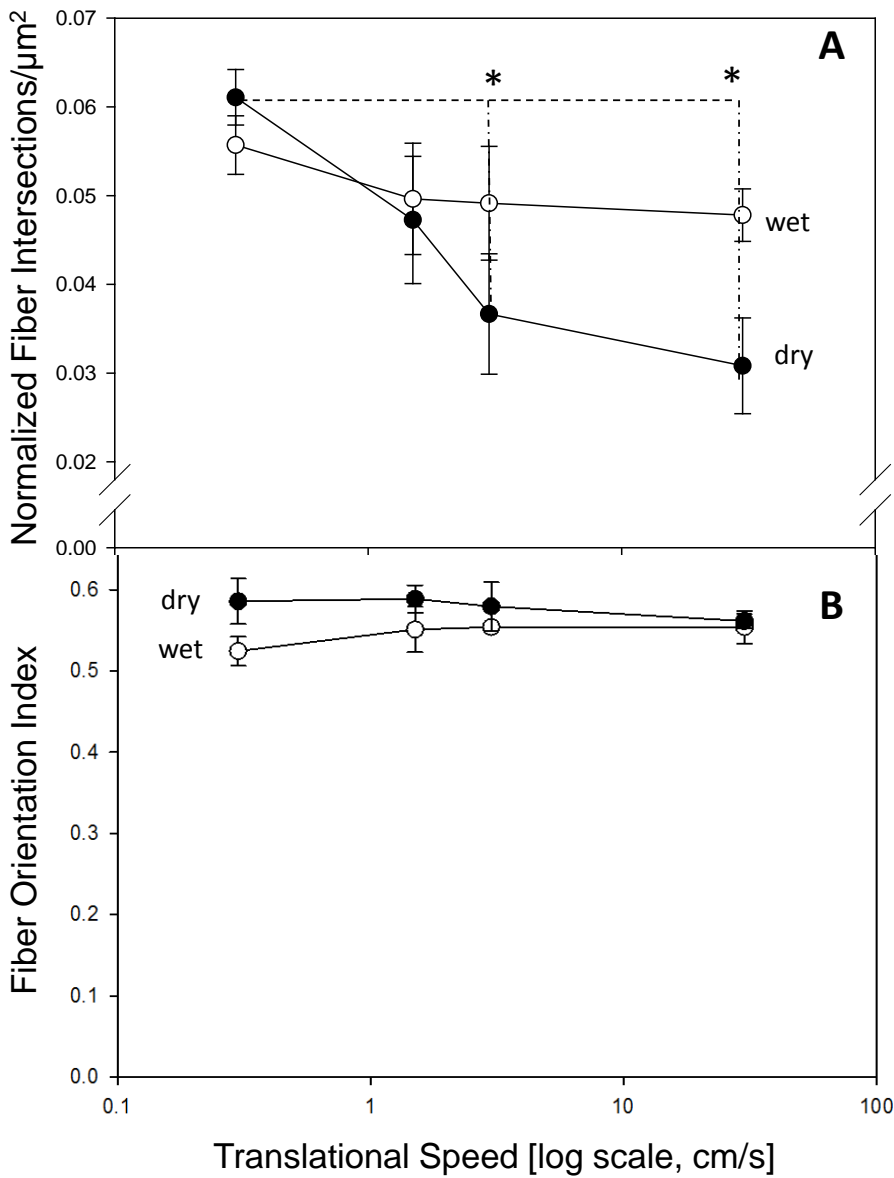


Figure 5. Comparison between 'wet' and 'dry' processed PEUU structural elements across translational speeds. **a.** Fiber intersection density, **b.** Fiber orientation index. * indicates $p < 0.05$

Inspection of SEM micrographs (**Figure 6**) demonstrated that smooth muscle cells or microspheres concurrently electrospayed into the PEUU scaffolds become an integral part of the fibrous network, in contact with multiple fibers. Interestingly, these particulates produced a significant increase in scaffold mechanical anisotropy beyond that found in either dry or wet PEUU at the same translational speed (**Figure 7**). This appears to be related to a stiffened longitudinal direction of the construct. In contrast, increasing the concentration of cells within the electrospay suspension did not affect the mechanical anisotropy, nor did replacing the cells with rigid polystyrene microspheres. No significant differences were observed between any micro-architectural parameters between microsphere integrated and wet PEUU. More importantly, it was shown that when cells are integrated into an electrospun construct in conjunction with the adoption of slow translational speed (0.3 cm/s) the resultant construct possesses a mechanical response that resembles highly anisotropic soft tissues (**Figure 7**).

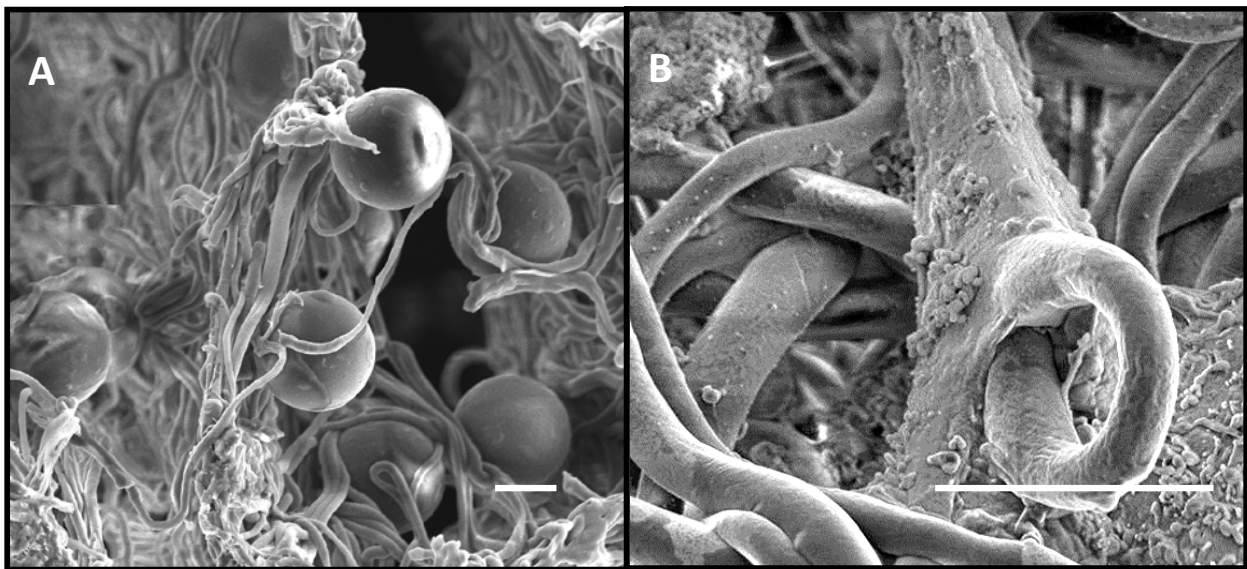


Figure 6 High resolution SEM micrographs depicting immediate microenvironment surrounding **A.** integrated microspheres and **B.** cells. Scale bar = 5 μ m

In the present study, we demonstrated that fiber topology and bulk mechanical response can be modulated by altering the net fiber interconnection densities without altering fiber alignment, achieved by translating the cylindrical collecting mandrel along its rotational axis at varying rates. It was further shown that constructs containing high densities of fiber interconnections were associated with higher strain energies and mechanical anisotropy. Fiber topology and bulk mechanical response were further altered through concurrent electrospaying of cell culture medium with or without living cells or rigid particulates during fabrication. It was discovered that a substantially higher degree of fiber intersections, but not fiber alignment, was associated with increased mechanical anisotropy and strain energy. Moreover, both fiber alignment and intersection density have fundamental implications for tailoring scaffold mechanical behavior and can be independently or synergistically applied to better approximate specific macro level native tissue mechanical responses. This knowledge provides additional levels of control at the fabrication level on micro-scale topology and macro-scale mechanical properties.

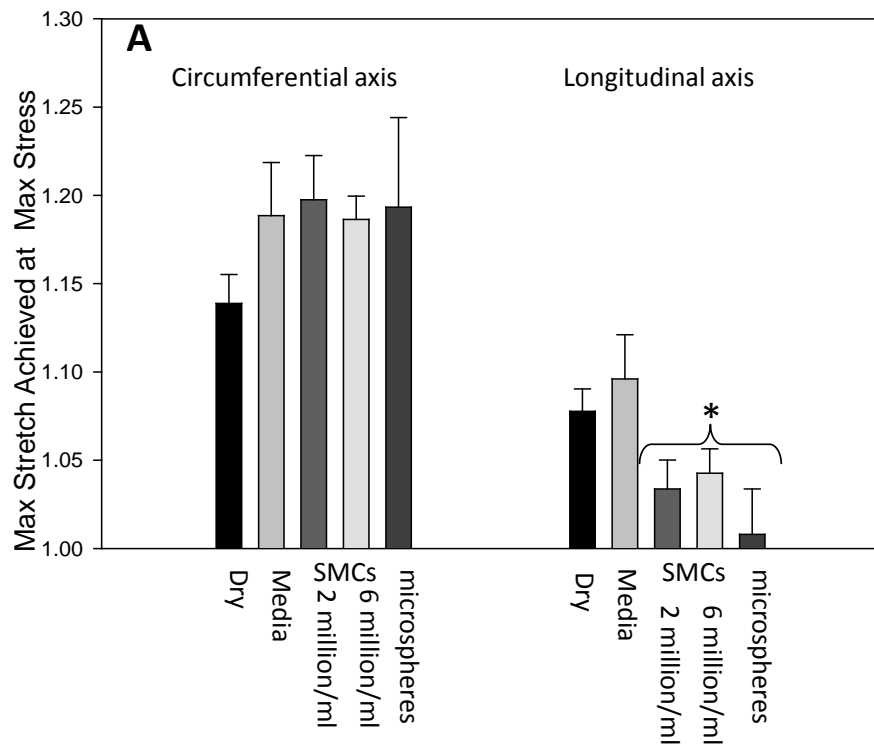
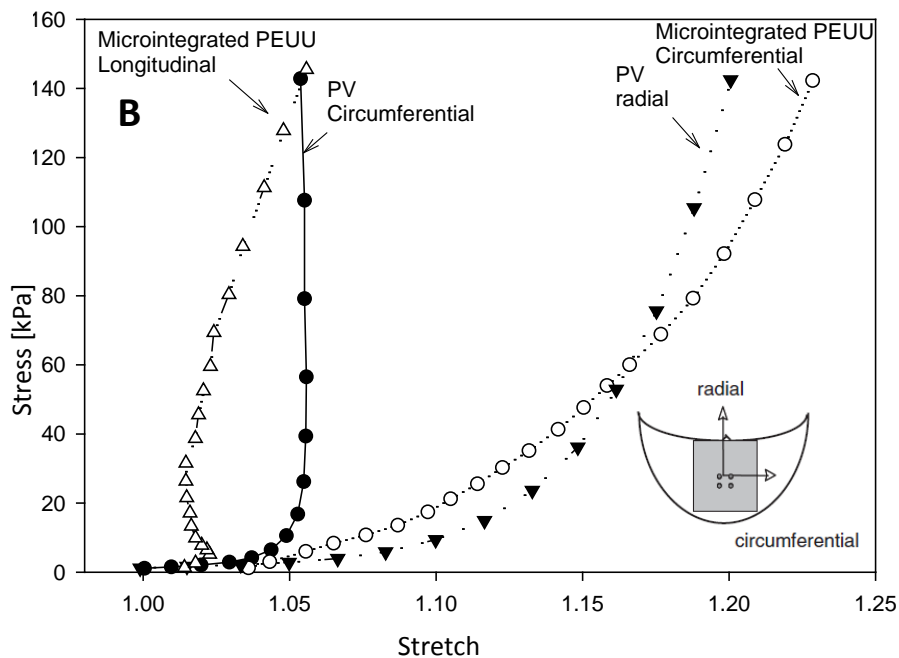


Figure 7. A. The change in biaxial mechanical response resultant from integrated particulates within PEUU fiber matrix. Translational speed during fabrication was 3.0 cm/s. * indicates statistically significant difference from both 'dry' and 'wet' groups. **B.** Combining slow translational speed with concurrent cell electrospaying produces a construct with mechanical anisotropy reminiscent of the native porcine pulmonary valve. (plots not significantly different from each other)



These studies were made largely possible due to the introduction of a new image analysis method for micro structural quantification. Current image processing techniques(68,75) can only quantify fiber angle distribution(s). In contrast, the importance of number and density of fiber intersections, network connectivity, and fiber diameter distributions on scaffold mechanical behavior has been discussed(111). While it was expected that an increase in translational speed would further orient the fibers due to physical motion of the mandrel, fiber alignment remained

consistent through an order of magnitude increase in translational speed despite a marked change in mechanical properties (**Figure 3**). Previous results(68) indicated that an alignment due to increased rotational velocity will stiffen the rotational axis, however this was not significant until the mandrel was rotated at a tangential speed higher than 2 m/s, a much faster rotational velocity than the one presented in this work. This finding suggests that fiber orientation alone does not adequately describe the mechanical response of these electrospun polyurethanes. An exponential decrease in fiber intersections was observed as translational speed was increased beyond 0.3 cm/s (**Figure 3 B**). This pattern is reminiscent of the change in circumferential axis compliance observed. Furthermore, fiber intersections were shown to be correlated with strain energy ($R^2=0.86$) (**Figure 3**). As all other structural parameters remained comparable (fiber diameter, connectivity, orientation index) across the translational speeds, it can be speculated that the fiber intersection density is related to and potentially responsible for the observed increase in mechanical anisotropy and strain energy, perhaps through directional restriction of fiber motion. The precise mechanism by which this effect occurs is currently unclear, and should be elucidated through structural deterministic modeling(111).

Concurrent electrospaying of cell culture medium onto the depositing scaffold during fabrication also induced a distinct change in scaffold microstructure. This is likely due to an aqueous layer that adhered to the forming scaffold as it rotated, delaying, but not preventing fiber bonding. It would follow that there would be more slack length, which would allow the additional, looping and undulation observed in SEM micrographs (**Figure 4**). At a translational speed of 0.3 cm/s, this leads to a more compliant mechanical response, however this appears to be overcome by increasing the translational speed. It follows logically that the increase in tortuosity might create artifactual fiber intersections at locations where fibers are not actually

securely bound together. This is admittedly a limitation with the current analysis, and has an implication in explaining the lack of definitive structural pattern with respect to translational speed in wet PEUU images while every mechanical trend observed in dry PEUU remains consistent.

When the electrosprayed medium is supplemented with particulates or cells, a distinct change occurs in the mechanical response of the scaffold. The microsphere size (10 μm) was chosen to be the same approximate physical size as the smooth muscle cells before they spread among the fibers. A consistent pattern of a stiffened longitudinal axis was observed in the mechanical response of particulate integrated constructs (**Figure 7 A**). A potential interpretation of this phenomenon is that particulates could serve as bridges connecting fibers to an extent beyond that which would be found with fiber intersections only. Following this assumption, particulates and cells would act as additional fiber bonding increasing the effective fiber intersection density and consequently raising the level of mechanical anisotropy. Additionally, previous work in structural modeling for valvular tissue(111) provides insights into the behavior of the longitudinal axis of these materials. Stella et al. observed that in anisotropic fibrous materials, biaxial mechanical loading can lead to micro-scale fiber rotations which, in turn, produce negative strain in the macro-scale response(111). This likely contributes to the phenomenon observed in this work and underscores the appropriateness of these scaffolds in the development of engineered heart valve tissues.

The complexity of electrospun scaffold morphology and the consequential difficulties in collecting quantitative structural information, particularly in wet processed PEUU, imply the clear need for additional studies aiming to consolidate the aforementioned hypothesis. Specifically in this context structural deterministic modeling represents an important approach in

future studies. Micro-meso architecture based mechanical models might, for instance, be adopted to investigate the influence of fiber intersection density on the material mechanical response.

While work in controlling bulk mechanical properties of electrospun scaffolds have focused on modifying fiber alignment through either electric field manipulation or high rotational velocities, the exact nature of the resulting fiber architectures and their relation to macroscopic mechanical behavior remain elusive. *The results of the present study indicate that fiber orientation alone does not adequately describe the mechanical response of elastomeric electrospun scaffolds.* Further, fiber alignment and intersection density can be controlled independently, allowing for an additional level of control on scaffold microstructure. Moreover, such control can be applied in conjunction with cell electrospaying to create highly anisotropic cellularized constructs without utilizing high rotational velocities, which are not amenable to the microintegration technique.⁽¹⁰²⁾ Mandrel translation was speculated to introduce macro-scale mechanical changes through modification of fiber intersection density. This method of scaffold fabrication was found to be nearly as effective in altering scaffold anisotropy as fiber alignment due to increasing tangential velocities. Practically, wet processing and mandrel translation can be successfully implemented as tools to reliably modify scaffold microarchitecture without altering fiber alignment.

3.0 MICROSTRUCTURE MANIPULATION TO TUNE BENDING STIFFNESS IN ELECTROSPUN SCAFFOLDS FOR HEART VALVE TISSUE ENGINEERING

This work has been adapted from the following previously published manuscript:

Amoroso NJ, D'Amore A, Hong Y, Rivera CP, Sacks MS, Wagner WR. Microstructural manipulation of electrospun scaffolds for specific bending stiffness for heart valve tissue engineering. *Acta Biomaterialia*. 2012;8(12):4268-77

3.1 INTRODUCTION

Flexural rigidity is a functional measure that quantifies a key aspect of a surgeon's perception regarding the appropriateness of a biomaterial for soft tissue repair. Beyond meeting perceived mechanical requirements prior to material implantation, the selection of a material with appropriate flexural rigidity is functionally important in avoiding a mechanical mismatch in situ, which could lead to patient discomfort, tissue damage, and a disruption of the desired healing process(112). In the specific case of heart valve tissue engineering, flexural properties are of paramount importance to achieving appropriate valve function(113–115). Surprisingly, however, scaffold flexural behavior is discussed least in the literature of the common mechanical responses.

The most common materials under development for the tissue engineering of heart valves include decellularized extracellular matrix (ECM) based scaffolds(116,117) and synthetic fibrous

scaffolds(118–120). Decellularized ECM scaffolds are typically sourced from human or xenograft valvular tissue(121,122) or small intestinal submucosa(123,124). However, decellularized, ECM-based scaffolds, depending upon the processing method employed, can be hindered by inconsistent performance in terms of their mechanics and local cytotoxicity due to residual processing agents(11)

Synthetic scaffolds have the advantage of consistent processing methodologies which can produce reliable and tunable mechanical properties and functional results. Varieties of non-woven fibrous scaffolds are commercially available and are typically based on polymers utilized in other devices that have obtained regulatory approval. Synthetic scaffolds can be seeded with cells(118–120) and have been shown to support host cell infiltration(108). However, many of the current materials used to produce such scaffolds have been limited by their high stiffness and lack of mechanical anisotropy, and thus fail to approximate native valvular tissue(68).

One method of producing non-woven fibrous scaffolds is electrospinning, which is notable for the ability to generate structural features on the nano to micro scale(46). Electrospun constructs are amenable to modification during, as well as following, fabrication to introduce functionality or modify microstructure and mechanical response. With respect to the latter, functional groups and peptides can be introduced onto electrospun fibers through common surface treatments(42) or by grafting them onto the polymer chain prior to solvent processing. Scaffold porosity and packing density can be altered by the introduction of a porogen such as salt crystals to create macro pores(31), laser ablation of scaffolds following fabrication(90), or concurrently electrospaying an aqueous medium to loosen interactions between polymer layers(11). It is further possible to alter electrospun scaffold microstructure in order to create anisotropy within the constructs. Fibers can be patterned(62) or aligned(68) to encourage contact

guidance of seeded cells(42) and produce tunable tensile mechanical anisotropy(68). While such structural manipulations have been employed to alter the mechanical behavior of electrospun scaffolds under tension, a reliable method of controlling the inherent bending modulus would be desirable to provide a more complete approach to meeting design objectives for soft tissue constructs.

The objective of this report was to examine specific microstructural features important to determining the flexural behavior of electrospun scaffolds suitable for heart valve tissue engineering. Methods are highlighted for tuning the flexural response by modifying fabrication parameters, or by introducing secondary fiber populations that may have a higher modulus or be selectively dissolved from the scaffold following fabrication. The effect of such construct modifications on in-plane tensile properties is also demonstrated, and effort was made to mimic the mechanical properties of a native pulmonary valve in both flexural and equi-biaxial tensile response.

3.2 MATERIALS AND METHODS

3.2.1 Scaffold Fabrication

Poly(ester urethane) urea (PEUU) was synthesized as described previously in Chapter 2. Scaffolds were fabricated in a manner similar to Chapter 2 with some modifications. Briefly, PEUU was dissolved in 1,1,1,3,3,3-hexafluoroisopropanol (HFIP) at a concentration of 12% (w/v) and electrospun onto a rotating and translating stainless steel mandrel (6 mm diameter) by feeding through a charged capillary (1.19 mm I.D.) at 1.5 mL/hr. The mandrel was located 17 cm

from the tip of the capillary and grounded with a voltage of -5 kV. The polymer feeding tube was charged to 12 kV. The mandrel was rotated with a tangential speed of 8 cm/s and translated along its axis at either 0.3, 1.5, 3.0, or 30.0 cm/s. (**Figure 8 A**)

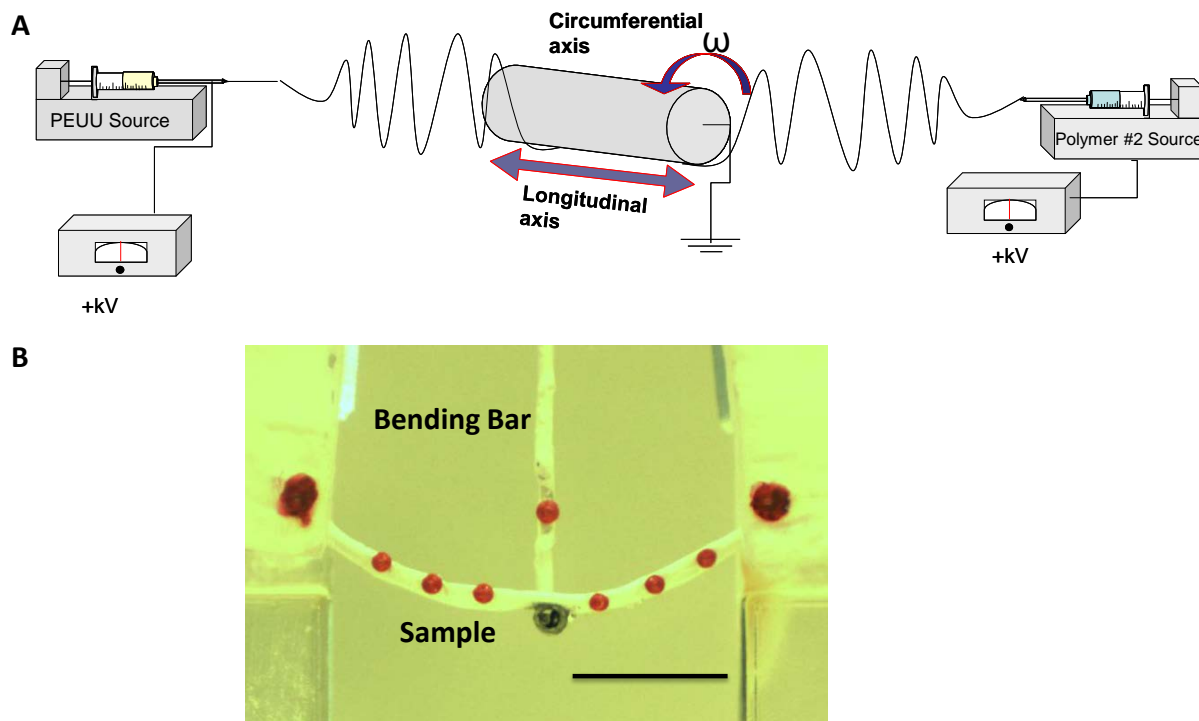


Figure 8. A. Schematic of electrospinning apparatus for two-component scaffolds. PEUU was fed from the same location for every group. The mandrel was rotated and translated along its longitudinal axis at varying speeds. Secondary polymer fibers were introduced through separate nozzles. **B.** Image of a polymeric specimen loaded in the bending device (scale bar = 1 cm)

Scaffolds were electrospun from PEUU in HFIP alone, or concurrently with a secondary polymer stream being fed from a capillary mounted in a separate location. Polycaprolactone (PCL, Sigma, Mn = 80,000 kDa) dissolved in HFIP (8% w/v) was electrospun from a capillary in a 180° opposing orientation from PEUU, at volume flow ratios of 100:0, 75:25, 50:50, 25:75, and 0:100 PEUU:PCL. In separate experiments, poly(ethylene) oxide (PEO) (Mv = 200 kDa) in cell culture medium (DMEM, 10% FBS, 5% penicillin/streptomycin) was electrospun from a perpendicular orientation to PEUU in volume flow ratios of 100:0, 85:15, 75:25, and 50:50

PEUU:PEO. Following fabrication, PEO-incorporated scaffolds were placed in distilled water for at least four hours, changing the water once, in order to dissolve the PEO fibers and to leach PEO out of the scaffold matrix. Scaffolds made from 25:75 PEUU:PEO did not maintain structural integrity following PEO fiber removal, and were therefore not included in the study. All mechanical characterizations PEUU:PEO blended constructs were completed following dissolution of the sacrificial fibers. All experimental groups were fabricated with a minimum sample number of $n = 5$ independently processed scaffolds.

3.2.2 Imaging and Structural Analysis

Scaffold microstructure for all constructs was determined through scanning electron microscopy (SEM, JEOL JSM6330F) after gold sputter coating. The resultant images were analyzed using an automated algorithm to provide quantitative comparisons of the following microstructural features: fiber diameter, orientation index (alignment angle distribution), and intersection density. This algorithm is designed to limit analysis to the surface fibers of the scaffold in order to minimize the recognition of fiber intersections when two fibers are not in contact(48). Fiber intersection density was normalized to fiber diameter for comparisons as previously presented [Chapter 2]. The distribution and morphology of distinct fiber populations in multi-polymer constructs was visualized by adding fluorescein isothiocyanate isomer I (0.001%, Fluka BioChemika) to the PEUU solution prior to electrospinning and Rhodamine 101 (0.001%, Fluka BioChemika) to the PEO or PCL solution prior to electrospinning thin mats of only several fiber layers thick. These constructs were imaged under fluorescent microscopy (Olympus 1X71).

3.2.3 Mechanical Testing

3.2.3.1 Uniaxial Mechanical Testing

Constructs previously immersed in distilled water were sectioned for uniaxial mechanical testing using a dog-bone shaped punch (Ray-Ran Testing Equipment) and tested with an MTS Tytron 250 MicroForce Testing Workstation at a 25 mm/min crosshead speed according to ASTM D638-98. Mechanical testing of PEUU/PEO blended scaffolds was performed following PEO dissolution. Sections were cut from each specimen so that the long axis being tested was consistent with the longitudinal axis of the mandrel.

3.2.3.2 Suture Retention Strength

Suture retention testing was performed according to American National Standard Institute Association for the Advancement of Medical Instruments (ANSI/ AAMI) VP20 standards. Briefly using 5 mm x 15 mm strips of each scaffold were sectioned so that the long axis matched with the longitudinal axis of the mandrel. A single loop of 4-0 braided polyester suture (Syneture) was placed in each section with a 2 mm bite. The suture was then pulled at 120 mm/min using the same MTS Tytron 250 MicroForce Testing Workstation as above. Suture retention strength was defined as the peak load before pullout/(suture diameter x sample thickness).

3.2.3.3 Biaxial Mechanical Testing

For biaxial mechanical testing, 10x10 mm sections were removed from each construct type. Polypropylene suture (Ethicon) was cut to form four small markers of ~1 mm diameter which were affixed to form a square in the central region of each specimen. Samples were then floated

in a room temperature physiological saline bath and subjected to a Lagrangian membrane tension (**T**) controlled protocol as previously described. Equi-biaxial tension was applied up to a maximum of 90 N/m to facilitate comparison with previous studies on valvular tissues. Data post-processing was completed using a preconditioned free-float reference, and was converted to stresses using measured specimen dimensions.

3.2.3.4 Flexural Mechanical Testing

Flexural mechanical testing was performed as previously described. Briefly, sections measuring 12x3 mm were removed from each electrospun construct and reserved for flexural testing. Sections were dried and 6 markers were affixed at even spacing along the edge of each specimen. Samples were immersed in a room temperature saline bath and mounted in a custom made holder. (**Figure 8 B**) The holder and bath were then raised and lowered with respect to a vertical loading bar which measured bending moment (**M**) up to a maximum sample curvature of $\Delta\kappa = 0.15 - 0.25 \text{ mm}^{-1}$, comparable to the maximum curvature experienced by functioning pericardial bioprosthetic heart valve leaflets and reported in previous work involving valvular biomaterials. Specimen dimensions were recorded automatically through imaging software, and used to calculate the second moment of area (**I**). The effective bending modulus (**E**) was calculated using the Bernoulli–Euler moment-curvature equation.

$$M = EI\Delta\kappa$$

3.2.4 Statistical Analyses

Statistical significance was determined using One Way Analysis of Variance with the Holm-Sidak method for post-hoc pairwise comparisons. Correlation coefficients were determined using Pearson's product moment correlation.

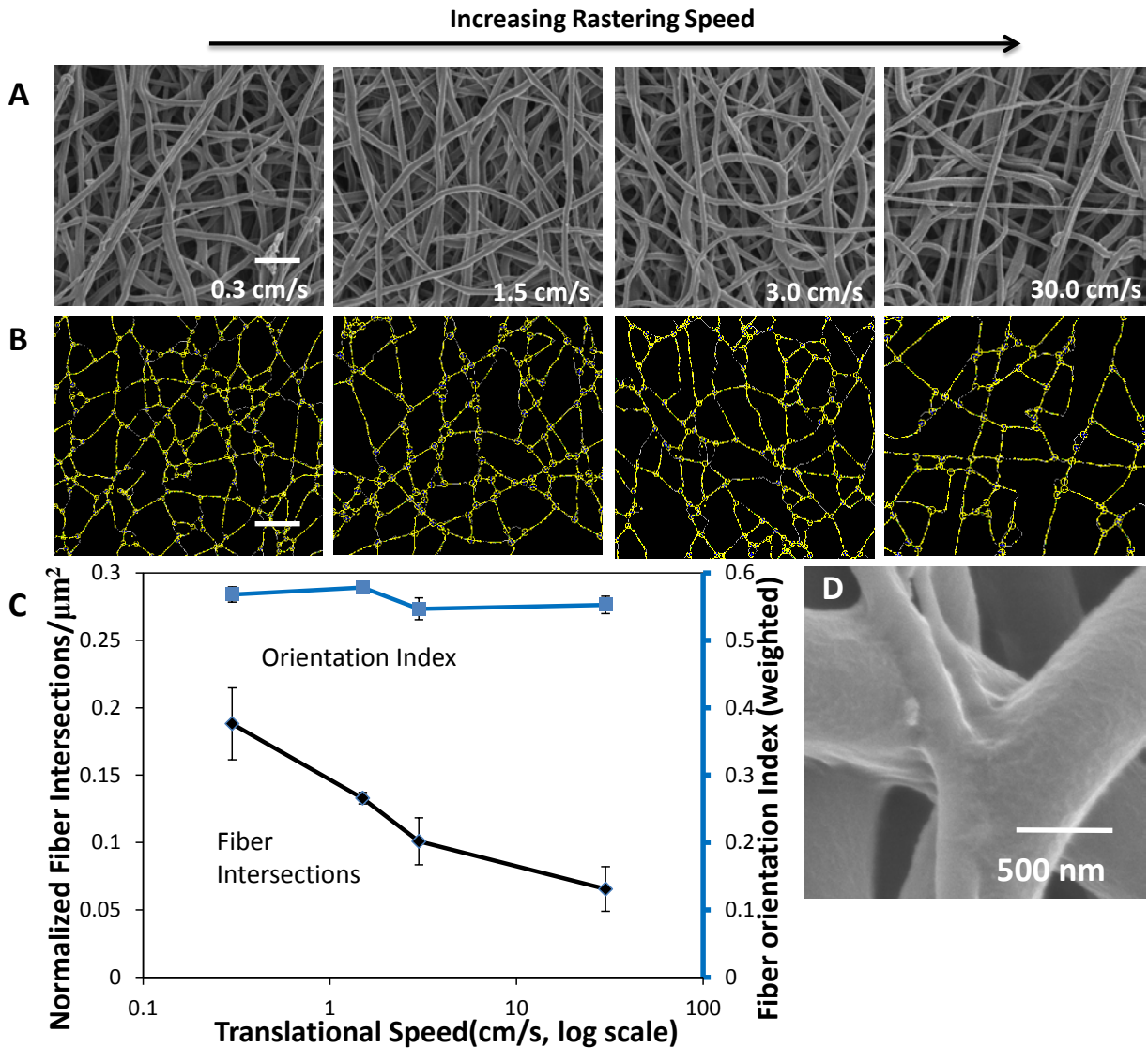


Figure 9. **A.** SEM micrographs of representative scaffolds from each translated group (Scale bar = 5 microns) and **B.** the corresponding digitized structure. **C.** A plot depicting the quantitative relationship between translational speed during fabrication and microstructural elements. **D.** High magnification morphology of a fiber intersection

3.3 RESULTS

3.3.1 Effect of Mandrel Translation on Dry PEUU

Altering the translational speed of the reciprocating target mandrel during electrospinning produced consistent microstructural and functional changes. These changes were subtle and not readily discernible by visual inspection of micrographs. (**Figure 9 A**) Structural analysis uncovered a trend relating increased mandrel translational speed during fabrication to a decrease in fiber intersection density of the electrospun scaffolds without change in any other structural measure evaluated. (**Figure 9 B,C**) Fiber diameters were not found to be significantly different between groups. (**APPENDIX B**) High resolution inspection of these fiber intersections demonstrated that fibers appear to be partially melded together at their interface. (**Figure 9 D**) Under further evaluation, fiber intersection density was found to be strongly inversely correlated ($R = -1.00$, $p < 0.001$) with a decrease in flexural modulus (**Figure 10 A**). No statistically significant differences were observed in initial uniaxial tensile moduli or suture retention strength for these constructs (**Figure 10 B,C**). Further, no significant differences were observed in the ultimate tensile strength or elongation at failure between the constructs generated at different translational speeds. (**APPENDIX C**)

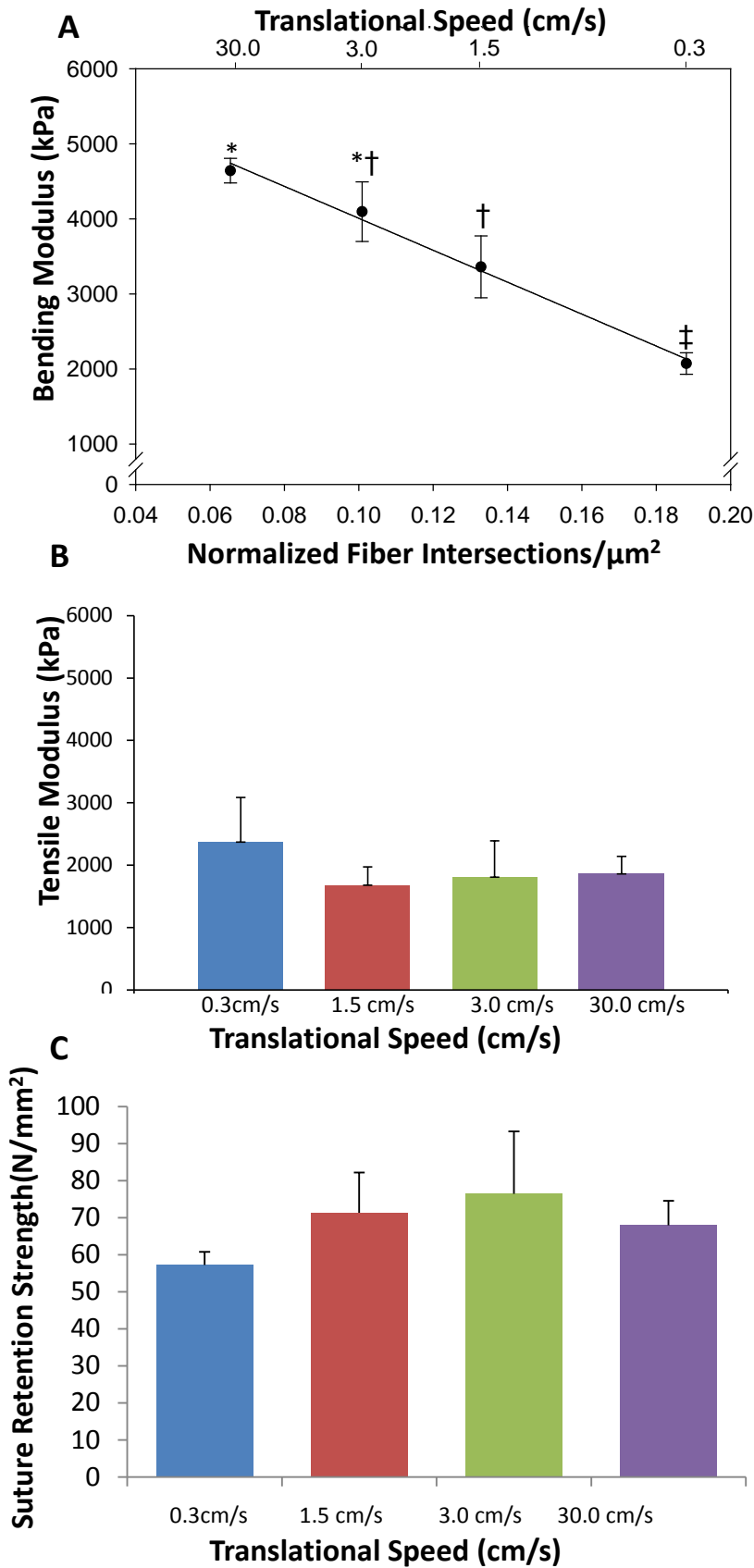


Figure 10. **A.** The relationship between translational velocity during fabrication (top x axis), fiber intersection density (bottom x axis), and bending modulus (y axis). **B.** Uniaxial tensile modulus of electrospun scaffolds fabricated under different translational velocities. **C.** Suture retention strengths of scaffolds fabricated under different translational velocities. Groups with different symbols (*, †, ‡) are significantly different from each other ($p < 0.05$)

3.3.2 Effect of Secondary Fiber Populations

Secondary fiber populations were introduced during construct fabrication to form uniform mixed fiber constructs of varying polymer ratios. Fluorescent dyes mixed with each polymer solution enabled visualization of independent fiber populations under confocal microscopy. Each fiber population appeared randomly distributed throughout each scaffold, and volume fractions of each polymer qualitatively matched that of the feed ratio used during fabrication. (**Figure 11 A**) SEM micrographs qualitatively depict a greater range of fiber diameters present within the constructs, however the fiber types cannot be differentiated under this imaging modality. (**Figure 11 B**) Structural analysis demonstrated that intersection density tended to increase with higher quantities of PCL (**Figure 11 C**).

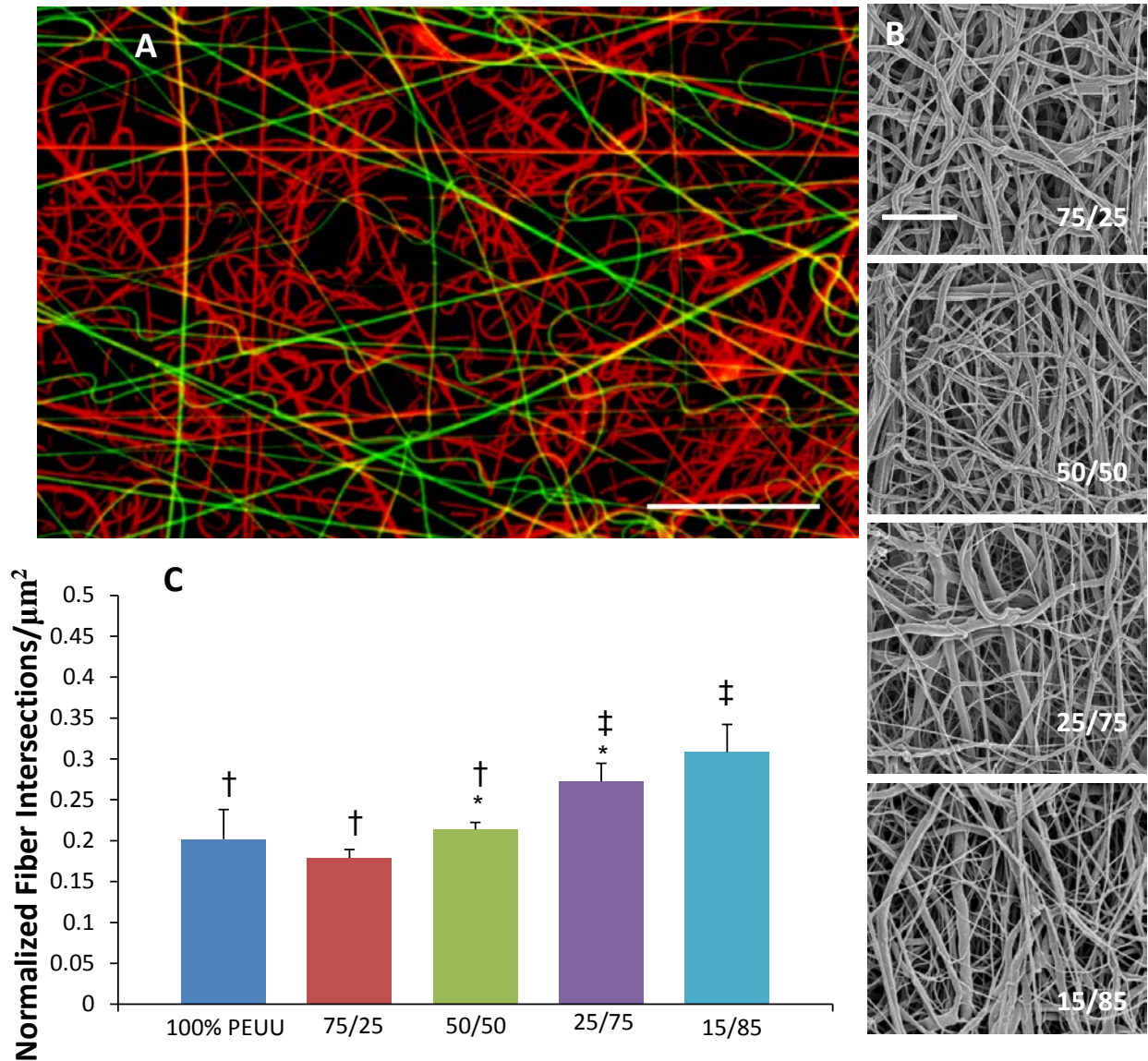


Figure 11. **A.** Fluorescent micrograph qualitatively depicting relative distribution of PEUU fibers (green) to PCL fibers (Red) in a 25/75 volume flow rate ratio construct. Scale bar = 20 microns **B.** Corresponding SEM micrographs representing each PEUU/PCL construct group. **C.** Change in fiber intersection density observed between PEUU/PCL ratios. No other differences in microstructural features were observed. Groups with different symbols (*, †, ‡) are significantly different from each other ($p < 0.05$)

Adding an increasing volume fraction of PCL fibers within the construct increased the tensile modulus under uniaxial load. (**Figure 12 A**) Under equal biaxial tension, all constructs containing PCL fibers were observed to be significantly ($p < 0.001$) stiffer and isotropic than unmodified PEUU fabricated under similar conditions. (**Figure 12 B**) No additional stiffening

was observed under biaxial tension at PCL concentrations above 25%. The addition of PCL fibers into PEUU scaffolds produced a significant increase in bending modulus. Fractional changes in the PEUU:PCL flow rate ratio resulted in changes to the observed bending moduli, with constructs containing the most PCL being more rigid in bending, while those with more PEUU remaining less stiff. The inclusion of any quantity of PCL fibers studied resulted in a significantly higher bending modulus than for simple PEUU scaffolds. (**Figure 13**)

Concurrent PEO and PEUU electrospinning produced constructs with fiber populations that appeared to be distinguishable by their diameters. Upon contact with water, constructs containing 75 and 50% PEO macroscopically contracted and curled slightly. No macroscopic changes were readily observed with constructs originally containing 15% PEO following water contact. The putatively smaller PEO fibers dissolved immediately upon contact with water, leaving PEUU fibers intact, but causing a distinct microstructural change. No changes in fiber morphology were appreciated following longer periods of water contact (**Figure 14 A,B**). Fiber intersection density within constructs that initially contained PEO fibers was higher following PEO dissolution than that found in similarly fabricated PEUU scaffolds without PEO fibers (**Figure 14 C**).

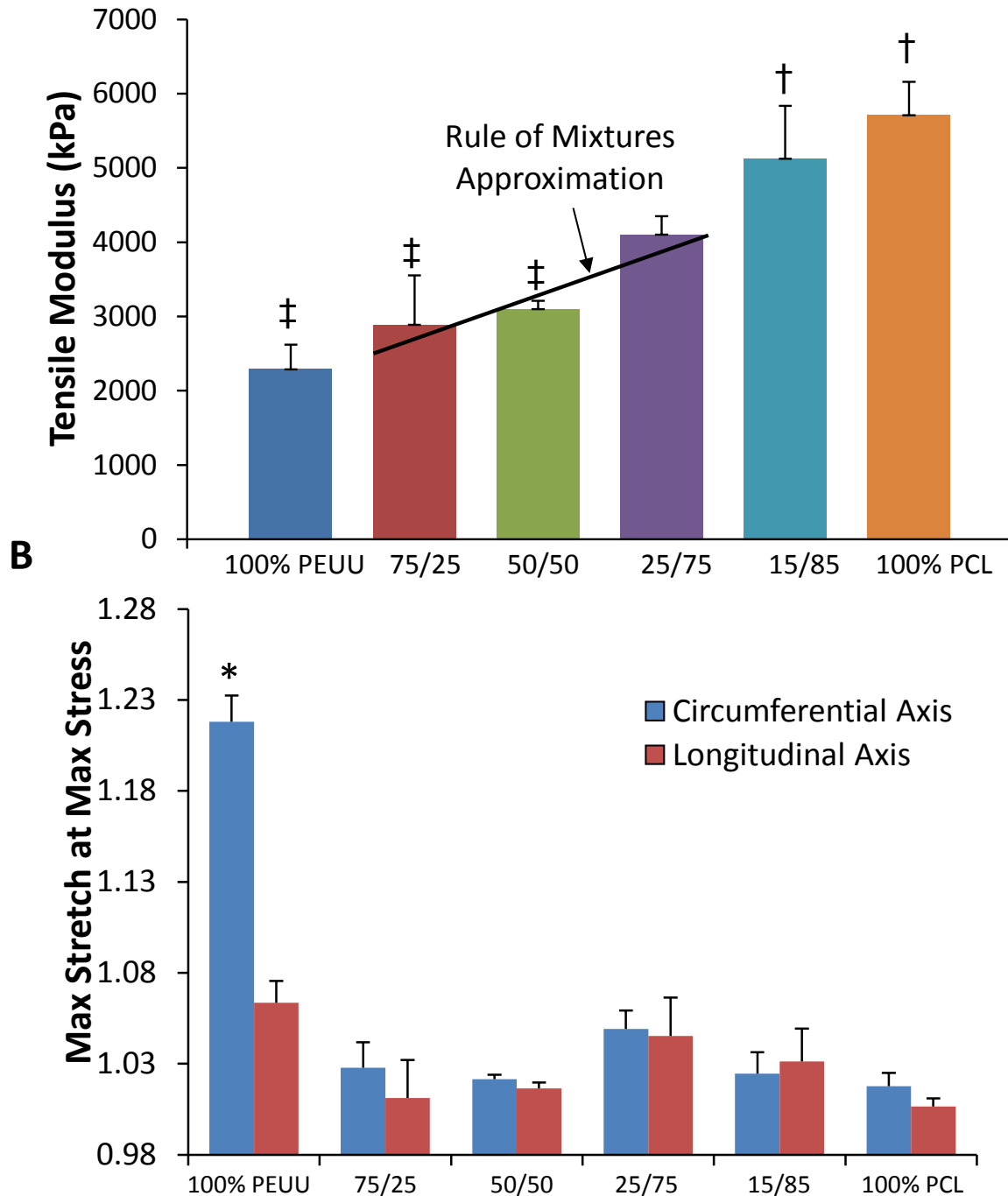


Figure 12. A. Uniaxial tensile mechanical response of constructs containing increasing quantities of PCL fibers. **B.** Planar biaxial mechanical properties of PEUU:PCL blended scaffolds Groups with different symbols (‡,†,*) are significantly different from one another ($p < 0.05$)

Qualitative assessment of scaffolds with dissolved PEO fiber populations found that these materials were more malleable than those made from PEUU alone. Constructs that initially contained 75% PEO did not maintain mechanical integrity following immersion in water, and

were not further evaluated. Higher volume fractions of sacrificial fibers within the PEUU based scaffolds were associated with decreasing uniaxial tensile moduli ($p < 0.05$) following fiber removal. (**Figure 15 A**) However, this did not appear to alter the suture retention strength of these constructs. (**Figure 15 B**) Additionally, no significant difference was observed between any PEO blended scaffold and pure electrospun PEUU under equal biaxial tension. (**Figure 15 C**) Scaffolds containing increasing initial amounts of PEO had a diminishing capacity to support their own weight when suspended as a cantilever following immersion in water (**Figure 16 A, Video 1**). This general phenomenon was shown quantitatively by the relationship between increasing quantities of sacrificial fibers and progressively lower flexural moduli following submersion in water. ($p < 0.05$, **Figure 16 B**) Scaffolds containing 50% PEO had a flexural modulus, that was statistically higher than that of the native pulmonary valve, but which was of the same order of magnitude.

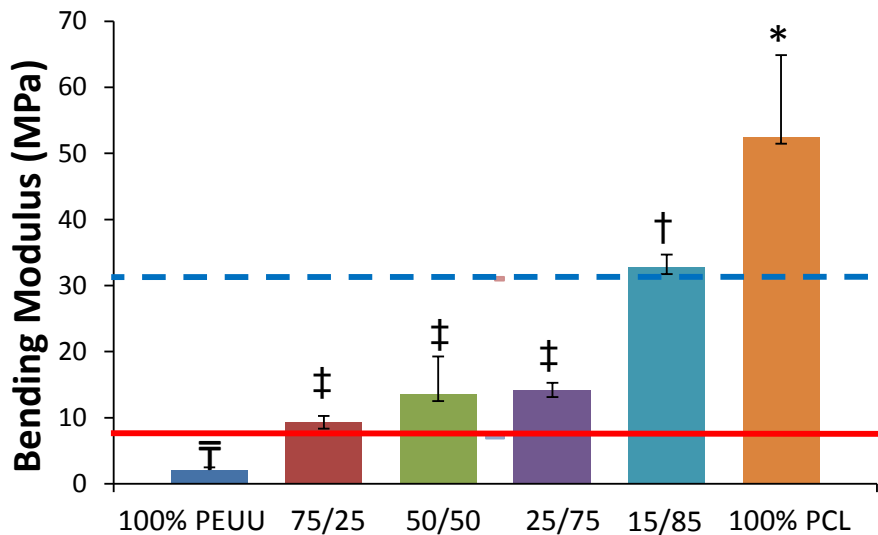


Figure 13. Bending modulus of mixed polymer constructs at varying ratios of PEUU:PCL. Red solid reference line indicates the bending modulus of native costal cartilage [123]. Blue dashed reference line indicates the bending modulus of intact septal cartilage [124]. Groups with different symbols (†, †, †, †, *) are significantly different from one another ($p < 0.05$).

3.4 DISCUSSION

How a biomaterial scaffold responds to physiologic loading is of critical importance to any tissue engineering application, and is of particular importance when seeking to reproduce the function of a cardiac valve. Materials utilized for valvular replacement will be subjected to cyclic forces up to 400-600 kPa thousands of times per day, every day. For a biomimetic valvular replacement to function successfully, it must not succumb to mechanical fatigue and be capable of passively stretching in the radial direction, while also remaining unyielding in the circumferential direction under such forces. Further, for natural leaflet movement, valvular materials must flex easily during normal function.

It is well established that electrospinning can be used to produce fibrous scaffolds with high levels of structural and mechanical anisotropy. During fabrication, fibers can be aligned through electrostatic or physical manipulation. It has been shown that when such scaffolds are comprised of compliant elastomers, the biaxial mechanical response can be designed to closely mimic that found in the native heart valve leaflet under physiologic loads(68). Chapter 2 has demonstrated that changes in the density of fiber intersections can be brought on without altering fiber orientation by introducing and varying the translational speed of the collecting mandrel during fabrication. In this manner, fiber orientation index and intersection density could be decoupled with orientation being controlled by mandrel rotation and intersection density by mandrel translation. This was possibly enabled by slow motion of the mandrel surface both in rotation and translation which could permit rapidly whipping fibers to deposit on top of one another more closely. A faster translational speed might create a more open structure. These subtle structural changes were also associated with changes in planar biaxial mechanical

response. However, to date reports seeking to understand the relationship between electrospun scaffold morphology and flexural properties have been lacking.

In the present chapter, the major experimental finding was a strong inverse correlation between fiber intersection density and bending modulus within electrospun polyurethanes. This suggests a functional relationship between network intersection density and flexural mechanical response. This phenomenon presents an apparent contradiction, as higher cross-link densities would generally be thought to result in stiffer mechanical behavior. In speculating as to what might cause this effect, it is noted that the whipping and pulling motion of the electrospinning process introduces crystallinity into the individual polymeric fibers. High magnification micrographs of fiber intersections demonstrate that fibers undergo some degree of melding at each intersection. (**Figure 9 D**) These interaction points might serve to locally disrupt the crystalline structure within the respective fibers. If this were the case, a local amorphous region might function as a hinge point that facilitates bending on a micro-scale. The additive combination of these weak points could translate into a lower bulk bending modulus. Such a hypothesis remains to be explored. It may be possible to examine the local crystallinity at fiber intersections using selected area electron diffraction or a similar technique.

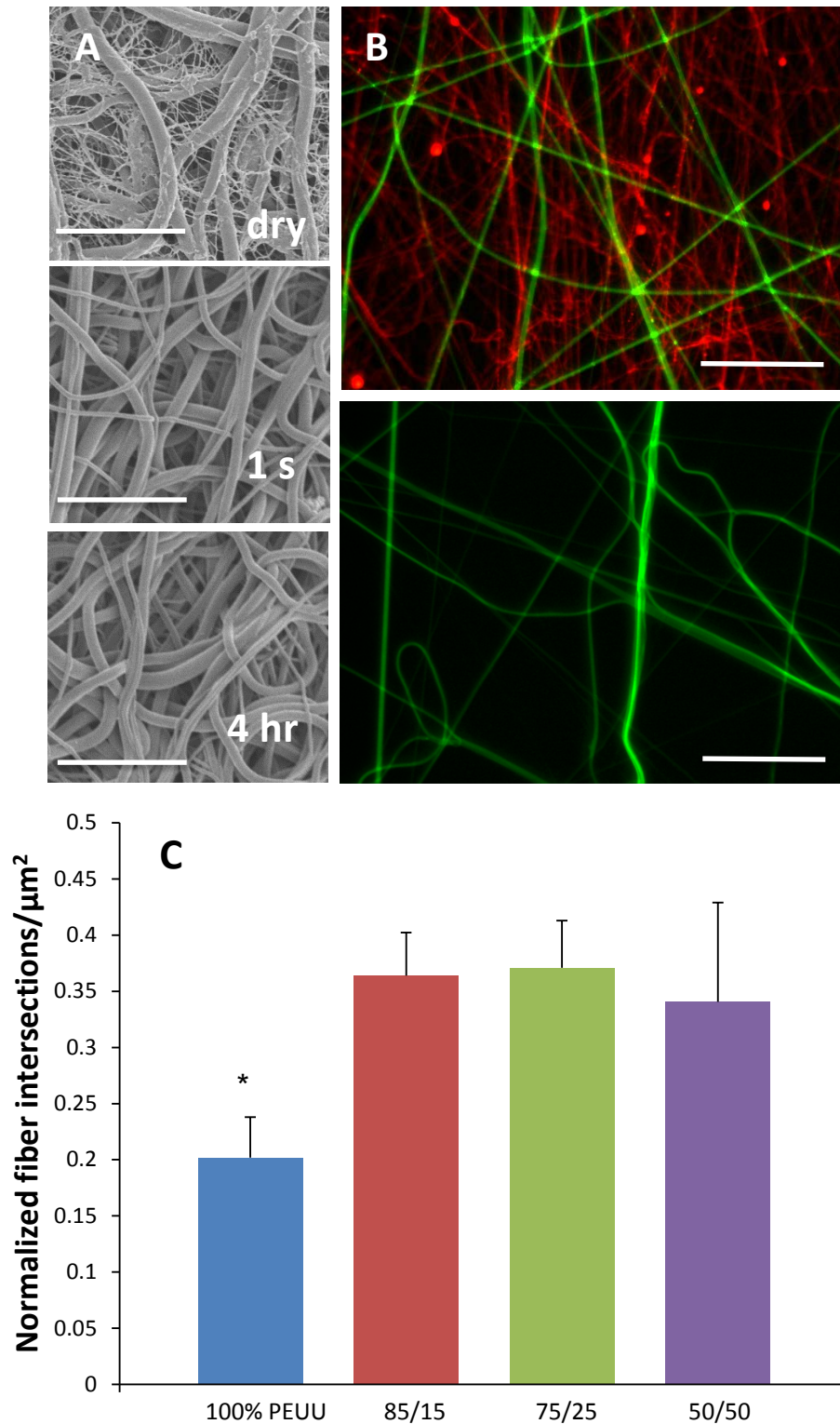


Figure 14. **A.** Representative structural images of PEUU/PEO 75/25 scaffolds as spun (dry), after 1 second (1s), and after 4 hours of soaking in water (4 hr). (Scale bar =10 microns. **B.** Fluorescent micrographs of PEUU (green)/PEO (red) blended constructs before (above) and after (below) treatment with water. Scale bar = 20 microns) **C.** Difference in normalized fiber intersection density between as spun 100% PEUU constructs and constructs following removal of PEO fibers *indicates $p < 0.05$

The potential to tune scaffold bending modulus was expanded upon by exploring the introduction of secondary fiber populations. PCL fibers were included within the PEUU fiber matrix as a means of mechanical reinforcement. Adding increasing volume fractions of PCL

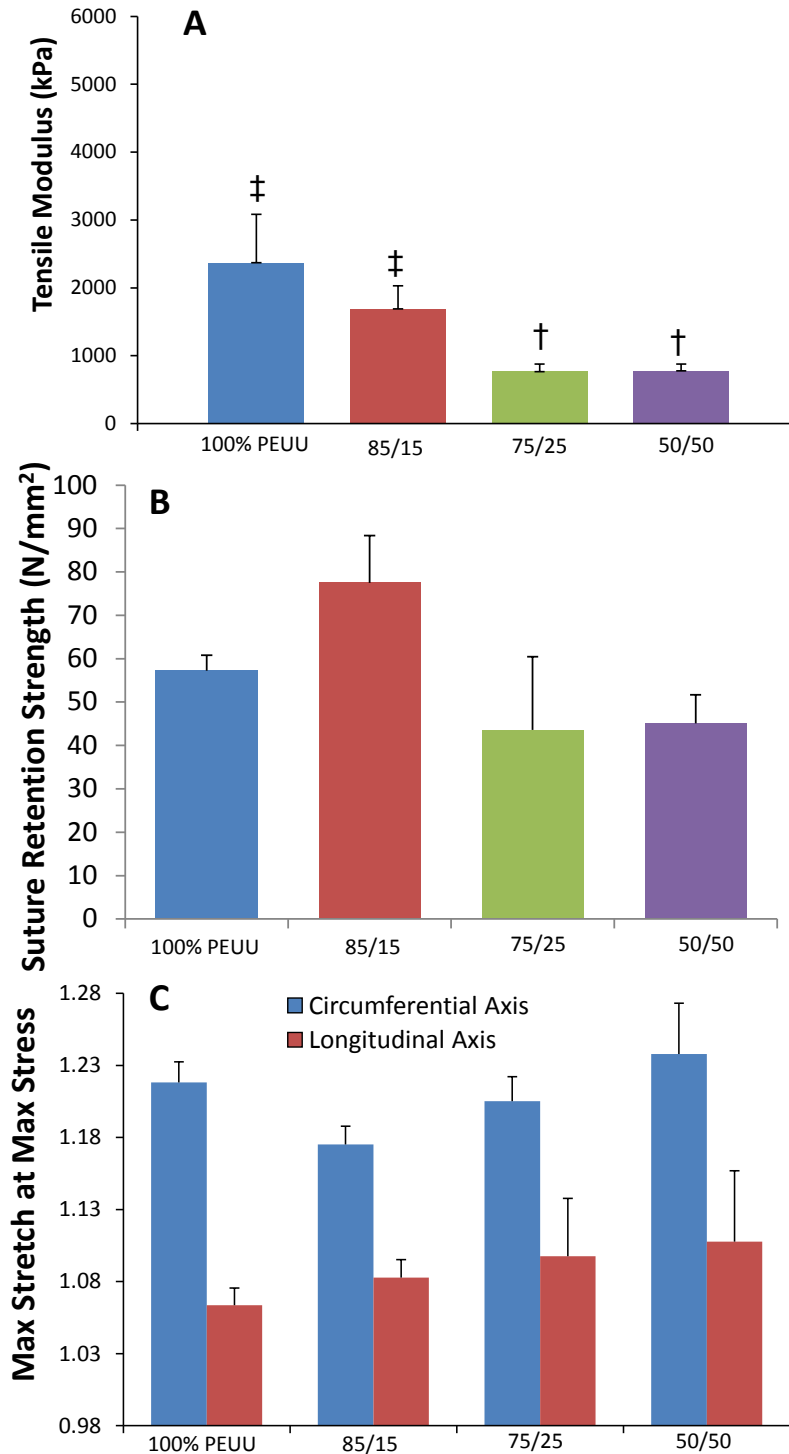


Figure 15. A. Tensile modulus of constructs containing varying quantities of PEO following contact with water. **B.** Suture retention strength of constructs following PEO fiber removal. **C.** Biaxial mechanical response of constructs following PEO fiber removal. Groups with different symbols (‡, †) are significantly different from one another. ($p < 0.05$)

fibers was found to increase tensile modulus under uniaxial tensile load. This was in approximate agreement with the rule of mixtures for non-unidirectional fiber reinforcement. However, no tunable response in stiffness was observed under equi-biaxial tension, as even a small quantity of PCL produced constructs with markedly reduced compliance. One possible explanation for such disparity between uniaxial and biaxial responses is that PCL fibers were able to rotate during uniaxial loading, whereas this deformation was restricted under planar biaxial loading. Structurally, such scaffolds were found to possess larger densities of fiber intersections with increased PCL. This may be due to the secondary fiber source producing fibers independently from the PEUU fiber source. A larger quantity of deposited fibers in a given area would logically increase the density of intersections within a construct. As expected, increased quantities of the much stiffer PCL produced scaffolds with larger bending moduli. Through this method, it was possible to produce constructs with bending moduli comparable to more rigid tissues such as costal cartilage and intact septal cartilage(93,125).

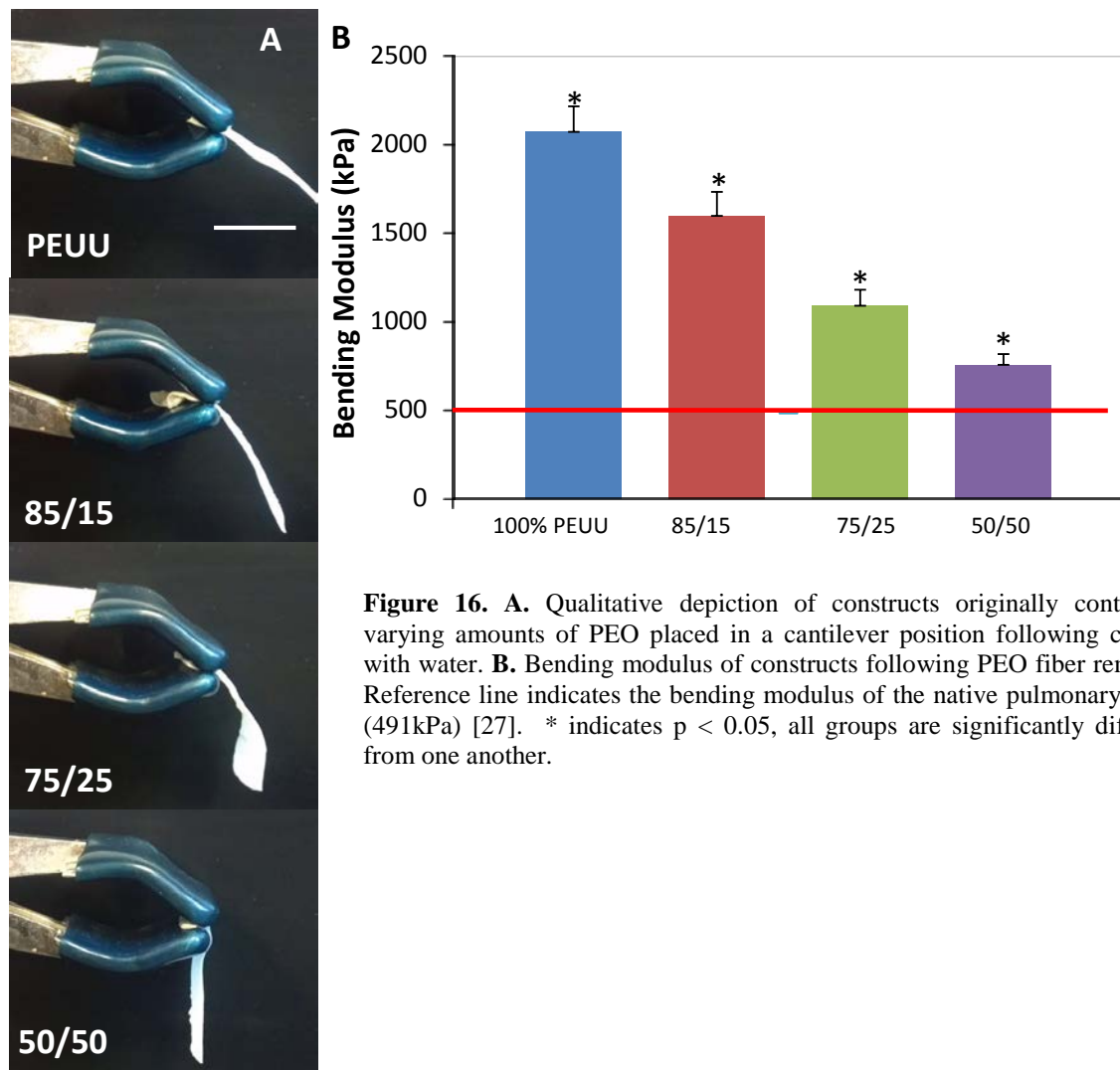


Figure 16. **A.** Qualitative depiction of constructs originally containing varying amounts of PEO placed in a cantilever position following contact with water. **B.** Bending modulus of constructs following PEO fiber removal. Reference line indicates the bending modulus of the native pulmonary valve (491kPa) [27]. * indicates $p < 0.05$, all groups are significantly different from one another.

A previous report by Baker et al.(93) introduced the technique of co-electrospinning PEO as a sacrificial fiber population in order to improve porosity and cell infiltration. Consistent with the results presented there, PEUU/PEO blended constructs possessed lower tensile moduli following removal of PEO fibers with increasing quantities of sacrificial PEO fibers. However, in the present work, a more dramatic microstructural change was observed following PEO dissolution. This difference is likely due to residual stress supported by the stiff PEO fibers as the construct was fabricated and is consistent with the work presented by Lowrey et al. Once those fibers were removed, the PEUU fibers were able to recoil. This may help explain the

decrease in tensile modulus observed under uniaxial loading, as well as the further decrease in bending modulus. In this work, PEO was dissolved in cell culture media in order to facilitate comparison with previous studies(108). This technique would also be amenable to encapsulating cells within the PEO fiber stream if the cells were not to be directly electrospayed(105). It is expected that some residual protein or PEO may adsorb onto the PEUU fibers. This would likely be in a monolayer, and SEM images do not suggest cross-linked protein residue that might produce substantial mechanical effect. However, it was unexpected that introducing PEO fibers to the fabrication process appeared to produce constructs with higher fiber intersection densities than single stream PEUU scaffolds fabricated under similar conditions. Electrostatic interactions between the two positively charged fiber streams during fabrication may have had an effect on fiber deposition patterns.

The combination of low mandrel translational speed and the introduction of a sacrificial fiber population during fabrication was able to produce scaffolds with little resistance to bending. For soft tissue repair, in general, this is an attractive feature in scaffold development to prevent injury to healthy surrounding tissue as well as to ingrowing tissue during healing. For example, an ideal mesh for abdominal wall repair must also drape properly for optimal healing and surgical handling during implantation. This behavior is directly related to the flexural rigidity of the mesh. The overall functional measure of flexural rigidity, neglecting tension and compression, is defined as $D = EI$, where I is the second moment of inertia, which is proportional to the thickness cubed. Therefore, it is possible to decrease the thickness of any material in order to produce a tissue construct that is functionally less stiff in bending despite its modulus. However this will necessarily be accompanied with decreased suture retention strength, increasing the risk of rupture at the anastomosis. Further, for degradable materials, there exists a

minimal thickness necessary for appropriate tissue ingrowth and remodeling prior to mechanical failure. This would depend on the structure of the material, mechanical response, and degradation rate in-vivo. Constructs fabricated thinner than the critical thickness would be expected to prematurely degrade before ingrown tissue can mechanically function under physiologic loads in situ. Altering the bending modulus of a construct can allow for a greater range of flexural rigidity while maintaining adequate suture retention strength and preventing premature degradation.

Results presented in this report demonstrate the capability of fabricating elastomeric scaffolds with good tensile strength, mechanical anisotropy, as well as a bending modulus that is significantly higher, but still on the order of magnitude of the native porcine pulmonary valve. By slightly decreasing the thickness of the construct, the methods described in this manuscript can be put into practice to produce mechanically strong elastomeric constructs with flexural rigidity equal to that of native heart valve tissue.

3.5 LIMITATIONS AND FUTURE WORK

Several additional experiments logically follow this work in order to address the inherent limitations of the current study. No degradation or fatigue studies were performed in order to evaluate potential long term function of these constructs. However, it would be expected that without cells, as the material degrades, the material will necessarily weaken and fail. The tissue engineering paradigm would require cells to elaborate ECM to take over the mechanical load from the degrading polymer fibers. Therefore, investigation of long term function must be completed either in a mechanically controlled bioreactor or in-vivo. Such a study would also

evaluate the appropriateness of the scaffolds' microstructure to support cellular infiltration and proliferation, as well as the effect of elaborated ECM on scaffold mechanical behavior. However, it may be possible to utilize these scaffolds in a blood-contacting position without cell seeding(126). This would be more attractive from a regulatory perspective and from a logistics perspective for 'off-the-shelf' use. In this case, it would be hypothesized that native vascular or circulating cells would populate the scaffold and secrete ECM.

3.6 CONCLUSION

The function of any biomimetic heart valve replacement is dependent on adequate mechanical response to allow for a reasonable approximation of natural leaflet movement. For this goal, tissue engineered constructs must be extensible and mechanically anisotropic under planar loads and possess sufficiently low flexural rigidity to allow for bending under physiologic pressures. While electrospun polyurethanes have been suggested to be attractive for heart valve applications, no information on their flexural properties have been published. In this manuscript, methods for producing constructs customized bending modulus are presented. Modification of mandrel translational speed during fabrication was shown to alter fiber intersection density which was directly relatable to flexural response. Mixed fiber constructs with higher modulus were found to have higher bending and tensile moduli when secondary fibers were stiffer than PEUU, whereas sacrificial fibers within scaffolds were found to decrease overall construct moduli. Moreover, combining low translational speed during fabrication with sacrificial fiber populations produced constructs with both high mechanical anisotropy and low bending modulus.

4.0 BIOMIMETIC ELECTROSPUN TISSUE CONSTRUCTS WITH CURVILINEAR MICROSTRUCTURES

4.1 INTRODUCTION

Heart valves are sophisticated mechanical structures, which essentially act as check valves, permitting unobstructed outward flow of blood, while preventing regurgitation. They are exquisitely designed to function in a complex and demanding mechanical environment, opening and closing more than 3 billion times during the average human lifetime(127).

An estimated 95,000 valve procedures are performed each year in the U.S., and aortic valve disease is responsible for more than 25,000 annual deaths(1). Even with recent advances in clinical care, such as percutaneous valve replacement, valve disease remains a pressing public health issue. By 2050, the percentage of the US population over the age of 65 is projected to increase to 23.5% from 13.4% in 2010, resulting in almost 36 million more seniors [US census]. Given that the prevalence of moderate to severe valve disease increases with age, from 0.7% in 18–44 year olds to 13.3% in the 75 years and older group(1), we can expect the number of patients to dramatically increase. Tissue engineering and stem cell therapies hold immense potential for the treatment of valvular heart disease.

The aortic valve ECM has a highly tuned laminar structure. Each layer comprises roughly one third of the valve thickness and serves a specific function in the valve mechanics and hemodynamics. The ECM nearest the aortic side of the leaflet is composed mostly of

fibrillar type I collagen oriented in the circumferential direction. This layer is primarily responsible for the planar mechanical response. The intermediate spongiosa layer is composed of sulfated glycosaminoglycans. It is hypothesized that this layer provides a damping function to reduce leaflet flutter under low loads(128,129). The ventricularis layer is composed of both collagen and elastin and is hypothesized to be responsible for the flexural properties and involved with closure(130).

Diseases of native aortic valves have been linked to mechanical factors, largely through observations that lesions occur at sites that correlate spatially with distinct and localized mechanical environments(131). For many years, valvular diseases including calcific aortic valve disease and degenerative aortic valve disease were thought to represent a passive, degenerative process, however, it has become increasingly clear that disease progression instead occurs through cell mediated processes, likely influenced by both endothelial and interstitial cell populations(132). Previous work has also demonstrated that varying tissue stretch levels alter cytokine effects, enzymatic activity, and protein biosynthesis. Clearly, an altered stress/strain field in AV tissue leads to multiple changes at the cellular level, leading to further changes in ECM content and mechanical response to physiologic loading(133,134).

Under quasistatic loading conditions sufficient to induce coaptation (approximately 4 mm Hg), Aortic and Pulmonary valves demonstrate a substantial increase in collagen fiber orientation as measured by Small Angle Light Scattering. This trend was maintained at physiologic transvalvular pressures. Most notably, upon loading the collagen demonstrated a significant curvilinear nature(135). From previous literature it is clear that the microstructure and fiber topology not only provides alignment cues, but also transmits organ level strains to the

resident cells. It was hypothesized that by more closely recapitulating native aortic valve collagen structure, a more effective tissue engineering scaffold will result.

Based on previous works with aligning fibers using high speed mandrels(68), it is commonly accepted that electrospinning has the capability of producing fibers that align to the entire surface of a mandrel. It is hypothesized that if a mandrel surface were designed to have a circular morphology when projected onto a flat surface, an electrospun mat fabricated with the mandrel should have a circular macrostructure when removed from the surface and its fibers should possess a curvilinear orientation similar to that observed in native tissue.

4.2 MATERIALS AND METHODS

4.2.1 Scaffold Fabrication

A previous report(135) has demonstrated using small-angle light scattering that collagen fibers within the belly region of valve leaflets take on a curvilinear orientation, with a change in angle of alignment of approximately 34° . This change in alignment corresponds to the change in slope of a line tangent to a circle with a radius of 5.13 cm (**Figure 17**).

In order to mimic this structure, a conical mandrel was designed to have a flattened projection containing a circle of radius 5.13 cm. (Figure 18) This mandrel was rotated at 1720

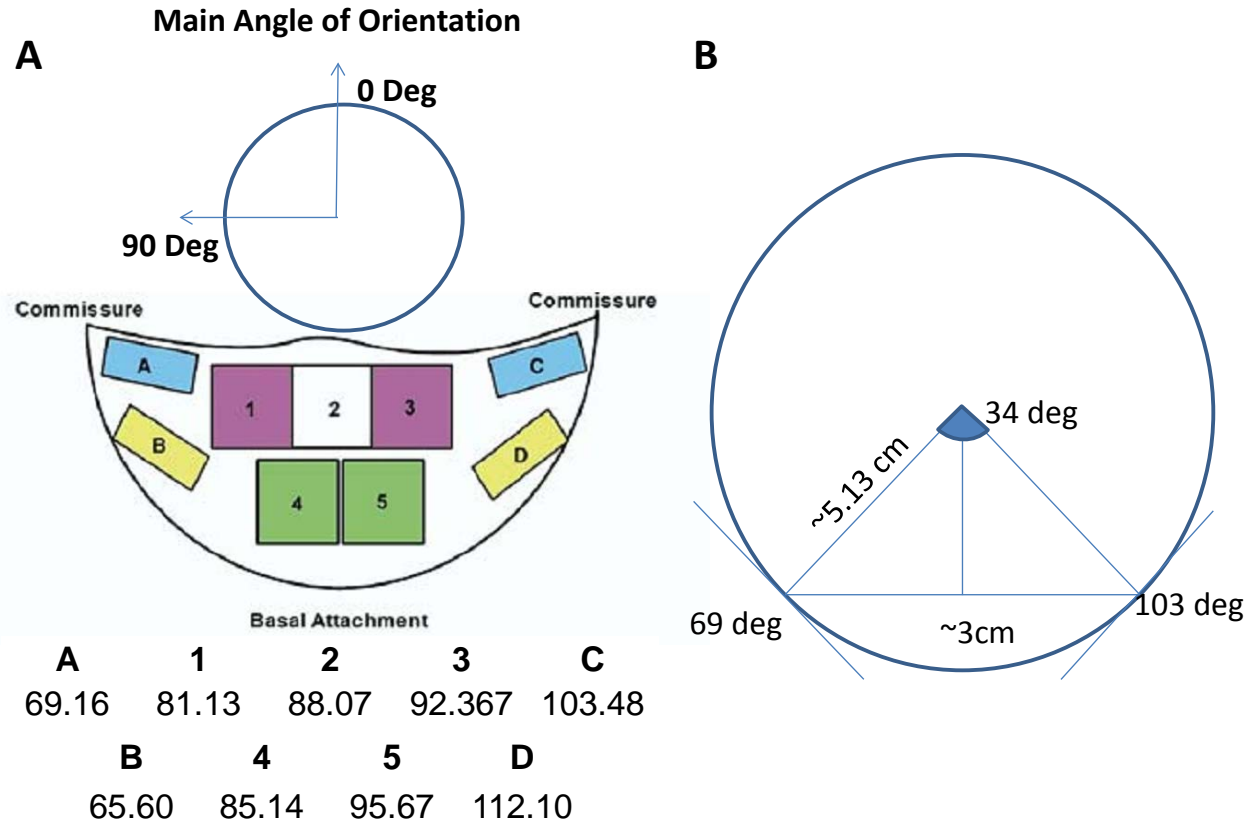


Figure 17 **A.** Graphical representation of the collagen fibril orientation in the native pulmonary valve (above) and the orientation angle values in each region (below). **B.** A circle of radius 5.13 cm will have a similar radius of curvature as the fibrils in native valve leaflets.

rpm to achieve a tangential velocity at the target radius of 4.5 m/s. The mandrel was charged to -5 kV. For electrospinning, PEUU (12%, w/v in 1,1,1,3,3,3-hexafluoroisopropanol (Sigma)) was fed through a stainless steel tube (ID = 1.19 mm) at a flow rate of 1.5 mL/hr. The tube was oriented horizontally perpendicular to the axis of rotation and charged to 11 kV. Prior to removal from the mandrel, a line was drawn on the electrospun mat using a solvent resistant marker in order to indicate the target radius of 5.13 cm. This line was readily visible under SEM. To validate that the tangential velocity was the only factor in producing any curvilinear

alignment, a second cone mandrel was fabricated with twice the height, and therefore, half of the original opening angle. Electrospinning was performed as described above, again targeted at a radius 5.13 cm. As a control, a cylindrical mandrel of similar size was also rotated to achieve a tangential velocity of 4.5 m/s.

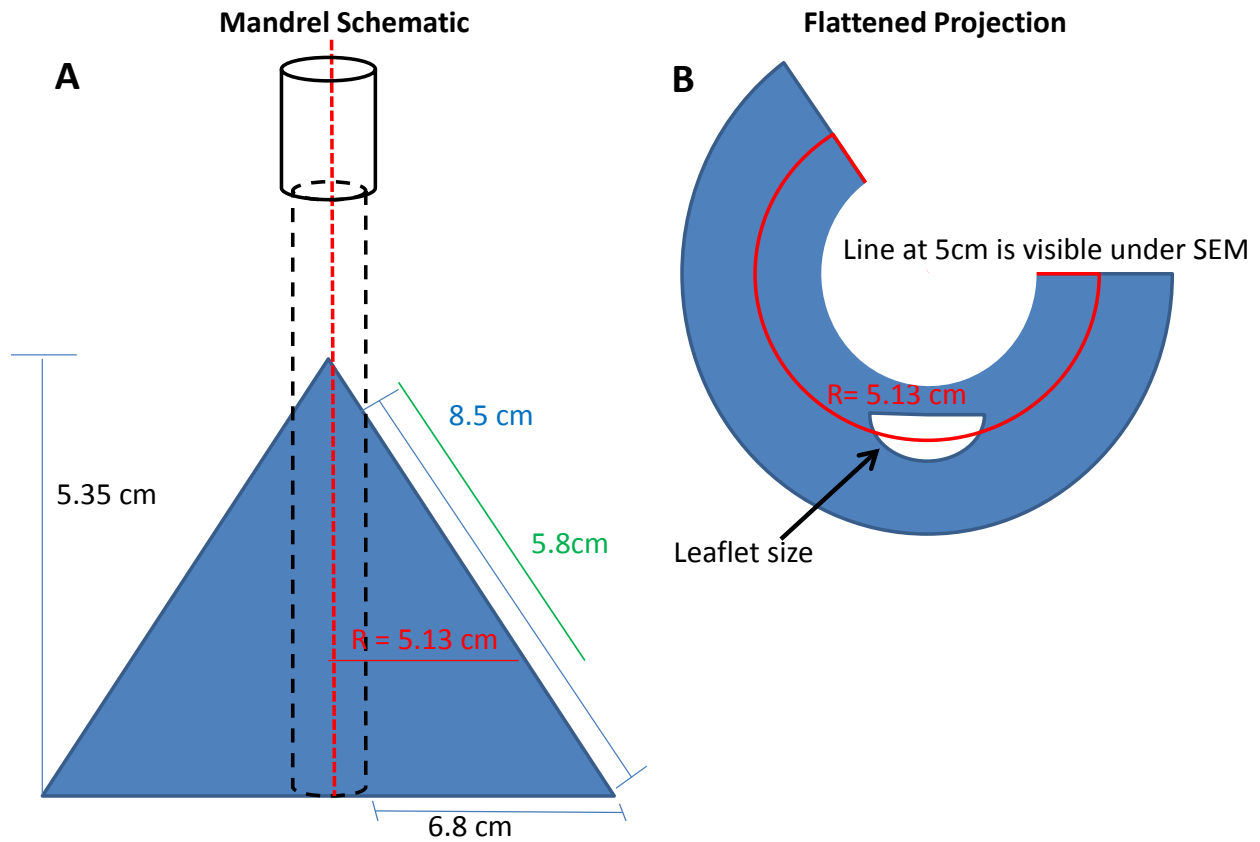


Figure 18 **A.** Schematic used to fabricate the conical mandrel used to collect fibers. **B.** The flattened projection of the conical mandrel surface includes a partial circle of radius 5.13 cm.

4.2.2 SEM Imaging and Structural Analysis

Constructs containing cells were prepared for SEM imaging (Jeol JSM6330F) by fixing in first in 2.5% glutaraldehyde, then in 1% OsO₄. Following that, they were dehydrated using a graded series of ethanol solutions followed by hexamethyldisilazane for final drying. Acellular materials were kept in a desiccator as produced until ready to be imaged. For imaging, scaffolds were Au/Pd sputter coated under vacuum to a thickness of 3.5 nm and mounted with known orientation with respect to original mandrel dimensions. Sets of 19 images were taken at a spacing of 1mm apart along the circumferential direction of the scaffold immediately adjacent to the radius of interest. Structural characterization was completed using a fully automated image analysis program as previously described(48). From each image, main fiber alignment angle, orientation index, fiber diameter, and intersection density were extracted.

4.2.3 Cell Culture

Ovine mesenchymal stem cells isolated from bone marrow were generously donated by the laboratory of Dr. John Mayer Jr., M.D. (Children's Hospital of Boston). The cells were cultured on tissue culture styrene using media containing Delbecco's Modified Eagle's Medium supplemented with 10% fetal bovine serum and 5% penicillin/streptomycin. Cells were plated onto scaffolds at a concentration of 1×10^6 cells/mL.

4.2.4 Biaxial Mechanical Testing

Specimens were removed from each scaffold along the radius of interest and trimmed to 10 x 10 mm square sections. Biaxial mechanical testing was completed as previously described(136). Briefly, blue polypropylene suture (Ethicon) was sectioned into 4 markers of approximately 1 mm in diameter and affixed to the surface of each section using cyanoacrylate. Subsequently, the sections were affixed to a custom built mechanical testing apparatus using sutures attached to four hooks per side. Samples were subjected to two equal biaxial tension controlled protocols up to 90 N/m. The first protocol was used for preconditioning and data were collected on the last cycle of the second protocol. Postprocessing was completed using a preconditioned freefloat reference. Tension data were converted to stresses using known specimen dimensions.

4.2.5 Uniaxial Mechanical Testing

Constructs were sectioned for uniaxial mechanical testing using a dog-bone shaped punch (Ray-Ran Testing Equipment). Sections were immersed in distilled water before testing with an MTS Tytron 250 MicroForce Testing Workstation at a 25 mm/min crosshead speed according to ASTM D638-98. Sections were cut from each specimen along the radius of interest in both the circumferential direction and radial direction.

4.2.6 Suture Retention Strength

Two 5 mm x 15 mm strips were sectioned from each scaffold for suture retention testing. Sections were oriented so that one would be cut parallel to the preferred fiber direction and one

would be cut perpendicular. These were considered circumferential and radial directions, respectively, as would be appropriate if constructs were cut into leaflets. Testing was performed according to American National Standard Institute – Association for the Advancement of Medical Instruments (ANSI/ AAMI) VP20 standards. A single loop of 4-0 braided polyester suture (Syneture) was placed in each section with a 2 mm bite and then pulled at 120 mm/min. (MTS Tytron 250 MicroForce Testing Workstation) Suture retention strength was defined as the peak load before pullout/(suture diameter x sample thickness).

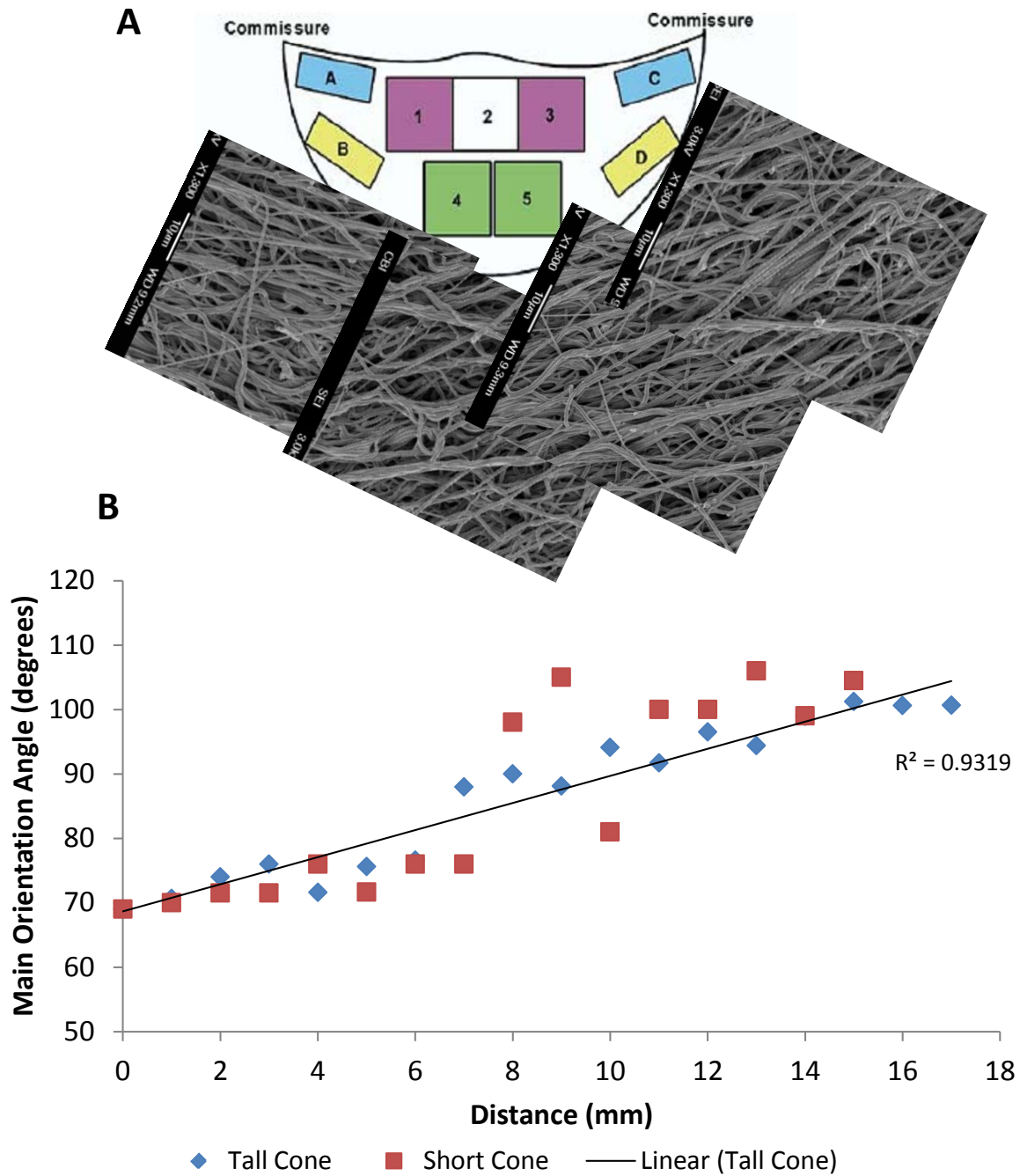


Figure 19 A. Qualitative depiction of fiber alignment over biologically relevant linear distances. B. Quantitative analysis of the change in main angle of alignment over linear distance on both conical mandrels evaluated.

4.2.7 Statistical Analyses

Statistical significance was determined using One Way Analysis of Variance with the Holm-Sidak method for post-hoc pairwise comparisons.

4.3 RESULTS

Consistent with the hypothesis and previously presented works, all scaffolds fabricated had highly anisotropic microstructures. Structural analysis quantified that the fibers that comprised these materials were all highly aligned ($OIW > 0.6$). The fibers in scaffolds fabricated using conical mandrels possessed main angles of alignment which consistently changed along the length of the material by approximately 1.8 degrees per millimeter. **Figure 19 A,B.** No other structural measure studied changed along the length of each section. Further, scaffolds fabricated on cylindrical mandrels possessed consistent main angles of alignment along section length.

Table 3. Uniaxial mechanical properties of electrospun scaffolds fabricated on conical and cylindrical mandrels

	Initial Modulus (MPa)	Linear Modulus (MPa)	Ultimate Tensile Strength (MPa)	Breaking Strain (%)
Conical Mandrel (PD)	2.9 +/- 0.7	28.2 +/- 6.6	16.2 +/- 1.6	173 +/- 18
Conical Mandrel (XD)	1.5 +/- 0.5	2.6 +/- 1.3	3.3 +/- 1.3	240 +/- 37
Cylindrical Mandrel (PD)	20.5 +/- 4.5	29.5 +/- 7.4	12.2 +/- 0.9	151 +/- 22
Cylindrical Mandrel (XD)	1.5 +/- 0.8	1.5 +/- 0.6	6.4 +/- 1.1	431 +/- 40

Consistent with previous reports(137), uniaxial mechanical testing demonstrated pronounced differences in mechanical responses between the circumferential and radial axes of constructs fabricated on a cylindrical mandrel in terms of initial moduli, linear moduli, and ultimate tensile stress. ($p < 0.05$, **Table 3**) Similar behavior was observed from electrospun constructs fabricated on conical mandrels except for a significant ($p = 0.008$) tow region in the circumferential axis under uniaxial tension (**Figure 20 A**). This tow region was not apparent in constructs fabricated on a cylindrical mandrel, nor was it apparent in the radial axis of any group studied. The modulus of conical mandrel scaffolds in the tow region was not significantly different from the initial modulus of conical mandrel scaffolds in the radial direction (**Table 3**). Interestingly, no statistically significant difference was observed in suture retention between the circumferential and radial axes of constructs fabricated on the conical mandrel, however the radial (crosspreferred) direction of cylindrical mandrel scaffolds possessed comparatively high suture retention strength. Both orientations of every construct evaluated in this study possessed higher suture retention strength than commercially available vascular graft material(26). (**Figure 20 B**)

Cultured ovine MDSCs were observed to survive and proliferate well on the conical mandrel scaffold surfaces, aligning with the fibers' main angle of orientation (**Figure 21 A**). Over 7 days of spinner flask culture, MDSCs formed a confluent monolayer covering the entire scaffold surface. (**Figure 21 B**)

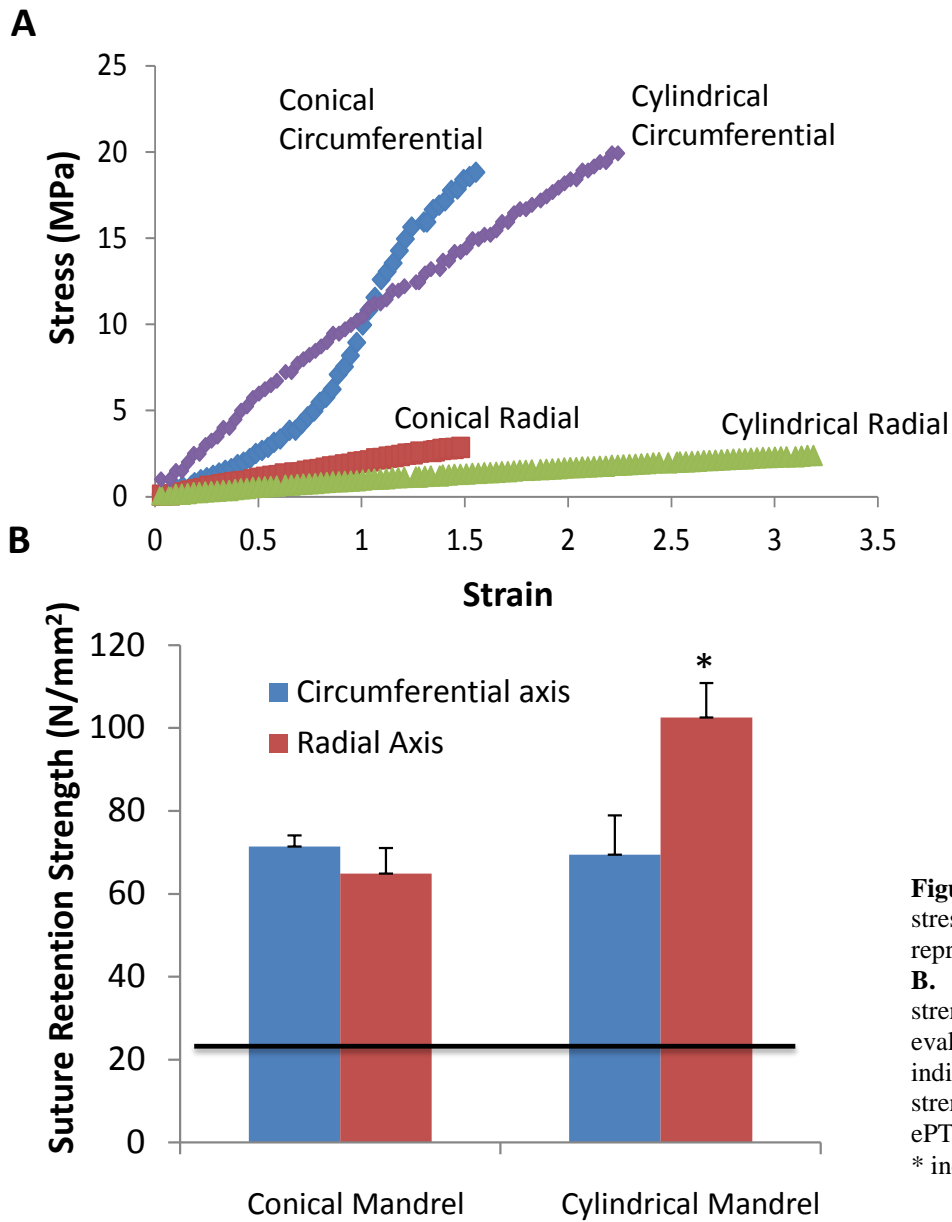


Figure 20 A. Uniaxial stress strain curves from representative constructs. B. Suture retention strength of constructs evaluated. Reference line indicates suture retention strength clinically used ePTFE vascular graft [26]. * indicates p < 0.05

Biaxial mechanical testing demonstrated pronounced mechanical anisotropy in all constructs evaluated and no significant difference was found in planar mechanics between constructs fabricated on a cylindrical mandrel and those fabricated on a conical mandrel. (**Figure 22**) Further, the electrospun constructs were found to have similar mechanical anisotropy to that found in the native pulmonary valve.

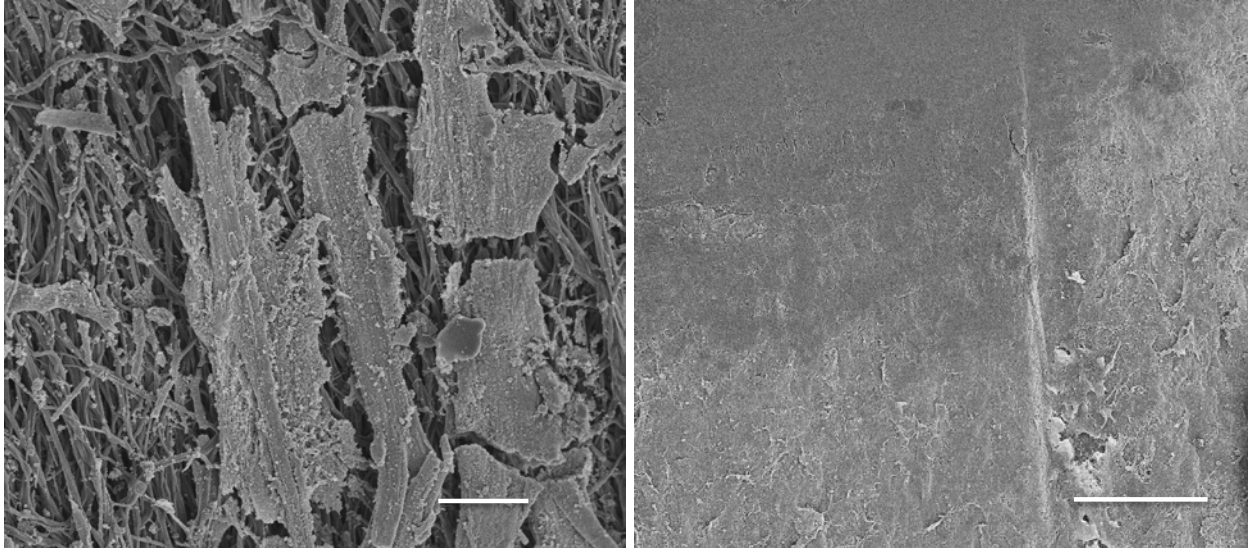


Figure 21. **A.** The morphology of sub-confluent MDSCs cultured on the surface of a scaffold with curvilinear fiber microarchitectures. **B.** MDSCs proliferated to a confluent layer on the surface of the scaffold. Scale bar = 100 μm .

4.4 DISCUSSION

Valvular endothelial cells (VECs) have been reported in the literature to be morphologically and behaviorally distinct from vascular endothelial cells. In-vivo, VECs align circumferentially along the leaflet(138) which is perpendicular to blood flow, contrary to the behavior of vascular endothelial cells. Similarly under in-vitro culture, VECs have been reported to align perpendicular to shear stress(138) as well as perpendicular to large tissue strains(139), which follows logically from the mechanical behavior of valvular tissue. During opening, valves experience significant flexure while VECs are exposed to shear due to blood flow(140). During coaptation, valve leaflets experience significant planar stresses and large strains in the radial direction(140). From clinical data, it is clear that both age and disease state produce alterations in native ECM stiffness, composition and structure which alter both conduit and valve mechanical response(132). Such changes in mechanical properties and tissue structure will have a direct

impact on leaflet motion, and therefore hemodynamic performance of diseased valves. Additionally, there is a body of literature which demonstrates that these changes in composition and structure result in changes to cellular level mechanical loading for both VECs and VICs(132,134,138,141). Further, altered micromechanics as well as fluid flow have been shown to produce changes in the behavior and ECM elaboration pattern of VICs(142). Clearly, valvular disease, malformed tissue structures, improper mechanical loading, and altered hemodynamics each play a role in a vicious cycle which can lead to significant regurgitation and severe clinical outcomes.

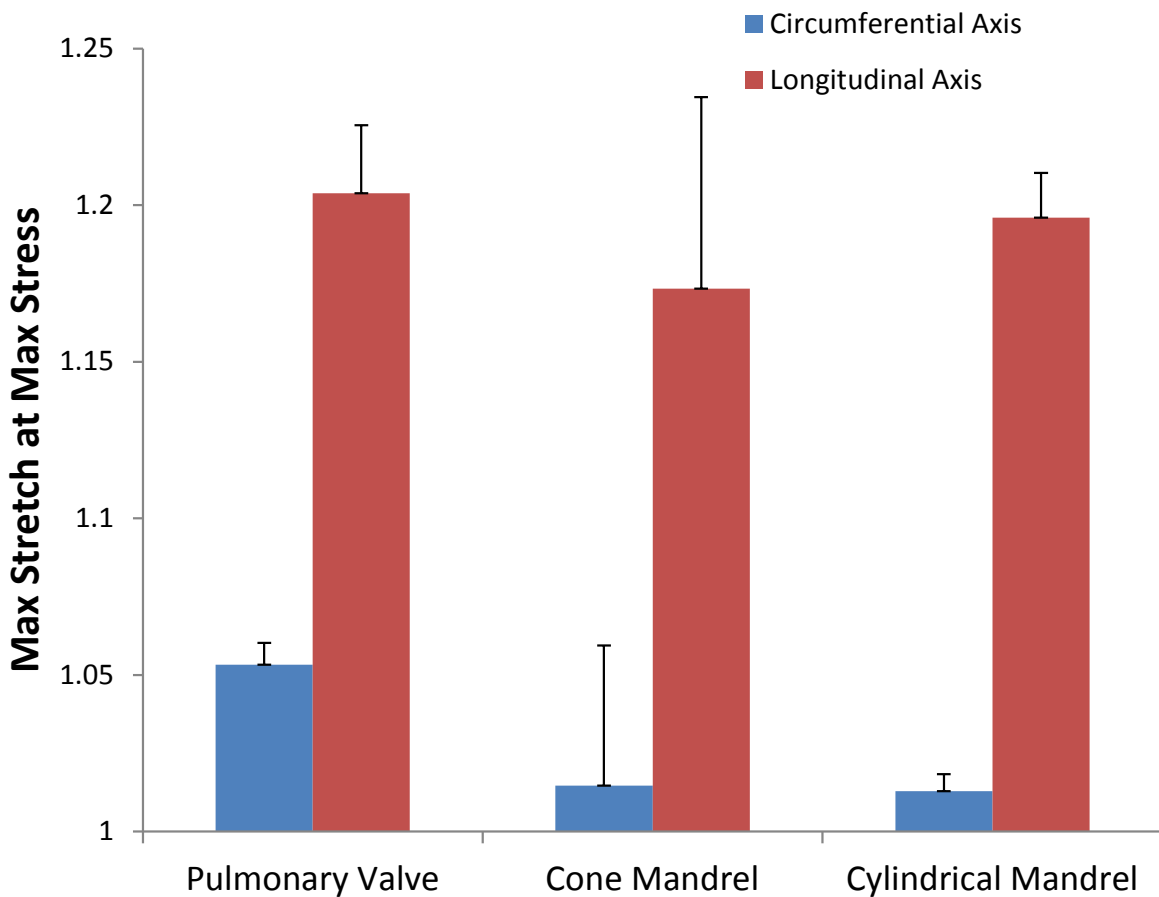


Figure 22 The biaxial mechanical response of scaffolds fabricated on conical and cylindrical mandrels in comparison to native pulmonary valve.

It is possible that a tissue engineered scaffold which recapitulates native mechanics and fiber microstructure may prevent the pathological remodeling seen in prosthetics to date(143). Previous attempts to fabricate electrospun scaffolds with mechanical behaviors similar to valve leaflets have focused on mimicking organ level mechanical response, and have achieved appropriate levels of planar mechanical anisotropy(68) and flexural modulus(113,144). The present work takes a divergent approach by focusing on the microstructural environment of the scaffolds. The hypothesis of the current work was that a curvilinear fiber orientation would create a more biomimetic microenvironment while maintaining physiologic mechanical anisotropy.

This was accomplished by electrospinning onto a conical mandrel rotating at a tangential velocity associated with aligned fiber morphologies. Consistent with previous results by our group(68), scaffolds fabricated in this manner on both cylindrical and conical mandrels were mechanically appropriate for cardiovascular biomaterial application and possessed highly anisotropic microstructures as well as planar biaxial mechanics that mimic the anisotropy of the native pulmonary valve at physiological load levels (**Figure 21**). Unlike scaffolds fabricated on cylindrical mandrels, the constructs fabricated in this work possessed constituent fibers with main angles of orientation that changed by 30° consistently along a linear distance consistent with valvular geometry (**Figure 19**). These scaffolds were shown to be capable of supporting and guiding the alignment and proliferation of ovine MDSCs, a cell type chosen for their ease of isolation and clinically relevant large animal model for pediatric valvular replacement.

Recently, Fisher et al. reported on a similar technique for fabricating electrospun scaffolds with curvilinear structures for knee meniscus tissue engineering(145). In that report, the authors electrospun onto a disk rotating at high speeds in order to circumferentially align the

constituent fibers. They found similar levels of alignment and change in orientation over linear distance. However it is important to note that in utilizing a rotating disk, more complex electrospinning modifications such as multiple polymer electrospinning for improved pore size(93) or concurrent cell electrospay may not be successful due to electrostatic repulsions between electrospinning or electrospay jets(146).

4.5 LIMITATIONS AND FUTURE WORK

Several additional experiments logically follow this work in order to best evaluate this technique for potential use in fabricating engineered heart valve tissue replacements. First, a blood compatibility study could be valuable in determining thrombogenicity and troubleshooting potential issues prior to animal implantations. It is likely that a confluent external layer of viable cells, particularly VECs or endothelial progenitor cells, would be of interest for this study. Additionally evaluation of local tissue strains and hemodynamic performance in a flow loop setting would be attractive in determining the success of biomimetic scaffold microstructures in producing more natural leaflet motion and minimizing regurgitation upon closure.

4.6 CONCLUSIONS

Disruptions in the structure and biomechanical response of native valve leaflets have been associated with changes in VIC and VEC behavior as well as pathological remodeling leading to organ failure(132,147). There is further evidence to suggest that similar changes in micro-scale

structure and mechanical function are responsible for bioprosthetic device failure in the clinic(138). It was hypothesized that an electrospun construct with biomimetic curvilinear fiber alignment would possess attractive mechanical properties and leaflet motion, as well as provide an adequate environment for cell growth. Toward that goal, a novel technique for the consistent production of electrospun scaffolds with circumferentially aligned constituent fibers was presented and evaluated structurally and mechanically. This work will serve as a starting point for the evaluation of biomimetic valvular prostheses in a pulsatile flow environment.

5.0 FATE AND FUNCTION OF INTEGRATED CELLS WITHIN ELECTROSPUN ELASTOMERIC CONSTRUCTS IN VIVO

5.1 INTRODUCTION

Surgical reconstruction of congenital cyanotic cardiac defects such as the Tetralogy of Fallot often require the use of biomaterial patches to complete closure when insufficient native tissue is available. Currently clinically used synthetic materials for these applications include Gore-Tex[®] and Dacron[®]. These materials, while durable and mechanically appropriate to withstand cardiovascular forces, are not inherently bioactive and are incapable of growth and remodeling. When these are applied to pediatric populations, reinterventions become necessary as the child grows in order to prevent or alleviate further complications such as stenosis and rejection(148,149).

The tissue engineering paradigm in this case, would serve to prevent many of these complications, as a biodegradable thermoplastic elastomer could be designed and employed to controllably degrade over time while maintaining sufficient mechanical strength to structurally support growing tissue. Such a construct could be further processed with intrinsic bioactivity through the incorporation of ECM proteins(150) or seeded cells(102,151). Thermoplastic elastomer based scaffolds are additionally advantageous for these purposes due to their amenability to various processing methods. Of such synthetic material processing methods,

electrospinning has been shown to be appropriate for cardiovascular tissue engineering for its ability to rapidly create fibrous constructs with physiological microstructural size scales(54). However, until recently, efforts toward seeding electrospun scaffolds with a uniform distribution of cells had met with little success due to insufficient pore sizes to permit cellular infiltration(55).

The past several years have seen a number of reports published dealing with modifications to electrospun constructs during fabrication(39,108) or following fabrication(91) which increase pore sizes and permit greater cell movement within electrospun scaffolds. Additionally, a method for fabricating fully cellularized electrospun constructs in a single step has been developed by our group(100). Such techniques have permitted a greater number of studies involving cellularized electrospun scaffolds implanted in animal models(28,39,41,80,151–156).

Despite this increasing body of literature dealing with cell seeded electrospun scaffolds in vivo, it is not currently clear how the implanted cells interact with their host. In each of these works, explanted scaffolds were found to be highly cellularized with a variety of cell types consistent with the well-established inflammatory and healing response. It is generally unknown how many of these cells were derived from the implanted cells. Some researchers have attempted to address this question using cell tracking(151–153), and in each instance have found some traces of implanted cells up to two months from the date of initial surgery(151,152), however these cells account for a minority of total cellular matter in every case. Further, several reports have shown significant differences between cellular implants and acellular implants in terms of functional or histological outcomes(28,30,151), signifying that if implanted cells only make up a

small portion of total cellularity at the experimental endpoints, they would logically serve some function prior to that point.

The hypothesis of the current work was that seeded cells serve a critical function in the early stages of the tissue repair process and continue to survive following the infiltration of host cells. This research question was approached through the use of a full thickness right ventricular outflow tract (RVOT) repair in an athymic nude rat model. The RVOT patch was fabricated without cells or pre-seeded with either muscle derived stem cells (MDSCs) or primary cells (smooth muscle cells and endothelial cells). It was expected that seeded cells of either type would improve the healing response in terms of vascularity and elaborated ECM compared to acellular constructs, however endothelial cells were hypothesized to provide an advantage in terms of endocardial endothelialization.

5.2 MATERIALS AND METHODS

5.2.1 Biaxial Mechanical Testing of the RVOT

The healthy RVOT of three animals was resected from harvested hearts of age-matched Lewis rats for mechanical evaluation in order to properly design scaffolds for passive mechanical behavior. Following harvesting, hearts were immersed in Ringer's solution (82mM NaCl, 60mM KCl, 2mM CaCl₂, 10mM Trizma-HCl, 10mM Trizma-base, 11mM dextrose) supplemented with verapamil (0.5mM) and ethylene glycol tetraacetic acid (EGTA, 0.5mM) for 1 h to obtain complete muscle fiber relaxation. The entire RVOT was excised and trimmed to a 6 mm x 6 mm square. Four 1 mm sections of polypropylene suture were affixed to the exterior

surface for strain tracking and the tissue was subjected to two 10 cycle equibiaxial tension controlled protocols up to 40 N/m. The first protocol was used to precondition the sample and data were recorded from the final cycle of the second protocol. Peak strains were compared with those from historical data(157) in order to choose appropriate fabrication conditions for generation of mechanically appropriate prosthetics.

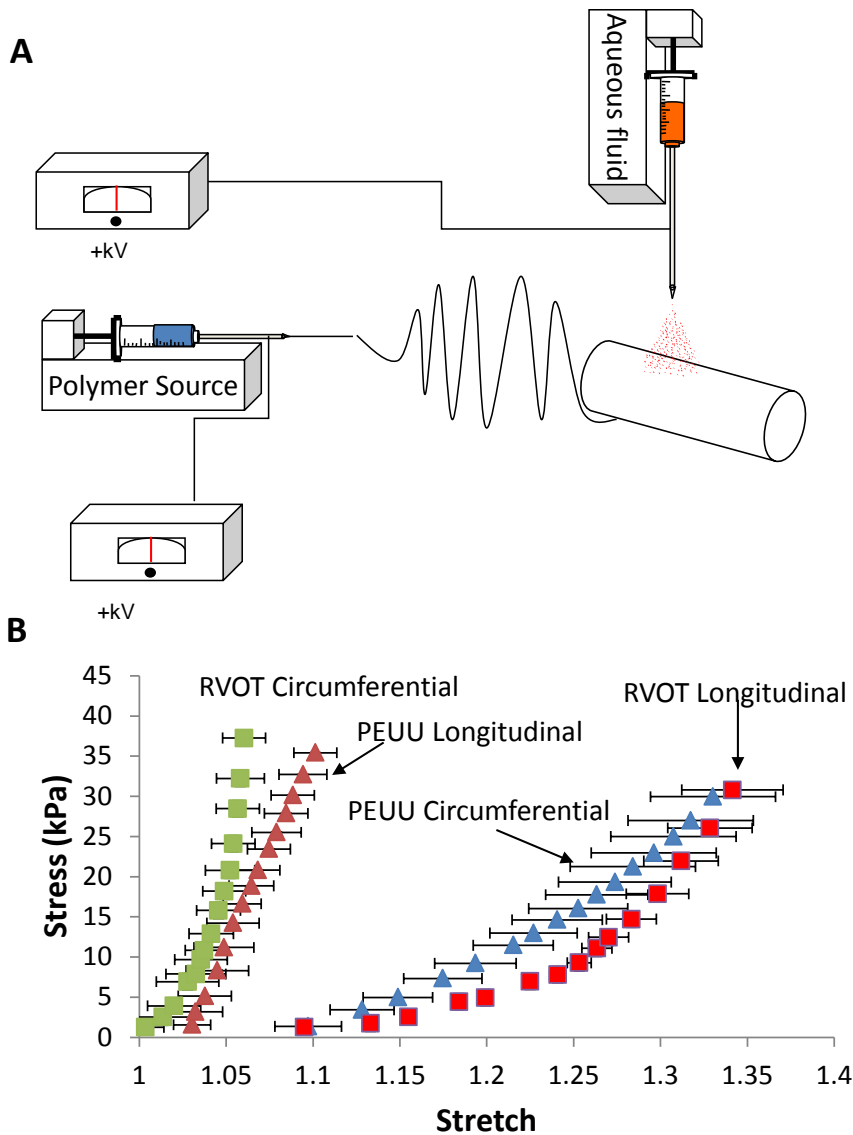


Figure 23 A. Schematic of the scaffold fabrication assembly. B. Mechanical response of the rat RVOT under equal biaxial tension, overlaid by the nearest fit of electrospun PEUU.

5.2.2 Scaffold Fabrication

Poly (ester urethane) urea (PEUU) was synthesized as described in Chapter 2. Electrospun scaffold fabrication was performed using methods similar to those previously reported (Chapter 2, **Figure 23 A**). Briefly, PEUU was dissolved in 1,1,1,3,3,3-hexafluoroisopropanol at a concentration of 12% (w/v) and fed through a stainless steel capillary (ID = 1.19 mm) at a rate of 1.5 mL/hr. This capillary was located 17 cm horizontally from and oriented perpendicularly to a rotating stainless steel mandrel (6 mm diameter) which was rotated at a tangential velocity of 8.0 cm/s and translated along its rotational axis at 0.3 cm/s. Concurrently, cell culture medium was electrospayed from a vertical orientation onto the same mandrel. For the MDSC integrated group, the cell culture medium contained a suspension of GFP+ MDSCs (10×10^6 cells/mL) (**Figure 24 A**). For the primary cell type group, a suspension of GFP+ SMCs (10×10^6 cells/mL) was electrospayed sequentially with a suspension of labeled ECs (10×10^6 cells/mL) (**Figure 24 B**). PEUU electrospinning was continued for two minutes between the two cell types in order to ensure distinct cellular regions through the construct thickness. Following fabrication, constructs were statically cultured overnight in preparation for surgery.

5.2.3 Cell Culture

Muscle derived stem cells (MDSCs) isolated from GFP(+) Lewis rats were generously donated by the Huard laboratory(158). MDSCs were expanded on tissue culture polystyrene using Dulbecco's modified Eagle medium (DMEM, Lonza) supplemented with 10% fetal bovine serum (FBS), 10% horse serum, and 1% penicillin-streptomycin. Vascular smooth muscle cells,(SMCs) were isolated from GFP+ Lewis rat aortas and were expanded on tissue culture

polystyrene culture flasks using DMEM (Lonza) supplemented with 10% FBS and 1% penicillin-streptomycin. Rat aortic endothelial cells (RAOEC, Cell Applications, Inc) were expanded on tissue culture polystyrene culture flasks coated with attachment factor solution (Cell Applications, Inc) using supplied endothelial growth medium according to supplier's instructions. Prior to electrospray processing, endothelial cells were labeled with PKH26 Claret Red Fluorescent Cell Linker Dye (Sigma) according to manufacturer's instructions.

5.2.4 RVOT Replacement Procedure

All animal procedures were performed in accordance with the National Institutes of Health guidelines for animal care, the Animal Welfare Act Regulations, and the principles set forth in

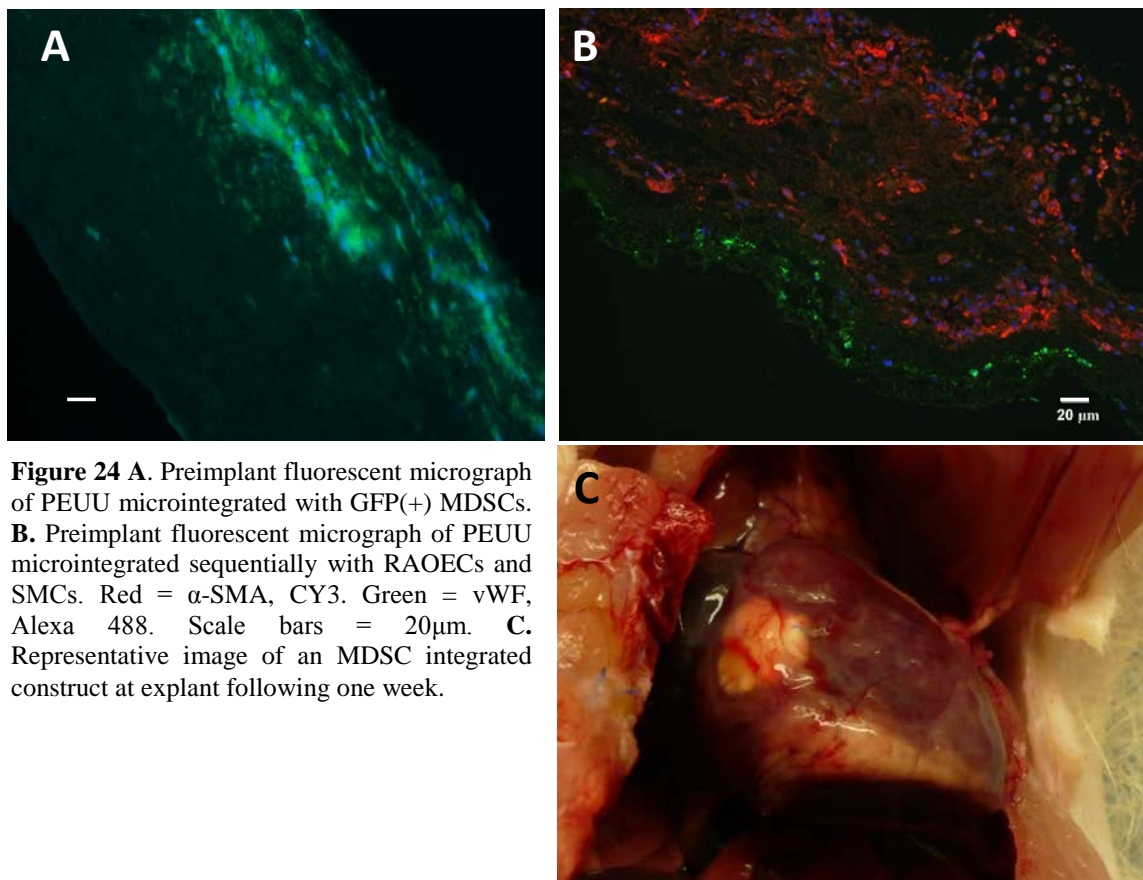


Figure 24 **A.** Preimplant fluorescent micrograph of PEUU microintegrated with GFP(+) MDSCs. **B.** Preimplant fluorescent micrograph of PEUU microintegrated sequentially with RAOECs and SMCs. Red = α -SMA, CY3. Green = vWF, Alexa 488. Scale bars = 20 μ m. **C.** Representative image of an MDSC integrated construct at explant following one week.

the Guide for Care and Use of Laboratory Animals, National Research Council, 1996. Procedures were approved by the Institutional Animal Care and Use Committee of the University of Pittsburgh. 6 week old Fox m1/rnu athymic nude rats (Charles River Laboratories) were anesthetized with an induction of 3% isoflurane and were subsequently endotracheally intubated and mechanically ventilated with a small animal respirator (Harvard apparatus) at a frequency of 60-70/min and tidal volume 2.0 mL. Animals were maintained under deep anesthesia with 100% O₂ and 1.5% isoflurane. The hearts were exposed through a median sternotomy and a purse-string suture was placed in the free wall of the RVOT to form a 6 mm diameter circular region with 7-0 polypropylene suture. Both ends of the stitch were passed through a 22 gauge plastic vascular cannula tightened as a tourniquet in order to distend the encircled cardiac wall, which was then resected. A 6 mm biopsy punch of a PEUU based patch processed with either GFP(+) MDSCs, sequentially seeded SMCs and ECs, or sterile cell culture media was then sutured along the margin of purse-string suture with over-and-over sutures to cover the defect. Each patch section was carefully aligned so that the mechanically stiffer direction (longitudinal axis) was aligned with the circumferential direction of the heart. Following completion of patch implantation, the tourniquet was released and the purse-string suture removed. The sternum was closed parasternally with four interrupted sutures of 6-0 polypropylene after expansion of lungs using positive end-expiratory pressure. The muscle and skin layers were then closed with 4-0 polyglactin absorbable suture (VICRYL, Ethicon, Inc.) Before the first skin incision and twice a day for the first three days post-implantation, cefuroxime (100 mg/kg) was administered as a prophylaxis against surgical infection. Tramadol (5 mg/kg) was also administered intramuscularly twice a day for the first three days post implantation for analgesia.

5.2.5 Patch Explantation

At 1 week and 2 weeks post implantation, animals were euthanized (n = 4 per group) with an overdose of anesthesia. The heart was exposed through a second median sternotomy and harvested. Each patch along with 1 mm of surrounding cardiac tissue was removed from the heart and bisected. One half was fixed with 2% paraformaldehyde for histological evaluation and the remainder was immediately snap frozen in liquid nitrogen for PCR.

5.2.6 RT-PCR

Total RNA was extracted from explanted constructs and similarly sized sections of healthy tissue using a SurePrep* TrueTotal* RNA Purification Kit (Fisher). Primers for Glyceraldehyde 3-phosphate dehydrogenase (GAPDH), Transforming growth factor beta (TGF β), Vascular endothelial growth factor (VEGF), Bone morphogenetic protein 2 (BMP-2), Granulocyte colony-stimulating factor (G-CSF), Stromal cell-derived factor-1 (SDF-1), and platelet derived growth factor (PDGF) were purchased from Applied Biosystems and used as received. These genes were selected based on previous works(159–161) which suggest their importance in cardiovascular repair and remodeling. RT-PCR was completed using a Power SYBR® Green RNA-to-CT™ 1-Step Kit according to package instructions. Data were analyzed using the $\Delta\Delta C_t$ method.

5.2.7 Histology and Immunohistochemistry

Explanted patches were fixed in 2% paraformaldehyde followed by 30% sucrose treatment and freezing in OCT medium. Specimens were then cryosectioned into 10-15 μm thick sections and processed for hematoxylin and eosin, Masson's Trichrome, and immunohistochemistry. Specimens selected for immunohistochemistry were reacted with antibodies for α -SMA and CD-31. GFP signaling was amplified using anti-GFP antibody (Abcam). Nuclei were stained with Hoechst 33342.

5.3 RESULTS

5.3.1 Biaxial Mechanics of the Native RVOT

Harvested full thickness RVOT wall sections were subjected to biaxial mechanical evaluation in order to determine appropriate processing conditions for the prosthetic patches. The native tissue was found to be mechanically anisotropic with a markedly stiffer circumferential axis compared to its longitudinal axis **Figure 23 B**. The peak strain ratios were matched with a database of previous work (Chapter 2) in order to determine appropriate processing conditions which would mimic the native planar biaxial mechanical response.

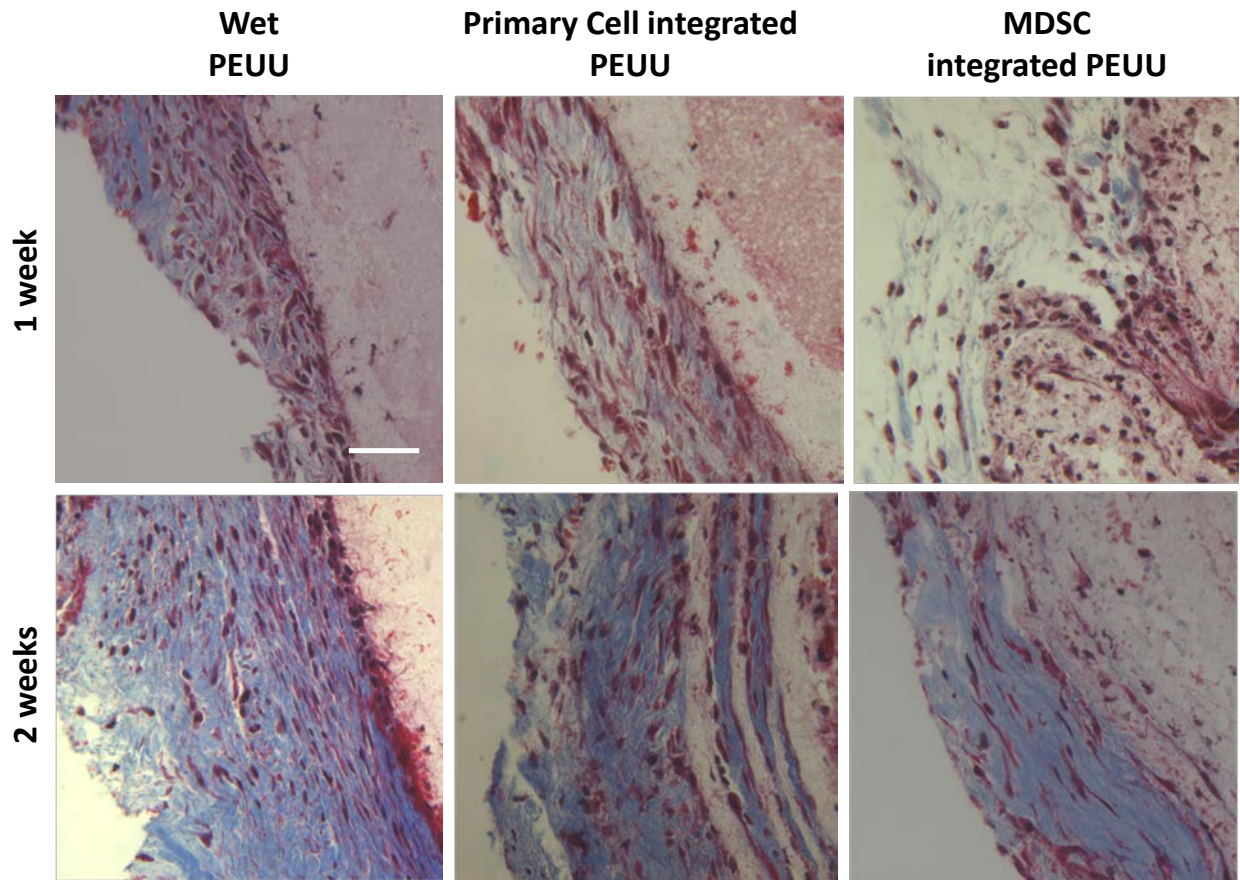


Figure 25 Representative micrographs of the endocardial surfaces of each explanted construct group at each timepoint. Sections stained with Masson's Trichrome stain. Scale bar = 50 μ m.

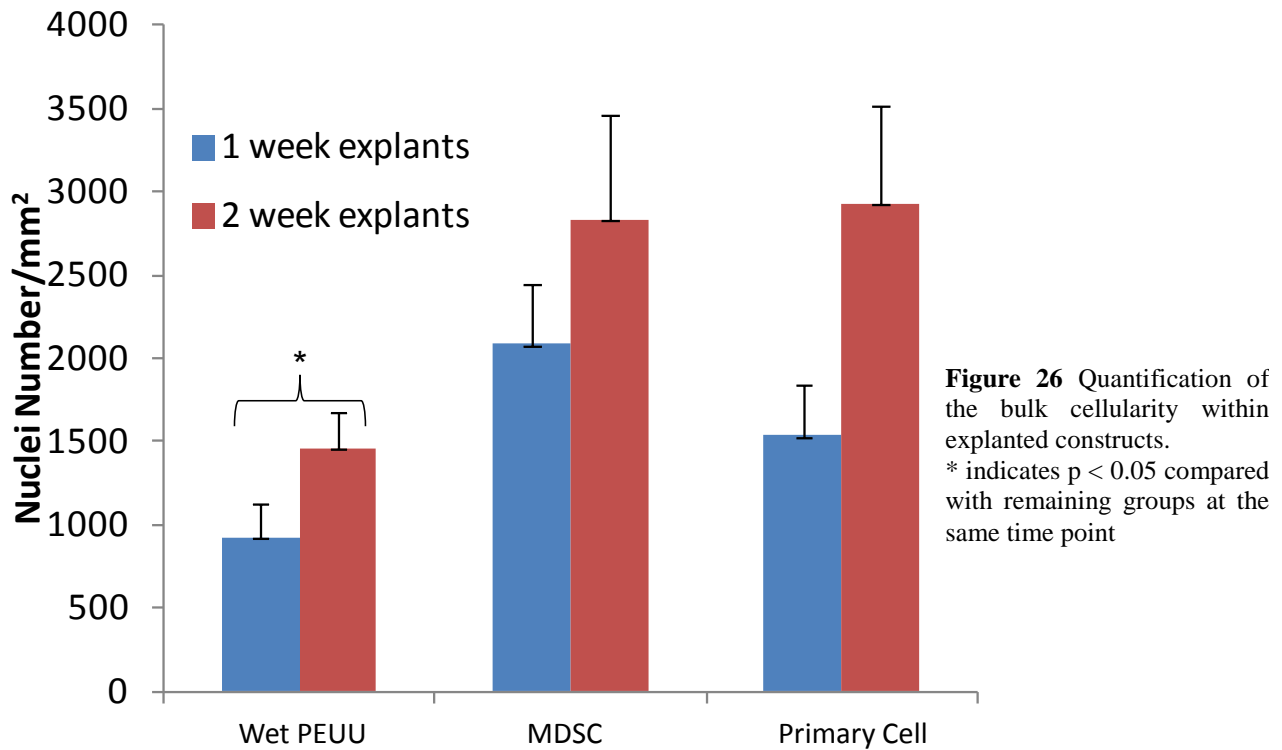
5.3.2 Postoperative Gross Observations

Twenty percent of animals did not survive the surgical procedure, as was expected from previous similar studies with the sensitive athymic rat model. At explantation, approximately 75% exhibited minimal thoracic adhesions (**Figure 24 C**) with no recognizable patterns between cell types or time points. No patches experienced any aneurism or dehiscence, nor was there gross evidence of thrombosis. No evidence of infection was observed.

5.3.3 Histology and Immunohistochemistry

5.3.3.1 Inflammatory Response and Cell Infiltration

Media wetted constructs consistently had thin regions of thrombus on their endocardial surfaces when viewed under histology. MT staining also indicated a pronounced inflammatory response



surrounding each scaffold, as indicated by the quantity of cell nuclei (**Figure 25**). Comparing the inflammatory responses between one week and two week explants, no difference was detected with respect to cell density, however cell nuclei appear to have elongated and elaborated ECM appears to be more dense.

Histological quantification determined that fewer cells existed within the bulk of explanted wet PEUU scaffolds compared to the cellular groups at similar timepoints ($p < 0.05$) (**Figure 26, APPENDIX D**). Further, at 1 week, media wetted scaffolds were heavily infiltrated by small, anuclear eosinophilic globular structures which stained positively for vWF. (**Figure 27**) These structures were also observed to a lesser extent at two weeks, and were rarely observed in other constructs. Masson's Trichrome images suggest that scaffolds fabricated concurrently with cell electrospaying possess modest quantities of ECM by two weeks while no ECM was observed within scaffolds from the acellular constructs at either timepoint (**Figure 28**).

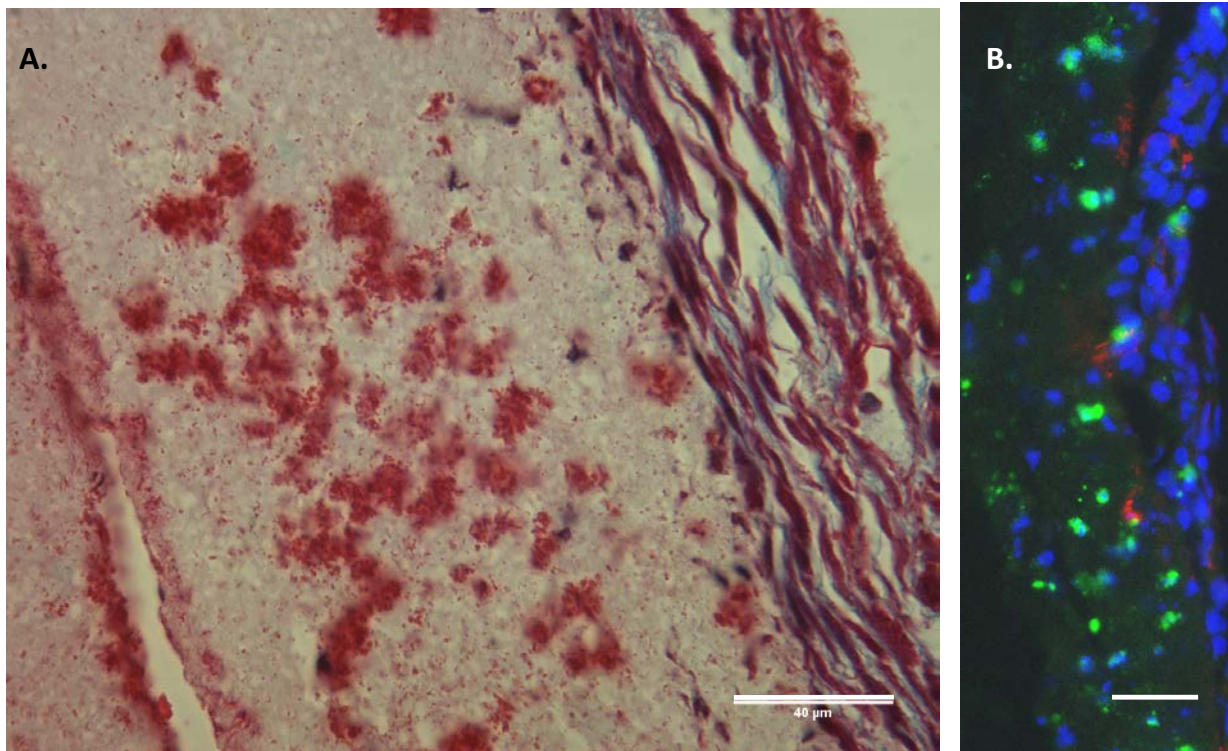


Figure 27. A. High magnification micrograph of a Masson's Trichrome stained section of a representative wet PEUU explant at one week. B. Immunofluorescent micrograph of the same section stained for vWF (green), α -SMA (red) and Hoescht (nuclei, blue)

5.3.3.2 Endothelialization and Neovascularization

Linear layers of vWF(+) structures indicative of endothelium were observed at the endocardial surfaces of some, but not all explanted constructs from the Wet PEUU and primary cell integrated groups at one and two week timepoints (**Figure 29**). Other wet PEUU constructs at the

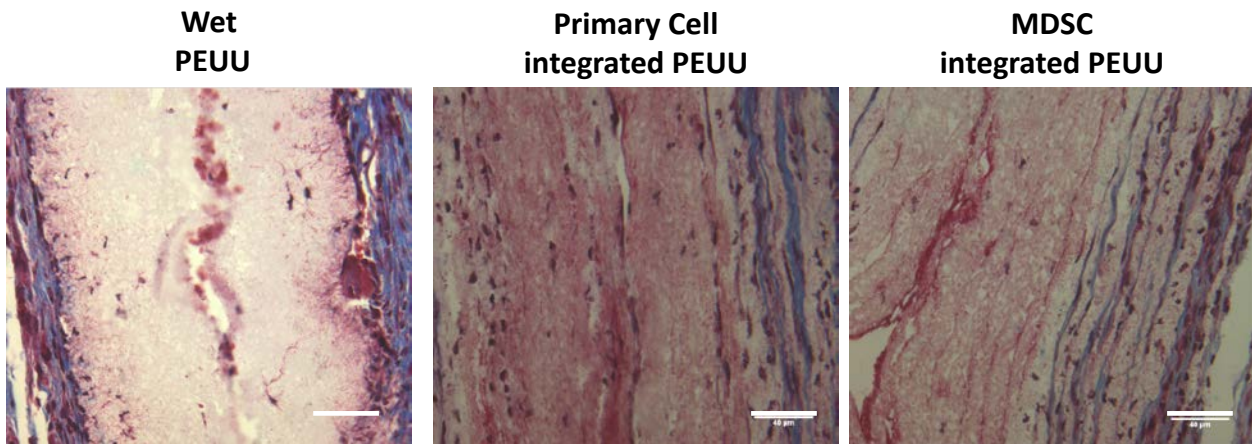


Figure 28. Masson's Trichrome staining depicting ECM elaboration within the bulk of representative sections from each group at two weeks post implantation. Scale bar = 50 μ m

one week explant displayed thrombus at their surfaces. No evidence of thrombus was observed on the cellularized explants at either timepoint. Further, a confluent endothelial layer was observed on all MDSC integrated explants at both one week and two weeks.

Neovasculature, identified by the presence of ringed vWF(+) structures surrounded by α -SMA staining, was present in each construct evaluated (**Figure 30 A,B**). Vessels were sparse within the acellular and primary cell integrated groups, but were significantly more dense within MDSC integrated scaffolds ($p < 0.05$). Vascular density was not found to be different within groups over time ($p > 0.1$)

5.3.3.3 Residual Cells

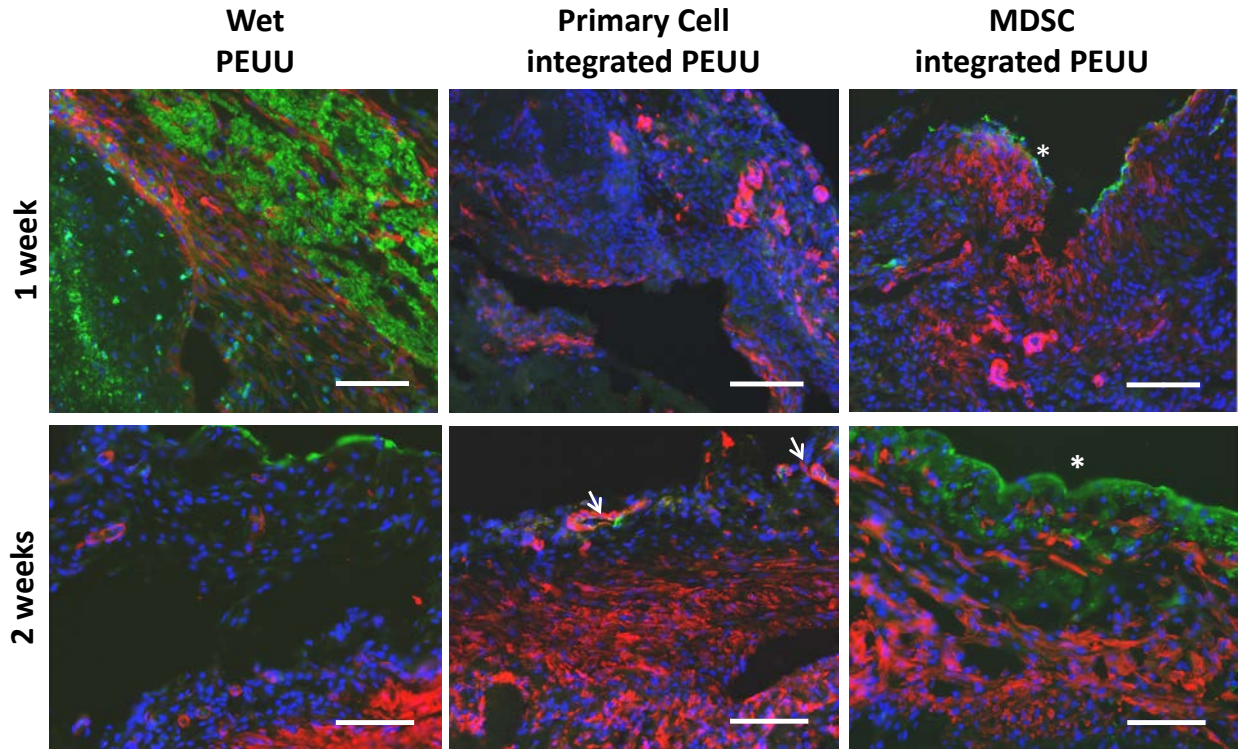


Figure 29 Immunofluorescent micrographs of explanted constructs at one week (top) and two week (bottom) timepoints. Red = α -SMA, Green = vWF, Blue = cell nuclei (Hoechst)

Figure 31 A,B indicate the presence of residual labeled cells at each experimental endpoint. These cells represent a low percentage of total cells observed in explanted constructs (10-30%, $p < 0.05$), however the total density of seeded cells remains consistent with that of the constructs as they were fabricated (**Figure 31 C**). When co-stained with α -SMA, it becomes clear that many of the remaining MDSCs are expressing contractile actin. Labeled endothelial cells were not observed in any endocardial surface endothelial layer, however some cells labeled with fluorescent dye were included in the neovascular structures discussed earlier. The remaining labeled RAOECs did not express vWF, however GFP (+) SMCs were still largely α -SMA (+).

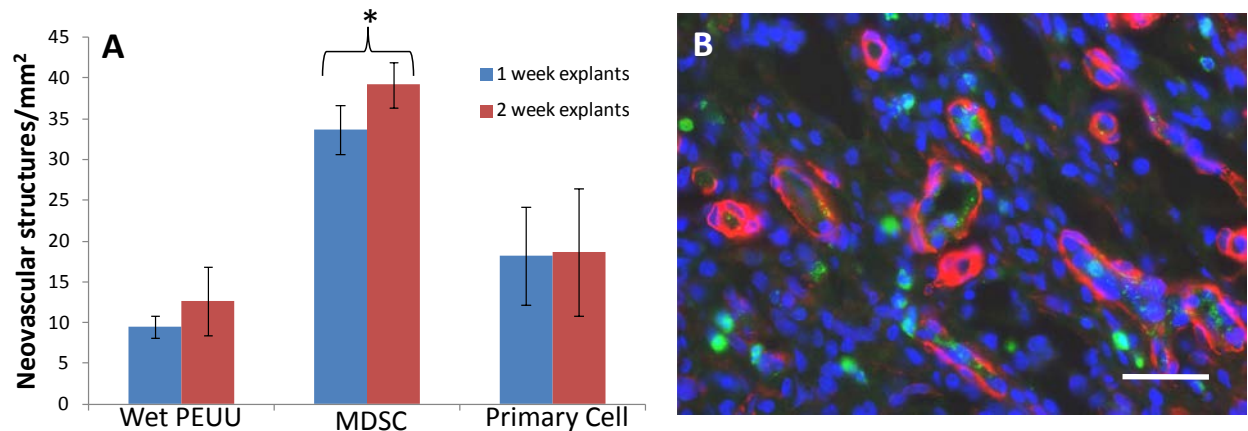


Figure 30 A. Density of neovascular structures within the bulk of explanted scaffolds. * indicates significantly different between other groups at the same timepoint. **B.** Immunofluorescent micrograph of neovascular structures. Green = vWF, Red = α -SMA. Scale bar = 40 μ m

Micrographs depicting the anastomosis between each patch and the healthy RVOT tissue (**Appendix E**) demonstrated dense nuclear staining in a gradient pattern from the cardiac muscle toward the scaffold border indicative of infiltrating inflammatory cells. It was common for some of the infiltrating cells to stain positively for α -SMA when they were in close proximity to the patch.

5.3.4 RT-PCR Results

PCR of explanted constructs revealed marked differences in expression of all genes studied compared to healthy tissue at one week for all cell integrated groups, whereas no expression beyond baseline was observed in the acellular group (**Figure 32**). PDGF was expressed significantly more than other genes studied in the primary cell integrated group ($p < 0.05$). Cells within MDSC explants expressed high levels of all genes studied, however VEGF, PDGF, TGFB, and SDF1 expression were all found to be higher than that of CSF and BMP2. At two weeks post implantation, expression of each gene evaluated within the cell integrated groups

dropped to equivalent levels found in the healthy RVOT wall (**Figure 33**). A modest increase in gene expression within wet electrospun explants was observed. CSF and SDF1 expression were highest in this case.

5.4 DISCUSSION

The preceding work focused on cell behavior when seeded into a cardiovascular graft in vivo. These results in conjunction with later term results help to close the gap in understanding

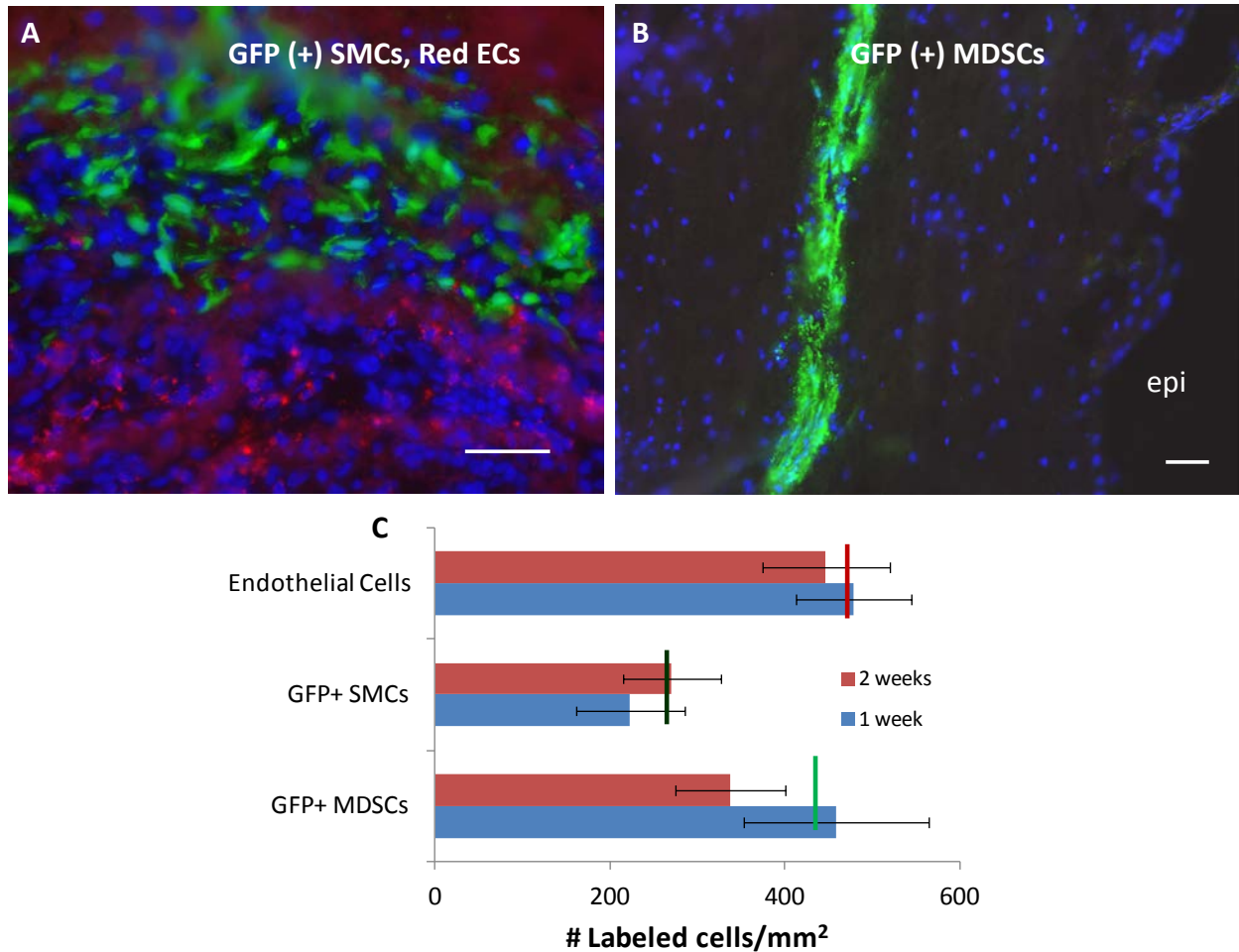


Figure 31 **A.** Residual cells within a primary cell microintegrated scaffold at two weeks. **B.** Residual cells within an MDSC integrated scaffold at two weeks. Green = GFP, Red = Fluorescent dye, Sections were stained for cell nuclei and GFP signal was amplified. **C.** Quantification of labeled cell density within the bulk of the scaffolds.

regarding the function of cells used for therapeutic purposes. Constructs were electrospun concurrently with cell electrospray in order to fabricate cellularized constructs. MDSCs and both primary cell types were all shown to survive the scaffold processing through two weeks within the cardiac environment. Upon scaffold harvest, these labeled cells were found to be the minority (15 -30%) of total cells observed within the scaffolds. Further quantification indicated that the labeled cell density quantified by histology was not statistically different from that observed in the constructs prior to implantation (**Figure 31 C**). This suggests that the microintegrated cells largely survived, but did not expand appreciably. Upon further investigation, large numbers of inflammatory cells were observed to invade the scaffold from the surrounding tissue. This produced a noticeable gradient in cellularity within each patch near the anastomosis (**APPENDIX E**). As such a gradient was not observed at the central endocardial surface of any construct, it is likely that the majority of host cells infiltrated parallel to the electrospun fibers as opposed to through the surface.

A higher density of colocalized vWF(+) and α -SMA(+) structures were observed in the cellular groups, indicative of neovascularization. In the case of the primary cell integrated group, some, but not all of the vascular structures observed within the scaffolds were found to be labeled with the fluorescent dye used to modify the seeded RAOECs. However, most of the RAOECs included within the scaffolds did not express vWF upon explant, suggesting some kind of change in phenotype over time. TGF β 1, which was found to be expressed in low levels in one week explants, has been shown to promote endothelial cell differentiation into a smooth muscle like lineage(162). This may partially explain the lack of vWF expression by many of the seeded RAOECs. Similarly, not all of the GFP (+) cells within the explanted primary cell group constructs stained positively for α -SMA. Such cells were found distant from the bulk of the

remaining GFP (+)/ α -SMA (+). This behavior is consistent with differentiation into a motile phenotype(163), which may have been initiated by the pronounced PDGF expression observed in RT-PCR (**Figure 32**)(160,164–166).

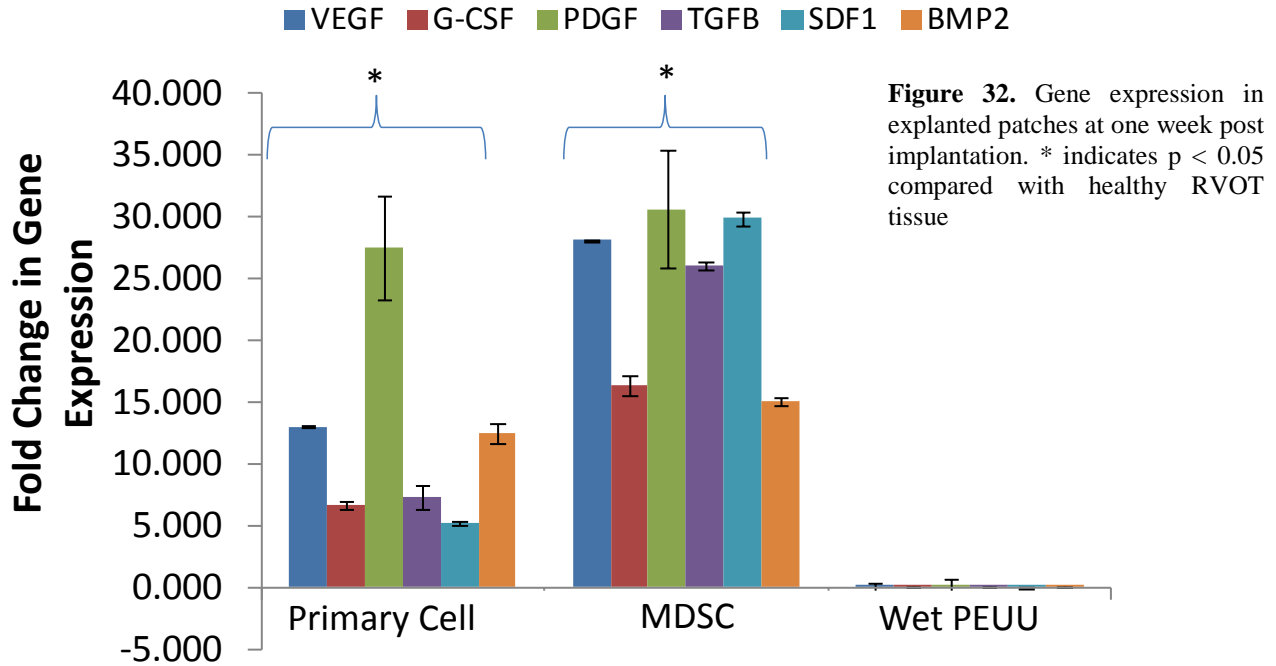


Figure 32. Gene expression in explanted patches at one week post implantation. * indicates $p < 0.05$ compared with healthy RVOT tissue

MDSC integrated scaffolds were shown to have significantly higher densities of neovascularization compared to both Wet PEUU scaffolds and primary cell integrated scaffolds (**Figure 30**). Interestingly, there did not appear to be evidence of GFP(+) cells actively involved within these structures, therefore the difference in vascular density necessarily has to be due to factors expressed by the MDSCs. Consistent with previous reports(167), the MDSCs were found to strongly express VEGF in vivo. This quantity was greater than that observed within the primary cell group ($p < 0.05$). VEGF expression was accompanied by similar levels of expression of SDF-1 and G-CSF, chemokines which have been associated with encouraging progenitor cell migration to ischemic tissues and promoting neovascularization(159). The major chemokines may have functioned together in order to produce the high vascular density observed, and may potentially be responsible for early endothelialization compared with the

other groups studied. Many GFP(+) cells within the MDSC integrated scaffolds were observed to stain positively for α -SMA, suggesting the start of a mesenchymal differentiation pathway, possibly similar to that observed in previous work(28). This may have been brought on by expression of one or more of the genes involved with differentiation of stem cells to cardiac TGF β , BMP-2, or PDGF.

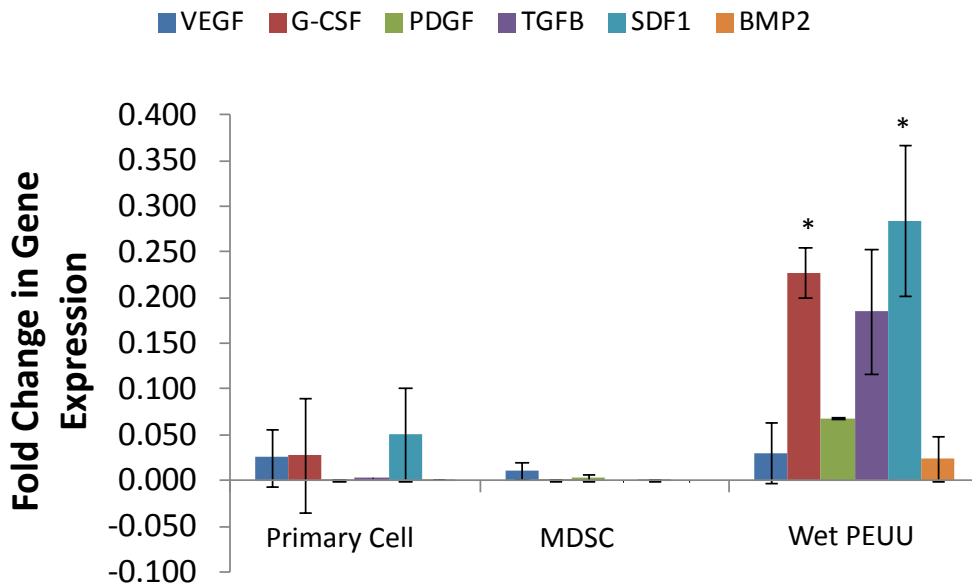


Figure 33. Gene expression in explanted patches at two weeks post implantation. * indicates $p < 0.05$ compared with healthy RVOT tissue

The acellular constructs evaluated in this work were characterized by a high quantity of small eosinophilic globular structures. These structures lacked nuclei, yet were vWF (+), and are therefore most likely platelet aggregates(168). Given the presence of thrombus on the scaffold endocardial surface (**Figure 29**), this logically follows, however there is evidence that platelets can be instrumental in accelerating the healing response(168). No gene expression beyond that observed in healthy cardiac tissue was observed in Wet PEUU explants at one week, despite the presence of cells within and surrounding the construct. This was likely due to cytokines delivered to the site by the platelet aggregates observed within and on the surface of the

explanted constructs. Gene expression was finally observed in this group at two weeks, with modest expression of SDF-1 and CSF, two chemokines responsible for encouraging progenitor cell infiltration into cardiac tissue(159). This was observed while the cells within the remaining two groups had decreased expression to that found in normal tissue. Further studies closely monitoring gene expression as these constructs are infiltrated and remodel would be required in order to determine if these trends continue.

The results presented here appear to be consistent with similar reports found in the literature. Kalfa et al. presented a report on RVOT repair with electrospun PDO seeded with mesenchymal stem cells (MSCs) in which the procedure was extended to eight months (151). In this report, the MSCs were tracked with quantum dots. Only a small number of labeled cells remained at one month, however those cells were not CD-45 (+), so it was ruled out that they were macrophages which had phagocytosed the MSCs(151). Consistent with the results presented here, by one month the cell seeded patch had endothelialized whereas the unseeded scaffold had not.

5.5 LIMITATIONS AND FUTURE WORK

There are several limitations that should be mentioned regarding this study. First is the time course of the study. In two weeks, it is not feasible to achieve robust tissue remodeling or scaffold degradation. However, this was not the purpose of this work, as close evaluation of early scaffold and cell function was desired. Follow-up studies with similar methodology and extended timepoints would be necessary to determine ultimately how successful these constructs will be, and what functions seeded cells serve in the longer term. Finally, a small animal model

of cardiac repair is simultaneously surgically challenging and less clinically relevant in terms of mechanical forces observed by the construct and therefore by the cells as well(106). It has been demonstrated in several cell types and environments that mechanical loading has a pronounced effect on cell phenotype and behavior(106,138,141,147,169–175), and therefore a large animal model would be preferable to a rodent model.

5.6 CONCLUSIONS

The preceding work focused on short term evaluation of cell seeded constructs in a cardiovascular setting. This study was done in order to gain an understanding of the fate and function of seeded cells during the early stages of tissue repair. The results suggest that stem cells encourage endothelialization and ECM deposition more readily than a sequential combination of endothelial cells and smooth muscle cells. However, the original hypothesis was found to be incorrect. The results presented suggest that integrated cells do not always actively participate in tissue repair by becoming functional part. GFP(+) MDSCs were not observed within neovasculature, and a majority of ECs presumably underwent a TGF β induced endothelial-mesenchymal transition. This evidence suggests that the primary role of the seeded cells within these constructs is not always to dominate the newly formed tissue, but rather to express growth factors responsible for recruiting host cells for tissue repair. Further, this function may in fact be temporary, as gene expression was observed to rapidly decrease to the level of healthy cardiac tissue.

6.0 CONCLUSIONS

Electrospinning is a powerful technique for the formation of fibrous scaffolds, and with new advances in technology it has become more robust. Recent developments have demonstrated modifications –chemical, structural and biological, which have permitted in vivo success in a number of regenerative medicine applications. Further, its low cost and physiologically compatible fiber diameter resolution makes electrospinning an attractive technique. However these advantages come with several limitations. In general, individual electrospun nanofibers are not controllable, and produce a construct with statistically predictable features, but randomly assembled fibers. Recently, some levels of precise control have been demonstrated at the cost of increased fiber diameter(58), however the achievable resolution and complexity using this technique remain unknown. Additionally, the electrospinning technique produces a 2D pattern onto the target which can be extrapolated to three dimensions through the thickness of the construct, and has been shown to accurately describe bulk mechanical response.(48) While much research has focused on the physics and mechanics of electrospun scaffolds, they have yet to be fully characterized in terms of how structure and composition affect the overall behavior of the construct. The preceding dissertation focused on structural and compositional modifications to electrospun scaffolds in order to more fully optimize their mechanical and biological functionality.

6.1 STRUCTURAL MODIFICATIONS

6.1.1 Fiber Intersections

As mentioned in Chapter 1, our group has recently developed an automated algorithm capable of digitizing the complete fiber network topology of electrospun scaffolds based on a series of SEM micrographs(48). This technique permitted a more in depth analysis of structure – mechanical function relationships than was previously possible, as fiber intersections were now able to be quantified.

During the electrospinning process, the majority of the solvent is evaporated as the polymer jet travels toward the mandrel. In most cases, however, fibers deposit on the mandrel with a very small quantity of solvent remaining, making the fibers slightly ‘wet’ and sticky for a brief period of time. This is important with respect to overall material mechanics, as it permits binding between two or more fibers as they contact each other(31,176), (**Figure 9**). This provides mechanical integrity between the layers of fibers, preventing the scaffold from unraveling and increasing the robust mechanical response. Despite the potential importance of these structures to the bulk mechanical integrity of electrospun constructs, few studies have focused on them.

Chapter 2 demonstrates a technique for modifying the density of fiber intersections independently from other microstructural elements such as fiber alignment. This was accomplished by varying the mandrel translational speed during electrospinning. A rapid translational motion was associated with lower fiber intersection densities whereas a much slower motion was associated with high fiber intersection densities. It was hypothesized that at slow translational speeds, fibers naturally overlapped densely, but as translational speed was

increased the mandrel began to move faster than the horizontal whipping speed of the fiber creating a more open microstructure. Changes in fiber intersection densities were not associated with altered uniaxial tensile mechanics, however under equibiaxial tension, high intersection densities were associated with increased strain energy and increases in planar anisotropy. Higher intersection densities necessarily created an electrospun construct with a more interconnected microstructure, changing the manner in which fibers rotate and interact with one another under biaxial loading.

Very recently, Shi et Al. reported on the mechanism of adhesion between polymeric fibers at their intersection points(177). Using nanoscale mechanical testing in conjunction with AFM, FTIR, and WAXD, they were able to quantify adhesive strength and provide evidence for this behavior. They found that molecular orientation was decreased locally at the adhesion site, permitting interdiffusion of chain segments. Weak van der Waals interactions between these segments were hypothesized to be responsible for adhesive strength(177). A local decrease in crystallinity within electrospun fibers at the adhesion site is consistent with the hypothesis presented for the results described in Chapter 3 of this dissertation. Local decreases in crystallinity would permit higher adhesive strength, but could also facilitate bending by acting as a hinge on the nano-scale. This is reinforced by the inverse linear relationship observed between fiber intersection density and bending modulus in electrospun scaffolds.

Electrospun constructs fabricated on a small diameter, low tangential velocity mandrel as described in Chapter 2 possess microstructures with slight structural anisotropy (orientation index > 0.5 , **Figure 3**), however low translational speeds permit a large quantity of undulation or looping within the fibers, a structure which was observed to be more pronounced in wet PEUU. The loops within each fiber permit further deformation in the circumferential direction before the

fiber is recruited in load support, creating a mechanical anisotropy with a stiffer longitudinal direction. The data from Chapter 2 demonstrate that higher interconnection densities were utilized to produce constructs which were more compliant, in general, under equi-biaxial loads. The fiber intersections were found to be correlated with strain energy under equi-biaxial tension. Expanding upon the hypothesis of Chapter 3, that each fiber bonding point would be a localized region of low crystallinity, they would also be localized regions of low tensile modulus. While it is likely that the sum of these low-modulus regions would be insufficient to overcome the effect of fiber rotation observed in fibrous materials scaffolds under uniaxial load, a clear trend could be observed under equi-biaxial tension. If this is the case, higher intersection densities would be expected to amplify any existing mechanical anisotropy within the construct. This hypothesis corresponds with the data presented in **Figure 3** **Figure 4**. Expanding on this hypothesis, if fiber intersection density were to be increased in a completely isotropic electrospun scaffold, it would not be expected to produce mechanical anisotropy. Future work should be completed to develop a complete structural deterministic model of electrospun scaffold mechanics. For applications in heart valve tissue engineering, such a model could be made to describe both planar and flexural mechanical behavior simultaneously.

Recent studies have determined that cells seeded onto fibrous constructs can respond to a number of structural cues including fiber diameter(178), orientation(179), and surface roughness(180). Some of these structural parameters have also been evaluated in vivo with consistent results(181–183). Further, scaffold microstructure has been demonstrated to have a strong effect on drug release kinetics(81). To date, the effect of fiber intersection density on cell and tissue behavior remains unclear. Such a study would be appropriately evaluated in a non-weight bearing subcutaneous implant model in order to decouple the mechanical response from

the structure. This is important, as there is evidence that mechanically functional tissues have a preferred pattern of ECM elaboration(108). It is currently unclear whether the effect is caused by local chemical signaling or by patterns of mechanical loading and stress from the surrounding tissue(106).

6.1.2 Curvilinear fibers

Chapter 4 presented a method of fabricating planar electrospun constructs with curvilinear fiber microarchitectures. SALS analysis and biomechanical modeling hypothesized that fibrous constructs with aligned structures which altered their main angle of alignment would behave in a manner consistent with native valve leaflets. This hypothesis was confirmed in that constructs designed to mimic the curvilinear architecture of a pulmonary valve possessed similar levels of planar mechanical anisotropy under equibiaxial loading, however more work remains in order to verify that similarly fabricated structures would be successful as a valve leaflet replacement.

As discussed in Chapter 3, the flexural response of potential biomimetic valve leaflet materials is of paramount importance. For this reason, electrospun constructs with curvilinear microarchitectures should be mechanically tested under flexure. Should these materials possess high bending moduli, they may be modified with sacrificial PEO fibers (Chapter 3). In this case, careful study would be necessary to prevent delamination due to the removed fibers. It is unlikely that attempts to modify fiber intersection density would be successful, as fiber intersection density is decreased with increasing fiber orientation index(48). Further evaluation could also be accomplished in a simulated in vivo environment such as a pulse duplicating flow loop. Such a device could be designed with stereoscopic imaging and strain tracking(184) in order to observe leaflet motion compared to native tissue under physiologic loads. Additionally,

contrast dye could be utilized to determine the presence of vortices which have been associated with negative phenotypic remodeling in vivo(138).

6.2 COMPOSITIONAL MODIFICATIONS

Compositional modifications to electrospun scaffolds have the capability to radically alter the mechanical and biological functionality of tissue engineering scaffolds. Such modifications have been extensively studied in vivo recently with promising results.

Electrospun constructs have been fabricated with multiple fiber populations for several years(185). Such constructs were most often utilized to impart biological functionality through drug incorporation(81) or ECM proteins(186). Secondary fiber populations have also been associated with increased mechanical strength under tension and altered degradation kinetics(83). Chapter 3 of this dissertation demonstrated that introduction of high modulus fibers within elastomeric electrospun constructs can be utilized to predictably increase bulk tensile and bending moduli. In this manner, high strength materials may be combined with alternate materials which may deform at lower stresses in order to more accurately mimic mechanical response of complex mechanically functional materials in both planar and flexural behavior. Moreover, secondary fiber populations can be designed with different degradation kinetics from the primary population. This could be utilized for controlled drug release or producing constructs with larger pore sizes and a more loose structure in the meso-scale.

Studies involving electrospun scaffolds implanted within functional in vivo environments indicate that while the nano-microfibrous topology can be instructive toward cellular behavior, meso-scale porosity is critical for tissue ingrowth and positive functional outcomes. Materials

implanted with compact structures on the meso scale demonstrated limited ingrowth and ECM elaboration(150) whereas when constructs were produced with loosened meso structures, rapid infiltration and remodeling was observed(92,181,187). One method of improving meso-scale porosity and cell infiltration involves electrospinning sacrificial fiber populations within electrospun constructs. First demonstrated by Baker et al, this technique was originally hypothesized to permit more robust cellular infiltration within the bulk of electrospun scaffolds(94). This technique has been repeated by several researchers and confirmed that in vivo cellularity is markedly improved by increasing inter-fiber space using this technique(92,181,187). Consistent with previous reports, Chapter 4 demonstrated a predictable decrease in tensile modulus with increasing sacrificial fiber content. This was further associated with a decrease in bending modulus compared with similarly fabricated PEUU constructs. It was hypothesized that the stiff-when-dry PEO fibers supported residual stress within the elastomeric PEUU fiber network which was responsible for the pronounced microstructural change observed when PEO fibers were dissolved (**Figure 14**). The resulting scaffold appeared contracted and more compact, however the structure was not tightly bound together in this conformation and was able to deform easily and permit infiltrating cells. This could reasonably be a mechanism for decreased moduli within these groups, however it follows logically that electrospun elastomeric constructs which share similar loose structures may also share similar mechanical behaviors.

The wet electrospinning technique is also capable of producing constructs with loose fiber structures which permit greater cell infiltration in vivo(108). During fabrication, a layer of aqueous fluid deposits over the entire surface of the mandrel and forms a thin layer which adheres to the rotating mandrel and scaffold surface. As fibers deposit on the fluid surface they

are likely slowed and partially coagulated due to non-solvent effects. If this hypothesis is valid, fibers would not be subjected to as large pulling forces due to mandrel motion and would also be less tightly bound to surrounding fibers which could permit motion rather than impose residual stress. It would also be likely that premature fiber coagulation would dampen the final elongation forces, and therefore form a larger final fiber diameter. Hashizume et al.(108) and 21 provide evidence of these structural changes which may be caused by the fluid layer present during wet electrospinning. Given this evidence, it is possible that molecular orientation may not be pronounced in wet electrospun constructs, and therefore it may be the case that wet electrospun polyurethanes possess attractive bending moduli for use in heart valve tissue engineering. These hypotheses could be verified through x-ray diffraction and flexural mechanical testing, respectively. It can further be predicted that the general patterns outlined in 37 with respect to fiber translational speed, fiber microarchitecture, and bending modulus would remain consistent with wet electrospun PEUU.

For future development of these techniques into potential cardiovascular therapies preliminary in vivo evaluation should be pursued. Insights from Chapter 5 as well as previous studies from our group(28) suggest that in a blood contacting environments, seeded cells help to prevent thrombosis. 78 describes the particular value of precursor cells in tissue engineering constructs. Microintegrated cells were not shown to proliferate in any meaningful way, however MDSCs were shown to express large quantities of cytokines that have been associated with cardiovascular repair. In this manner, constructs seeded with MDSCs developed an endothelial layer faster than constructs seeded with endothelial cells. These results may be extrapolated into design for future heart valve tissue engineering research. Mechanically optimized, seeded polyurethane scaffolds could be fabricated using techniques developed in this dissertation

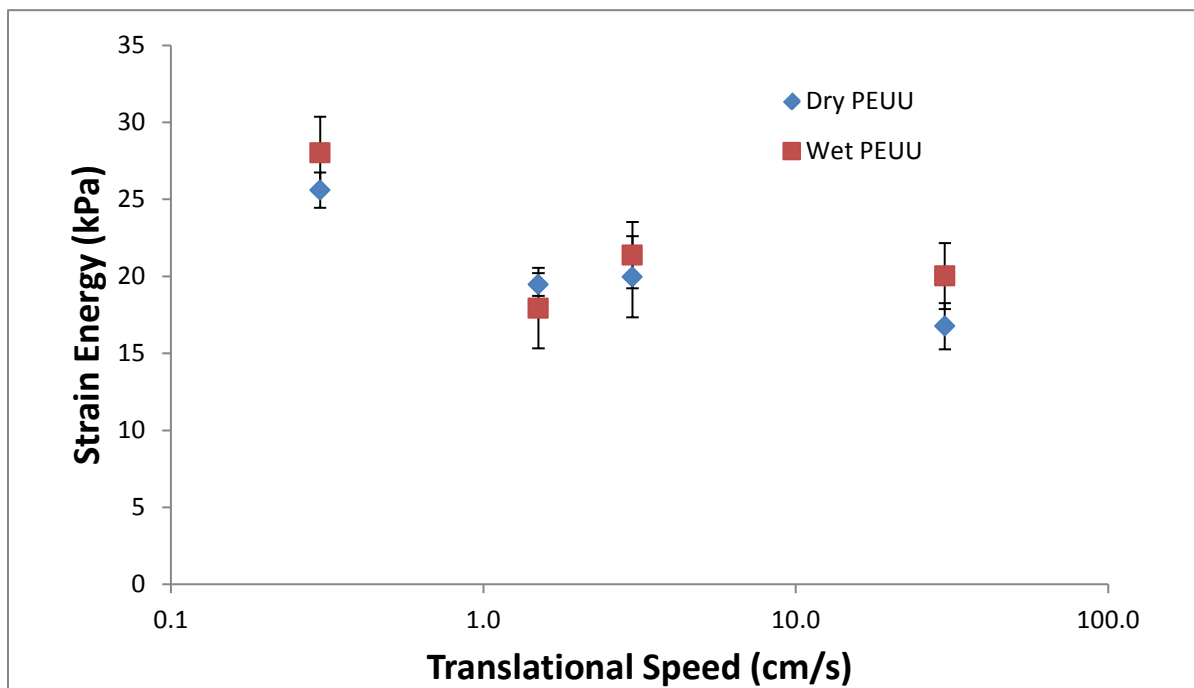
including simultaneous precursor cell electrospray and sacrificial fiber electrospinning. Following in vitro characterization including flexural testing, leaflets could be implanted in an ovine heart valve model. Based on previous results from several groups, as well as those presented in Chapter 5, few cells penetrate perpendicularly through electrospun scaffold surfaces, even in constructs designed to improve cellular infiltration. Therefore, ideal evaluation would attach leaflet scaffolds to native tissue, rather than a polymeric conduit. It would be expected that cell infiltration into the bulk of the scaffold would most likely originate in the vascular anastomosis rather than from circulating progenitor cells.

6.3 CLOSING REMARKS

The preceding dissertation outlines a series of experiments designed to modify the topology and composition of electrospun constructs in order to guide mechanics and bioactivity toward cardiovascular tissue engineering, specifically heart valves and cardiac wall. This research represents a small increase in the understanding of the in vitro and in vitro mechanical and biological behavior of complex electrospun scaffolds. A great deal of work remains to be done, however it is the hope of this author that techniques or results from this research may impact clinically relevant treatments.

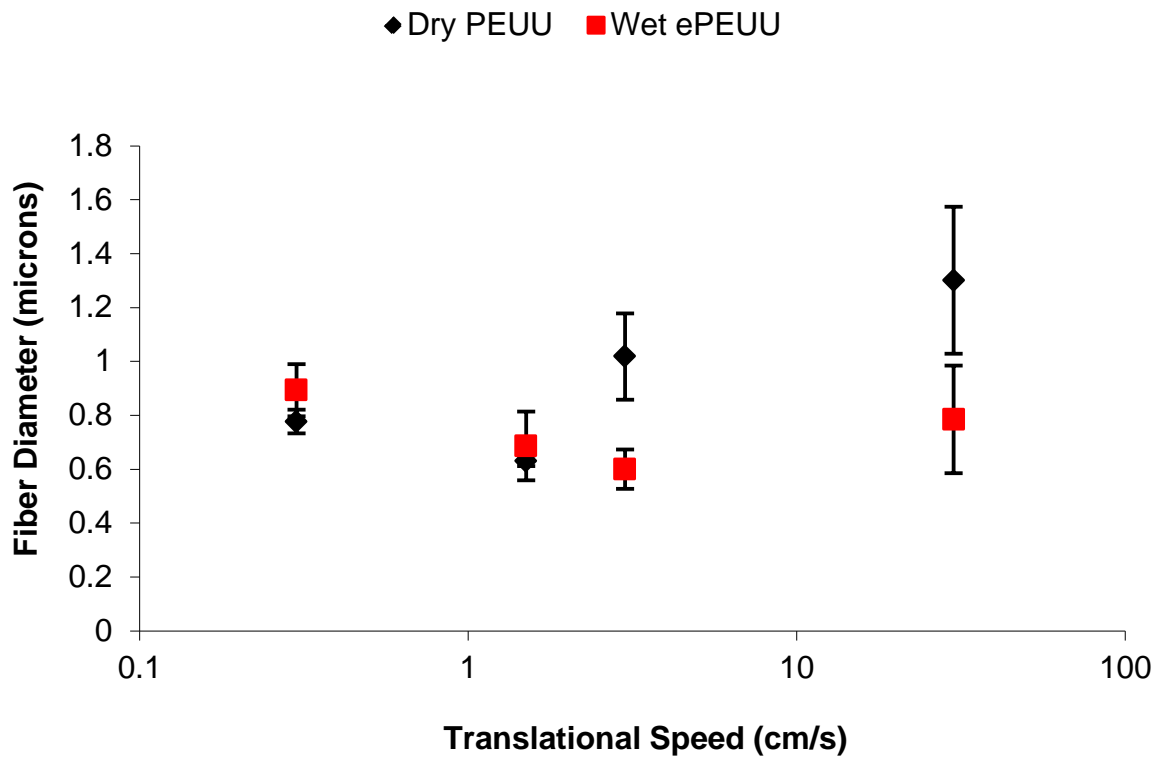
APPENDIX A

STRAIN ENERGY COMPARISON BETWEEN WET AND DRY ELECTROSPUN PEUU



APPENDIX B

FIBER DIAMETER AS A FUNCTION OF TRANSLATIONAL SPEED IN WET AND DRY PEUU



APPENDIX C

UNIAXIAL TENSILE MECHANICS OF DRY PEUU

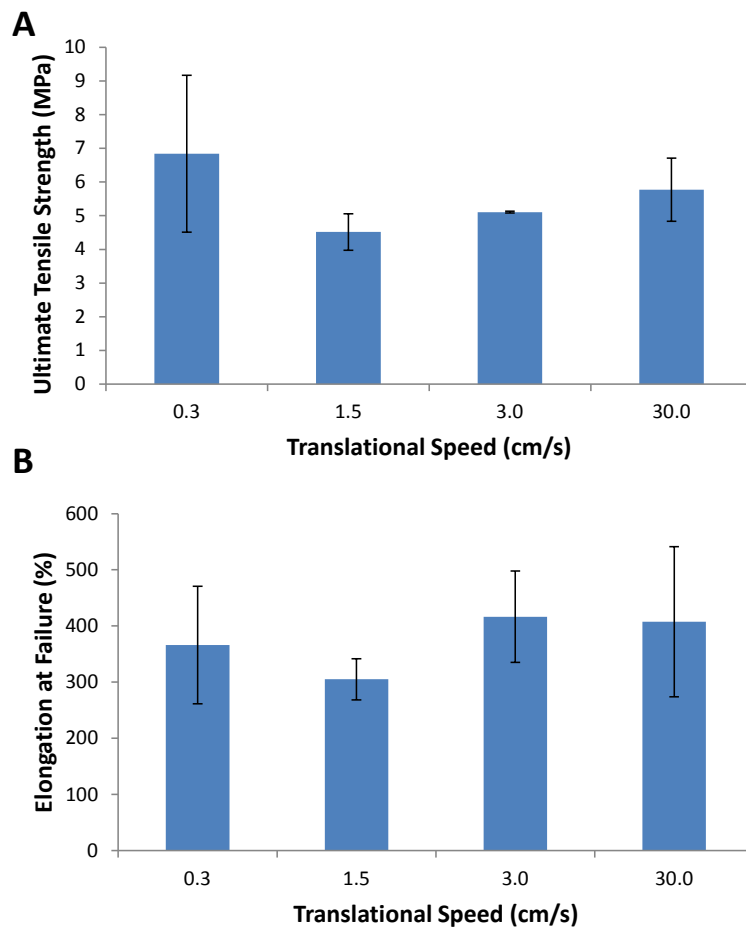


Figure 34 A. Ultimate tensile strength of dry PEUU under uniaxial load.. Elongation at failure of dry PEUU under uniaxial tensile load. Constructs fabricated at different translational speeds were not significantly different under these measures.

APPENDIX D

BULK CELLULARITY IN EXPLANTED CONSTRUCTS

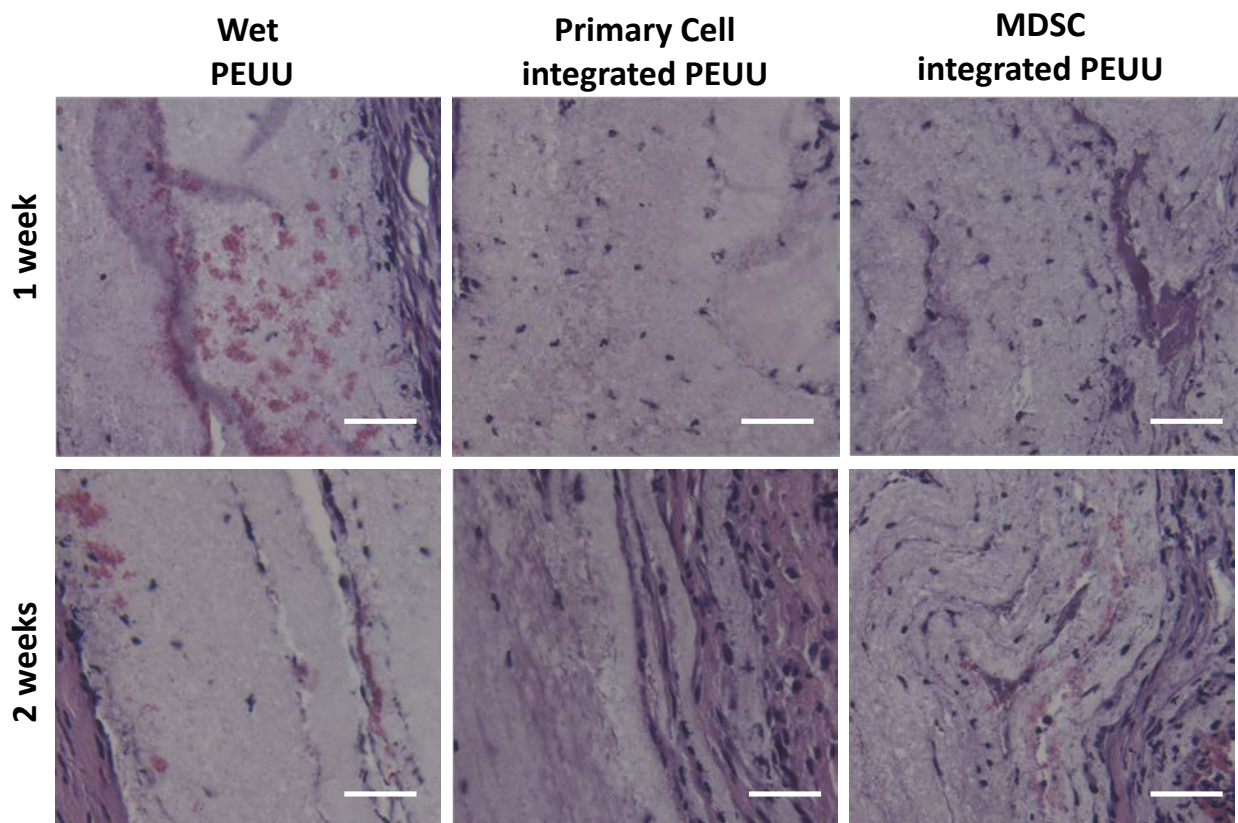


Figure 35. H&E stained micrographs depicting cellularity in the central region of electrospun PEUU patches in each group at each timepoint. Scale bar = 50 μ m

APPENDIX E

ANASTOMOSIS WITH HEALTHY TISSUE

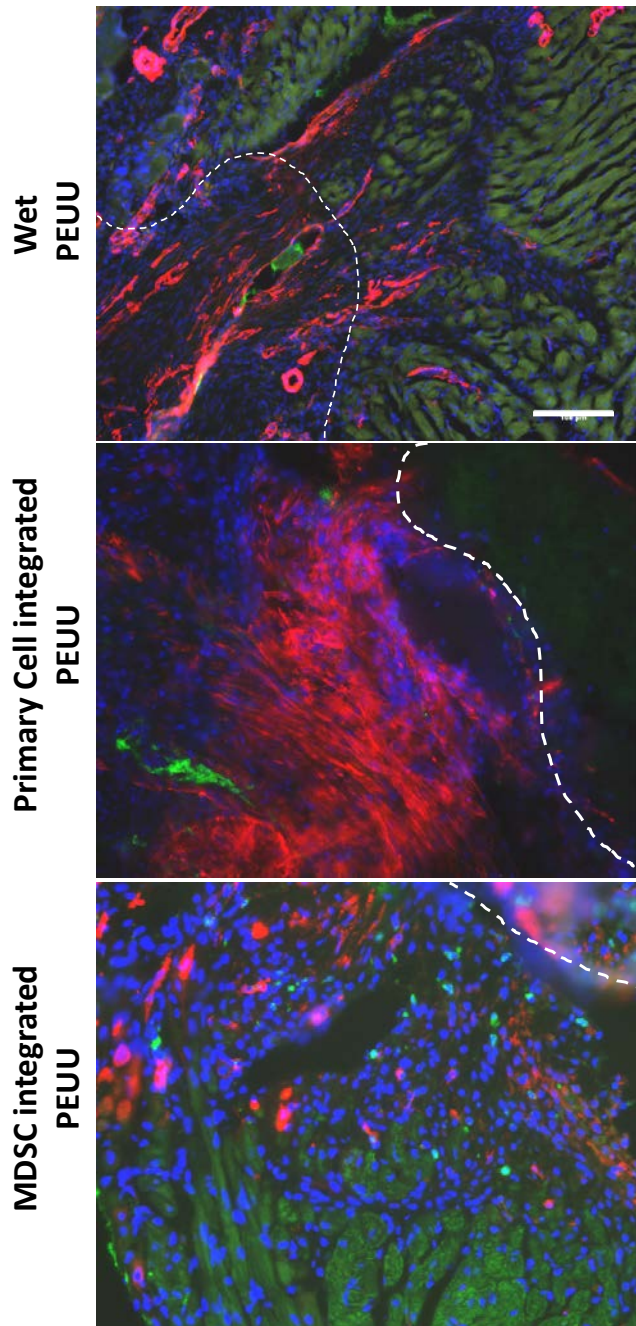


Figure 36. Immunofluorescent micrographs depicting the anastomosis with healthy RVOT tissue in each group at two weeks post implantation. Dotted line = PEUU border. Green = vWF, Red = α -SMA, Blue = cell nuclei. Scale bar = 100 μ m

BIBLIOGRAPHY

1. Roger VL, Go AS, Lloyd-Jones DM, Benjamin EJ, Berry JD, Borden WB, et al. Heart disease and stroke statistics--2012 update: a report from the American Heart Association. *Circulation*. 2012;125(1):e13–e228.
2. Schmidt CE, Baier JM. Acellular vascular tissues: natural biomaterials for tissue repair and tissue engineering. *Biomaterials*. 2000;21(22):2215–31.
3. Gilbert TW. Strategies for tissue and organ decellularization. *Journal of Cellular Biochemistry*. 2012;113(7):2217–22.
4. Badylak SF, Freytes DO, Gilbert TW. Extracellular matrix as a biological scaffold material: Structure and function. *Acta Biomaterialia*. 2009;5(1):1–13.
5. Manni ML, Czajka CA, Oury TD, Gilbert TW. Extracellular matrix powder protects against bleomycin-induced pulmonary fibrosis. *Tissue Engineering: Part A*. 2011;17(21 and 22):2795–804.
6. Badylak SF, Vorp DA, Spievack AR, Simmons-Byrd A, Hanke J, Freytes DO, Thapa A, Gilbert TW, Nieponice A. Esophageal reconstruction with ECM and muscle tissue in a dog model. *The Journal of Surgical Research*. 2005;128(1):87–97.
7. Remlinger NT, Czajka CA, Juhas ME, Vorp DA, Stolz DB, Badylak SF, Gilbert S, Gilbert TW. Hydrated xenogeneic decellularized tracheal matrix as a scaffold for tracheal reconstruction. *Biomaterials*. 2010;31(13):3520–6.
8. Yang S, Leong K-F, Du Z, Chua C. The design of scaffolds for use in tissue engineering. Part I. Traditional factors. *Tissue Engineering*. 2001;7(6):679–89.
9. Kim B, Baez CE, Atala A. Biomaterials for tissue engineering. *World Journal of Urology*. 2000;1(18):2–9.
10. LifeNet Health. Product information for sterile decellularized dermis. 2007 p. 0–1.
11. Rippel RA, Ghanbari H, Seifalian AM. Tissue-engineered heart valve: future of cardiac surgery. *World Journal of Surgery*. 2012;36(7):1581–91.

12. Guan J, Wagner WR. Synthesis, characterization and cytocompatibility of polyurethaneurea elastomers with designed elastase sensitivity. *Biomacromolecules*. 2005;6(5):2833–42.
13. Guan J, Sacks MS, Beckman EJ, Wagner WR. Synthesis, characterization, and cytocompatibility of elastomeric, biodegradable poly(ester-urethane)ureas based on poly(caprolactone) and putrescine. *Journal of Biomedical Materials Research*. 2002;61(3):493–503.
14. Guelcher SA, Gallagher KM, Didier JE, Klinedinst DB, Doctor JS, Goldstein AS, Wilkes GL, Beckman EJ, Hollinger JO. Synthesis of biocompatible segmented polyurethanes from aliphatic diisocyanates and diurea diol chain extenders. *Acta Biomaterialia*. 2005;1(4):471–84.
15. Wang F, Li Z, Lannutti JL, Wagner WR, Guan J. Synthesis, characterization and surface modification of low moduli poly(ether carbonate urethane)ureas for soft tissue engineering. *Acta Biomaterialia*. 2009;5(8):2901–12.
16. Zhang J-Y, Beckman EJ, Hu J, Yang G-G, Agarwal S, Hollinger JO. Synthesis, biodegradability, and biocompatibility of lysine diisocyanate-glucose polymers. *Tissue Engineering*. 2002;8(5):771–85.
17. Fujimoto KL, Ma Z, Nelson DM, Hashizume R, Guan J, Tobita K, Wagner WR. Synthesis, characterization and therapeutic efficacy of a biodegradable, thermoresponsive hydrogel designed for application in chronic infarcted myocardium. *Biomaterials*. 2009;30(26):4357–68.
18. Zhang J, Doll BA, Beckman EJ, Hollinger JO. A biodegradable polyurethane-ascorbic acid scaffold for bone tissue engineering. *Journal of Biomedical Materials Research. Part A*. 2003;67(2):389–400.
19. Runge MB, Dadsetan M, Baltrusaitis J, Knight AM, Ruesink T, Lazcano EA, Lu L, Windebank AJ, Yaszemski MJ. The development of electrically conductive polycaprolactone fumarate-polypyrrole composite materials for nerve regeneration. *Biomaterials*. 2010;31(23):5916–26.
20. Sivak WN, Zhang J, Petoud S, Beckman EJ. Incorporation of ionic ligands accelerates drug release from LDI-glycerol polyurethanes. *Acta Biomaterialia*. 2010;6(1):144–53.
21. Woo KM, Chen VJ, Ma PX. Nano-fibrous scaffolding architecture selectively enhances protein adsorption contributing to cell attachment. *Journal of Biomedical Materials Research. Part A*. 2003;67(2):531–7.
22. Ranieri JP, Bellamkonda R, Bekos EJ, Gardella JA, Mathieu HJ, Ruiz L, Aebischer P. Spatial control of neuronal cell attachment and differentiation on covalently patterned

- laminin oligopeptide substrates. *International Journal of Developmental Neuroscience*. 1994;12(8):725–35.
23. Soletti L, Nieponice A, Hong Y, Ye S-H, Stankus JJ, Wagner WR, Vorp DA. In vivo performance of a phospholipid-coated bioerodable elastomeric graft for small-diameter vascular applications. *Journal of Biomedical Materials Research. Part A*. 2011;96(2):436–48.
 24. Oh H-I, Ye S-H, Johnson CA, Woolley JR, Federspiel WJ, Wagner WR. Hemocompatibility assessment of carbonic anhydrase modified hollow fiber membranes for artificial lungs. *Artificial Organs*. 2010;34(5):439–42.
 25. Guan J, Fujimoto KL, Wagner WR. Elastase-sensitive elastomeric scaffolds with variable anisotropy for soft tissue engineering. *Pharmaceutical Research*. 2008;25(10):2400–12.
 26. Hong Y, Fujimoto K, Hashizume R, Guan J, Stankus JJ, Tobita K, Wagner WR. Generating elastic, biodegradable polyurethane/poly(lactide-co-glycolide) fibrous sheets with controlled antibiotic release via two-stream electrospinning. *Biomacromolecules*. 2008;9(4):1200–7.
 27. Ma Z, Hong Y, Nelson DM, Pichamuthu JE, Leeson CE, Wagner WR. Biodegradable polyurethane ureas with variable polyester or polycarbonate soft segments: effects of crystallinity, molecular weight, and composition on mechanical properties. *Biomacromolecules*. 2011;12(9):3265–74.
 28. Nieponice A, Soletti L, Guan J, Hong Y, Gharaibeh B, Maul TM, Huard J, Wagner WR, Vorp DA. In vivo assessment of a tissue-engineered vascular graft combining a biodegradable elastomeric scaffold and muscle-derived stem cells in a rat model. *Tissue Engineering. Part A*. 2010;16(4):1215–23.
 29. Fujimoto KL, Tobita K, Merryman WD, Guan J, Momoi N, Stolz DB, Sacks MS, Keller BB, Wagner WR. An elastic, biodegradable cardiac patch induces contractile smooth muscle and improves cardiac remodeling and function in subacute myocardial infarction. *Journal of the American College of Cardiology*. 2007;49(23):2292–300.
 30. Fujimoto KL, Guan J, Oshima H, Sakai T, Wagner WR. In vivo evaluation of a porous, elastic, biodegradable patch for reconstructive cardiac procedures. *The Annals of Thoracic Surgery*. 2007;83(2):648–54.
 31. Wright LD, Young RT, Andric T, Freeman JW. Fabrication and mechanical characterization of 3D electrospun scaffolds for tissue engineering. *Biomedical Materials*. 2010;5(5):055006-1-9.
 32. Soletti L, Nieponice A, Guan J, Stankus JJ, Wagner WR, Vorp DA. A seeding device for tissue engineered tubular structures. *Biomaterials*. 2006;27(28):4863–70.

33. Yang F, Qu X, Cui W, Bei J, Yu F, Lu S, Wang S. Manufacturing and morphology structure of polylactide-type microtubules orientation-structured scaffolds. *Biomaterials*. 2006;27(28):4923–33.
34. Greiner A, Wendorff JH. Electrospinning: A fascinating method for the preparation of ultrathin fibers. *Angewandte Chemie*. 2007;46(30):5670–703.
35. Lannutti J, Reneker D, Ma T, Tomasko D, Farson D. Electrospinning for tissue engineering scaffolds. *Materials Science and Engineering: C*. 2007;27(3):504–9.
36. Nisbet DR, Rodda AE, Horne MK, Forsythe JS, Finkelstein DI. Neurite infiltration and cellular response to electrospun polycaprolactone scaffolds implanted into the brain. *Biomaterials*. 2009;30(27):4573–80.
37. Kai D, Prabhakaran MP, Jin G, Ramakrishna S. Guided orientation of cardiomyocytes on electrospun aligned nanofibers for cardiac tissue engineering. *Journal of Biomedical Materials Research. Part B, Applied Biomaterials*. 2011; 16:1–8.
38. Phipps MC, Clem WC, Catledge SA, Xu Y, Hennessy KM, Thomas V, Jablonsky MJ, Chowdhury S, Stanishevsky AV, Vohra YK, Bellis SL. Mesenchymal stem cell responses to bone-mimetic electrospun matrices composed of polycaprolactone, collagen I and nanoparticulate hydroxyapatite. *PloS one*. 2011;6(2):e16813.
39. Blakeney BA, Tambralli A, Anderson JM, Andukuri A, Lim D-J, Dean DR, Jun HW. Cell infiltration and growth in a low density, uncompressed three-dimensional electrospun nanofibrous scaffold. *Biomaterials*. 2011;32(6):1583–90.
40. Lowery JL, Datta N, Rutledge GC. Effect of fiber diameter, pore size and seeding method on growth of human dermal fibroblasts in electrospun poly(epsilon-caprolactone) fibrous mats. *Biomaterials*. 2010;31(3):491–504.
41. Mei F, Zhong J, Yang X, Ouyang X, Zhang S, Hu X, Ma Q, Lu J, Ryu S, Deng X. Improved biological characteristics of poly(L-lactic acid) electrospun membrane by incorporation of multiwalled carbon nanotubes/hydroxyapatite nanoparticles. *Biomacromolecules*. 2007;8(12):3729–35.
42. Nisbet DR, Forsythe JS, Shen W, Finkelstein DI, Horne MK. A review of the cellular response on electrospun nanofibers for tissue engineering. *Journal of Biomaterials Applications*. 2009;24(1):7–29.
43. Reneker DH, Yarin AL. Electrospinning jets and polymer nanofibers. *Polymer*. 2008;49(10):2387–425.
44. McKee MG, Elkins CL, Long TE. Influence of self-complementary hydrogen bonding on solution rheology/electrospinning relationships. *Polymer*. 2004;45(26):8705–15.

45. Shenoy S, Bates W, Frisch H, Wnek G. Role of chain entanglements on fiber formation during electrospinning of polymer solutions: good solvent, non-specific polymer-polymer interaction limit. *Polymer*. 2005;46(10):3372–84.
46. Rutledge GC, Fridrikh S V. Formation of fibers by electrospinning. *Advanced Drug Delivery Reviews*. 2007;59(14):1384–91.
47. Feng C, Khulbe KC, Matsuura T. Recent progress in the preparation , characterization , and applications of nanofibers and nanofiber membranes via electrospinning / interfacial polymerization. *Journal of Applied Polymer Science*. 2010;115:756–76.
48. D'Amore A, Stella JA, Wagner WR, Sacks MS. Characterization of the complete fiber network topology of planar fibrous tissues and scaffolds. *Biomaterials*. 2010;31(20):5345–54.
49. Han T, Yarin AL, Reneker DH. Viscoelastic electrospun jets: Initial stresses and elongational rheometry. *Polymer*. 2008;49(6):1651–8.
50. Thompson CJ, Chase GG, Yarin AL, Reneker DH. Effects of parameters on nanofiber diameter determined from electrospinning model. *Polymer*. 2007;48(23):6913–22.
51. Fridrikh S, Yu J, Brenner M, Rutledge G. Controlling the Fiber Diameter during Electrospinning. *Physical Review Letters*. 2003;90(14):144502-1-4.
52. Dong Z, Wu Y, Clark RL. Thermodynamic modeling and investigation of the formation of electrospun collagen fibers. *Langmuir*. 2011;27(20):12417-22.
53. Lu C, Chen P, Li J, Zhang Y. Computer simulation of electrospinning. Part I. Effect of solvent in electrospinning. *Polymer*. 2006;47(3):915–21.
54. Pham QP, Sharma U, Mikos AG. Electrospinning of polymeric nanofibers for tissue engineering applications: a review. *Tissue Engineering*. 2006;12(5):1197–211.
55. Rnjak-Kovacina J, Weiss AS. Increasing the Pore Size of Electrospun Scaffolds. *Tissue Engineering. Part B, Reviews*. 2011;17(5):365-72.
56. De Vrieze S, Camp T, Nelvig A, Hagström B, Westbroek P, Clerck K. The effect of temperature and humidity on electrospinning. *Journal of Materials Science*. 2008;44(5):1357–62.
57. Vaquette C, Cooper-White J. The use of an electrostatic lens to enhance the efficiency of the electrospinning process. *Cell and Tissue Research*. 2012;815–26.
58. Brown TD, Dalton PD, Hutmacher DW. Direct writing by way of melt electrospinning. *Advanced Materials*. 2011;23(47):5651–7.

59. Liu Y, Zhang X, Xia Y, Yang H. Magnetic-field-assisted electrospinning of aligned straight and wavy polymeric nanofibers. *Advanced Materials*. 2010;22(22):2454–7.
60. Theron A, Zussman E, Yarin AL. Electrostatic field-assisted alignment of electrospun nanofibres. *Nanotechnology*. 2001;12:384–90.
61. Xu C, Inai R, Kotaki M, Ramakrishna S. Aligned biodegradable nanofibrous structure: a potential scaffold for blood vessel engineering. *Biomaterials*. 2004;25(5):877–86.
62. Neves NM, Campos R, Pedro A, Cunha J, Macedo F, Reis RL. Patterning of polymer nanofiber meshes by electrospinning for biomedical applications. *International Journal of Nanomedicine*. 2007;2(3):433–48.
63. Kakade M V, Givens S, Gardner K, Lee KH, Chase DB, Rabolt JF. Electric field induced orientation of polymer chains in macroscopically aligned electrospun polymer nanofibers. *Journal of the American Chemical Society*. 2007;129(10):2777–82.
64. Chaurey V, Chiang P-C, Polanco C, Su Y-H, Chou C-F, Swami NS. Interplay of electrical forces for alignment of sub-100 nm electrospun nanofibers on insulator gap collectors. *Langmuir*. 2010;26(24):19022–6.
65. Ding Z, Salim A, Ziaie B. Selective nanofiber deposition through field-enhanced electrospinning. *Langmuir*. 2009;25(17):9648–52.
66. Li D, Ouyang G, McCann JT, Xia Y. Collecting electrospun nanofibers with patterned electrodes. *Nano Letters*. 2005;5(5):913–6.
67. Stankus JJ, Guan J, Wagner WR. Fabrication of biodegradable elastomeric scaffolds with sub-micron morphologies. *Journal of Biomedical Materials Research. Part A*. 2004;70(4):603–14.
68. Courtney T, Sacks MS, Stankus J, Guan J, Wagner WR. Design and analysis of tissue engineering scaffolds that mimic soft tissue mechanical anisotropy. *Biomaterials*. 2006;27(19):3631–8.
69. Li W-J, Mauck RL, Cooper JA, Yuan X, Tuan RS. Engineering controllable anisotropy in electrospun biodegradable nanofibrous scaffolds for musculoskeletal tissue engineering. *Journal of Biomechanics*. 2007;40(8):1686–93.
70. Teo WE, Kotaki M, Mo XM, Ramakrishna S. Porous tubular structures with controlled fibre orientation using a modified electrospinning method. *Nanotechnology*. 2005;16(6):918–24.
71. Wang C-Y, Liu J-J, Fan C-Y, Mo X-M, Ruan H-J, Li F-F. The Effect of Aligned Core-Shell Nanofibres Delivering NGF on the Promotion of Sciatic Nerve Regeneration. *Journal of Biomaterials Science. Polymer Edition*. 2010;20(1-4):167-84

72. Yin Z, Chen X, Chen JL, Shen WL, Hieu Nguyen TM, Gao L, Ouyang HW. The regulation of tendon stem cell differentiation by the alignment of nanofibers. *Biomaterials*. 2010;31(8):2163–75.
73. Baker BM, Mauck RL. The effect of nanofiber alignment on the maturation of engineered meniscus constructs. *Biomaterials*. 2007;28(11):1967–77.
74. Ifkovits JL, Wu K, Mauck RL, Burdick JA. The influence of fibrous elastomer structure and porosity on matrix organization. *PLoS one*. 2010;5(12):e15717.
75. Ayres CE, Jha BS, Meredith H, Bowman JR, Bowlin GL, Henderson SC, Simpson DG. Measuring fiber alignment in electrospun scaffolds: a user's guide to the 2D fast Fourier transform approach. *Journal of Biomaterials Science. Polymer Edition*. 2008;19(5):603–21.
76. Casper CL, Yamaguchi N, Kiick KL, Rabolt JF. Functionalizing electrospun fibers with biologically relevant macromolecules. *Biomacromolecules*. 2007;6(4):1998–2007.
77. Srivastava Y, Loscertales I, Marquez M, Thorsen T. Electrospinning of hollow and core/sheath nanofibers using a microfluidic manifold. *Microfluidics and Nanofluidics*. 2007;4(3):245–50.
78. Prabhakaran M, Kai D, Ghasemi-Mobarakeh L, Ramakrishna S. Electrospun biocomposite nanofibrous patch for cardiac tissue engineering. *Biomedical Materials*. 2011;6(5):055001.
79. Sun Z, Zussman E, Yarin AL, Wendorff JH, Greiner A. Compound Core–Shell Polymer Nanofibers by Co-Electrospinning. *Advanced Materials*. 2003;15(22):1929–32.
80. Luong-Van E, Grøndahl L, Chua KN, Leong KW, Nurcombe V, Cool SM. Controlled release of heparin from poly(epsilon-caprolactone) electrospun fibers. *Biomaterials*. 2006;27(9):2042–50.
81. Szentivanyi A, Chakradeo T, Zernetsch H, Glasmacher B. Electrospun cellular microenvironments: Understanding controlled release and scaffold structure. *Advanced Drug Delivery Reviews*. 2011;63(4-5):209–20.
82. Drexler JW, Powell HM. Regulation of electrospun scaffold stiffness via coaxial core diameter. *Acta Biomaterialia*. 2011;7(3):1133–9.
83. Baker BM, Nerurkar NL, Burdick JA, Elliott DM, Mauck RL. Fabrication and modeling of dynamic multipolymer nanofibrous scaffolds. *Journal of Biomechanical Engineering*. 2009;131(10):101012-1-10.
84. Chen ZCC, Ekaputra a K, Gauthaman K, Adaikan PG, Yu H, Hutmacher DW. In vitro and in vivo analysis of co-electrospun scaffolds made of medical grade poly(epsilon-

- caprolactone) and porcine collagen. *Journal of Biomaterials Science. Polymer Edition*. 2008;19(5):693–707.
85. Zhang Y, Su B, Venugopal J, Ramakrishna S, Lim C. Biomimetic and bioactive nanofibrous scaffolds from electrospun composite nanofibers. *International Journal of Nanomedicine*. 2007;2(4):623–38.
 86. Kenar H, Kose GT, Toner M, Kaplan DL, Hasirci V. A 3D aligned microfibrillar myocardial tissue construct cultured under transient perfusion. *Biomaterials*. 2011;32(23):5320–9.
 87. Soliman S, Sant S, Nichol JW, Khabiry M, Traversa E, Khademhosseini A. Controlling the porosity of fibrous scaffolds by modulating the fiber diameter and packing density. *Journal of Biomedical Materials Research. Part A*. 2011;96(3):566–74.
 88. Van Tienen TG, Heijkants RGJC, Buma P, De Groot JH, Pennings AJ, Veth RPH. Tissue ingrowth and degradation of two biodegradable porous polymers with different porosities and pore sizes. *Biomaterials*. 2002;23(8):1731–8.
 89. Milleret V, Hefti T, Hall H, Vogel V, Eberli D. Influence of fiber diameter and surface roughness of electrospun vascular grafts on blood activation. *Acta Biomaterialia*. 2012;8(12):4349–56.
 90. McCullen SD, Gittard SD, Miller PR, Pourdeyhimi B, Narayan RJ, Lobo EG. Laser ablation imparts controlled micro-scale pores in electrospun scaffolds for tissue engineering applications. *Annals of Biomedical Engineering*. 2011;39(12):3021-30
 91. Shim IK, Jung MR, Kim KH, Seol YJ, Park YJ, Park WH, Lee SJ. Novel three-dimensional scaffolds of poly(L-lactic acid) microfibers using electrospinning and mechanical expansion: Fabrication and bone regeneration. *Journal of Biomedical Materials Research. Part B, Applied Biomaterials*. 2010;95(1):150–60.
 92. Phipps MC, Clem WC, Grunda JM, Clines GA, Bellis SL. Increasing the pore sizes of bone-mimetic electrospun scaffolds comprised of polycaprolactone, collagen I and hydroxyapatite to enhance cell infiltration. *Biomaterials*. 2012;33(2):524–34.
 93. Baker BM, Gee AO, Metter RB, Nathan AS, Marklein RA, Burdick JA, Mauck RL. The potential to improve cell infiltration in composite fiber-aligned electrospun scaffolds by the selective removal of sacrificial fibers. *Biomaterials*. 2008;29(15):2348–58.
 94. Baker BM, Shah RP, Silverstein AM, Esterhai JL, Burdick JA, Mauck RL. Sacrificial nanofibrous composites provide instruction without impediment and enable functional tissue formation. *Proceedings of the National Academy of Sciences of the United States of America*. 2012;109(35): 14176-81

95. Simonet M, Schneider OD, Neuenschwander P, Stark WJ. Ultraporous 3D polymer meshes by low-temperature electrospinning : Use of ice crystals as a removable void template. *Polymer Engineering and Science*. 2007;47(12):2020–6.
96. Schneider OD, Weber F, Brunner TJ, Loher S, Ehrbar M, Schmidlin PR, Stark WJ. In vivo and in vitro evaluation of flexible, cottonwool-like nanocomposites as bone substitute material for complex defects. *Acta Biomaterialia*. 2009;5(5):1775–84.
97. Cho WJ, Kim JH, Oh SH, Nam HH, Kim JM, Lee JH. Hydrophilized polycaprolactone nanofiber mesh-embedded poly(glycolic-co-lactic acid) membrane for effective guided bone regeneration. *Journal of Biomedical Materials Research. Part A*. 2009;91(2):400–7.
98. Kolambkar YM, Dupont KM, Boerckel JD, Huebsch N, Mooney DJ, Hutmacher DW, Guldberg RE. An alginate-based hybrid system for growth factor delivery in the functional repair of large bone defects. *Biomaterials*. 2011;32(1):65–74.
99. Redman SN, Oldfield SF, Archer CW. Current strategies for articular cartilage repair. *European Cells & Materials*. 2005;9:23–32.
100. Stankus JJ, Guan J, Fujimoto K, Wagner WR. Microintegrating smooth muscle cells into a biodegradable, elastomeric fiber matrix. *Biomaterials*. 2006;27(5):735–44.
101. Jayasinghe SN, Warnes G, Scotton CJ. Bio-electrosprayed living composite matrix implanted into mouse models. *Macromolecular Bioscience*. 2011;11(10):1364–9.
102. Stankus JJ, Soletti L, Fujimoto K, Hong Y, Vorp DA, Wagner WR. Fabrication of cell microintegrated blood vessel constructs through electrohydrodynamic atomization. *Biomaterials*. 2007;28(17):2738–46.
103. Bartolovic K, Mongkoldhumrongkul N, Waddington SN, Jayasinghe SN, Howe SJ. The differentiation and engraftment potential of mouse hematopoietic stem cells is maintained after bio-electrospray. *Analyst*. 2010;135(1):157–64.
104. Paletta JRJ, Mack F, Schenderlein H, Theisen C, Schmitt J, Wendorff JH, Agarwal S, Fuchs-Winkelmann S, Schofer MD. Incorporation of osteoblasts (MG63) into 3D nanofibre matrices by simultaneous electrospinning and spraying in bone tissue engineering. *European Cells & Materials*. 2011;21:384–95.
105. Patel AS, Smith A, Attia RQ, Mattock K, Humphries J, Lyons O, Saha P, Modarai B, Jayasinghe SN. Encapsulation of angiogenic monocytes using bio-spraying technology. *Integrative Biology*. 2012;4(6):628–32.
106. Stella JA, Liao J, Hong Y, Merryman WD, Wagner WR, Sacks MS. Tissue-to-cellular level deformation coupling in cell micro-integrated elastomeric scaffolds. *Biomaterials*. 2008;29(22):3228–36.

107. Stella JA, Amoroso NJ, D'Amore A, Mayer JE, Wagner WR, Sacks MS. Effects of finite deformation on extracellular matrix production and mechanical properties. *Proceedings of Heart Valve Biology and Tissue Engineering*. 2012. p. 13.
108. Hashizume R, Fujimoto KL, Hong Y, Amoroso NJ, Tobita K, Miki T, Keller BB, Sacks MS, Wagner WR. Morphological and mechanical characteristics of the reconstructed rat abdominal wall following use of a wet electrospun biodegradable polyurethane elastomer scaffold. *Biomaterials*. 2010;31(12):3253–65.
109. Criscione JC, Sacks MS, Hunter WC. Experimentally tractable, pseudo-elastic constitutive law for biomembranes: II. Application. *Journal of Biomechanical Engineering*. 2003;125(1):100-5.
110. Criscione JC, Sacks MS, Hunter WC. Experimentally tractable, pseudo-elastic constitutive law for biomembranes: I. Theory. *Journal of Biomechanical Engineering*. 2003;125(1):94-9.
111. Billiar KL, Sacks MS. Biaxial mechanical properties of the native and glutaraldehyde-treated aortic valve cusp: Part II--A structural constitutive model. *Journal of Biomechanical Engineering*. 2000;122(4):327–35.
112. Bringman S, Conze J, Cuccurullo D, Deprest J, Junge K, Klosterhalfen B, Parra-Davila E, Ramshaw B, Schumpelick V. Hernia repair: the search for ideal meshes. *Hernia*. 2010;14(1):81–7.
113. Durst CA, Cuchiara MP, Mansfield EG, West JL, Grande-Allen KJ. Flexural characterization of cell encapsulated PEGDA hydrogels with applications for tissue engineered heart valves. *Acta Biomaterialia*. 2011;7(6):2467–76.
114. Mirnajafi A, Raymer JM, McClure LR, Sacks MS. The flexural rigidity of the aortic valve leaflet in the commissural region. *Journal of Biomechanics*. 2006;39(16):2966–73.
115. Gloeckner DC, Billiar KL, Sacks MS. Effects of Mechanical Fatigue on the Bending Properties of the Porcine Bioprosthetic Heart Valve. *ASAIO Journal*. 1999;45(1):59–63.
116. Dainese L, Guarino A, Burba I, Esposito G, Pompilio G, Polvani G, Rossini A. Heart valve engineering: decellularized aortic homograft seeded with human cardiac stromal cells. *Artificial Cells, Blood Substitutes and Biotechnology*. 2012;21(1):125–34.
117. Cebotari S, Tudorache I, Jaekel T, Hilfiker A, Dorfman S, Ternes W, Haverich A, Lichtenberg A. Detergent decellularization of heart valves for tissue engineering: Toxicological effects of residual detergents on human endothelial cells. *Artificial Organs*. 2010;34(3):206–10.
118. Shinoka T. Tissue engineered heart valves: Autologous cell seeding on biodegradable polymer scaffold. *Artificial Organs*. 2002;26(5):402–6.

119. Hoerstrup SP, Kadner A, Melnitchouk S, Trojan A, Tracy J, Sodian R, Visjager JF, Grunenfelder J, Zund G, Turina MI. Tissue engineering of functional trileaflet heart valves from human marrow stromal cells. *Circulation*. 2002;106(12 Suppl 1):i145-50.
120. Schmidt D, Mol A, Breymann C, Achermann J, Odermatt B, Gössi M, Neuenschwander S, Prêtre R, Genoni M, Zund G, Hoerstrup SP. Living autologous heart valves engineered from human prenatally harvested progenitors. *Circulation*. 2006;114(1 Suppl):i125–31.
121. Stock U, Schenke-Layland K. Performance of decellularized xenogeneic tissue in heart valve replacement. *Biomaterials*. 2006;27(1)1-2.
122. Takagi K, Fukunaga S, Nishi A, Shojima T, Yoshikawa K, Hori H, Akashi H, Aoyagi S. In vivo recellularization of plain decellularized xenografts with specific cell characterization in the systemic circulation: histological and immunohistochemical study. *Artificial Organs*. 2006;30(4):233–41.
123. White J, Agnihotri A, Titus J, Torchiana D. A stentless trileaflet valve from a sheet of decellularized porcine small intestinal submucosa. *Annals of Thoracic Surgery*. 2005;80(2):704–7.
124. Ruiz C, Iemura M, Medie S, Varga P, Van Alstine W, Mack S, Deligio A, Fearnot N, Beier UH, Pavcnik D, Hijazi ZM, Kiupel M. Transcatheter placement of a low-profile biodegradable pulmonary valve made of small intestinal submucosa: a long-term study in a swine model. *Journal of Thoracic and Cardiovascular Surgery*. 2005;130(2):477–84.
125. Roy R, Kohles SS, Zaporozhan V, Peretti GM, Randolph MA, Xu J, Bonassar LJ. Analysis of bending behavior of native and engineered auricular and costal cartilage. *Journal of Biomedical Materials Research. Part A*. 2004;68(4):597–602.
126. Williams SK, Kleinert LB, Patula-Steinbrenner V. Accelerated neovascularization and endothelialization of vascular grafts promoted by covalently bound laminin type 1. *Journal of Biomedical Materials Research. Part A*. 2011;99(1):67–73.
127. Merryman WD, Huang H-YS, Schoen FJ, Sacks MS. The effects of cellular contraction on aortic valve leaflet flexural stiffness. *Journal of Biomechanics*. 2006;39(1):88–96.
128. Eckert CE, Fan R, Mikulis B, Barron M, Carruthers CA, Friebe VM, Vyavahare NR, Sacks MS. On the biomechanical role of glycosaminoglycans in the aortic heart valve leaflet. *Acta Biomaterialia*. 2012;9(1):4653–60.
129. Tseng H, Grande-Allen KJ. Elastic fibers in the aortic valve spongiosa: a fresh perspective on its structure and role in overall tissue function. *Acta Biomaterialia*. 2011;7(5):2101–8.
130. Schoen F. Aortic valve structure-function correlations: role of elastic fibers no longer a stretch of the imagination. *The Journal of Heart Valve Disease*. 1997;6(1):1–6.

131. Schoen F, Levy R. Calcification of tissue heart valve substitutes: progress toward understanding and prevention. *The Annals of Thoracic Surgery*. 2005;79(3):1072-80
132. Merryman WD. Insights into (the interstitium of) degenerative aortic valve disease. *Journal of the American College of Cardiology*. 2008;51(14):1415.
133. Hu J-G, Zhang Y-X, Qi Q, Wang R, Shen L, Zhang C, Xi J, Zhou JS, Lu HZ. Expression of BMP-2 and BMP-4 proteins by type-1 and type-2 astrocytes induced from neural stem cells under different differentiation conditions. *Acta Neurobiologiae Experimentalis*. 2012;72(1):95–101.
134. Weinberg EJ, Shahmirzadi D, Mofrad MRK. On the multiscale modeling of heart valve biomechanics in health and disease. *Biomechanics and Modeling in Mechanobiology*. 2010;9(4):373–87.
135. Joyce EM, Liao J, Schoen FJ, Mayer JE, Sacks MS. Functional collagen fiber architecture of the pulmonary heart valve cusp. *The Annals of Thoracic Surgery*. 2009;87(4):1240–9.
136. Sacks MS. Biaxial mechanical evaluation of planar biological materials. *Journal of Elasticity*. 2000;61:199–246.
137. Mauck RL, Baker BM, Nerurkar NL, Burdick JA, Li W-J, Tuan RS, Elliott DM. Engineering on the straight and narrow: the mechanics of nanofibrous assemblies for fiber-reinforced tissue regeneration. *Tissue Engineering. Part B, Reviews*. 2009;15(2):171–93.
138. Merryman DW. Mechano-potential etiologies of aortic valve disease. *Journal of Biomechanics*. 2010;43(1):87–92.
139. Weiler M, Hwai Yap C, Balachandran K, Padala M, Yoganathan AP. Regional analysis of dynamic deformation characteristics of native aortic valve leaflets. *Journal of Biomechanics*. 2011;44(8):1459–65.
140. Sacks M, Merryman WD, Schmidt D. On the biomechanics of heart valve function. *Journal of Biomechanics*. 2009;42(12):1804–24.
141. Sewell-Loftin MK, Chun YW, Khademhosseni A, Merryman WD. EMT-inducing biomaterials for heart valve engineering: Taking cues from developmental biology. *Journal of Cardiovascular Translational Research*. 2011;4(5):658–71.
142. Butcher JT, Penrod AM, García AJ, Nerem RM. Unique morphology and focal adhesion development of valvular endothelial cells in static and fluid flow environments. *Arteriosclerosis, Thrombosis, and Vascular Biology*. 2004;24(8):1429–34.

143. Merryman WD, Engelmayr GCJ, Liao J, Sacks MS. Defining biomechanical endpoints for tissue engineered heart valve leaflets from native leaflet properties. *Progress in Pediatric Cardiology*. 2006;21(2):153–60.
144. Amoroso NJ, D'Amore A, Hong Y, Rivera CP, Sacks MS, Wagner WR. Microstructural manipulation of electrospun scaffolds for specific bending stiffness for heart valve tissue engineering. *Acta Biomaterialia*. 2012;8(12):4268–77.
145. Fisher MB, Henning EA, Söegaard N, Esterhai JL, Mauck RL. Organized nanofibrous scaffolds that mimic the macroscopic and microscopic architecture of the knee meniscus. *Acta Biomaterialia*. 2012;9(1):4496-504.
146. Seol Y-J, Kim K-H, Kim IA, Rhee S-H. Osteoconductive and degradable electrospun nonwoven poly(epsilon-caprolactone)/CaO-SiO₂ gel composite fabric. *Journal of Biomedical Materials Research. Part A*. 2010;94(2):649–59.
147. Balachandran K, Alford PW, Wylie-Sears J, Goss JA, Grosberg A, Bischoff J, Aikawa E, Levine RA, Parker KK. Cyclic strain induces dual-mode endothelial-mesenchymal transformation of the cardiac valve. *Proceedings of the National Academy of Sciences of the United States of America*. 2011;108(50):19943–8.
148. Hickey EJ, Veldtman G, Bradley TJ, Gengsakul A, Manlhiot C, Williams WG, Webb GD, McCrindle BW. Late risk of outcomes for adults with repaired Tetralogy of Fallot from an inception cohort spanning four decades. *European Journal of Cardio-Thoracic Surgery*. 2009;35(1):156–64.
149. Sinzobahamvya N, Boscheinen M, Blaschczok HC, Kallenberg R, Photiadis J, Haun C, Hraska V, Asfour B. Survival and reintervention after neonatal repair of truncus arteriosus with valved conduit. *European Journal of Cardio-Thoracic Surgery*. 2008;34(4):732–7.
150. Hong Y, Takanari K, Amoroso NJ, Hashizume R, Brennan-Pierce EP, Freund JM, Badylak SF, Wagner WR. An elastomeric patch electrospun from a blended Solution of dermal extracellular matrix and biodegradable polyurethane for rat abdominal wall repair. *Tissue Engineering. Part C*. 2012;18(2):122–33.
151. Kalfa D, Bel A, Chen-Tournoux A, Della Martina A, Rochereau P, Coz C, Bellamy V, Bensalah M, Vanneaux V, Lecourt S, Mousseaux E, Bruneval P, Larghero J, Menasché. A polydioxanone electrospun valved patch to replace the right ventricular outflow tract in a growing lamb model. *Biomaterials*. 2010;31(14):4056–63.
152. Steigman SA, Ahmed A, Shanti RM, Tuan RS, Valim C, Fauza DO. Sternal repair with bone grafts engineered from amniotic mesenchymal stem cells. *Journal of Pediatric Surgery*. 2009;44(6):1120–6.

153. Luong-Van E, Grøndahl L, Song S, Nurcombe V, Cool S. The in vivo assessment of a novel scaffold containing heparan sulfate for tissue engineering with human mesenchymal stem cells. *Journal of Molecular Histology*. 2007;38(5):459–68.
154. Ho STB, Hutmacher DW, Ekaputra AK, Hitendra D, Hui JH. The evaluation of a biphasic osteochondral implant coupled with an electrospun membrane in a large animal model. *Tissue Engineering. Part A*. 2010;16(4):1123–41.
155. Srouji S, Kizhner T, Suss-Tobi E, Livne E, Zussman E. 3-D Nanofibrous electrospun multilayered construct is an alternative ECM mimicking scaffold. *Journal of Materials Science: Materials in Medicine*. 2008;19(3):1249–55.
156. Lu H, Chen W-J, Xing Y, Ying D-J, Jiang B. Design and preparation of an electrospun biomaterial surgical patch. *Journal of Bioactive and Compatible Polymers*. 2009;24(1 Suppl):158–68.
157. Amoroso NJ, D'Amore A, Hong Y, Wagner WR, Sacks MS. Elastomeric electrospun polyurethane scaffolds: the interrelationship between fabrication conditions, fiber topology, and mechanical properties. *Advanced Materials*. 2011;23(1):106-111.
158. Gharaibeh B, Lu A, Tebbets J, Zheng B, Feduska J, Crisan M, Péault B, Cummins J, Huard J. Isolation of a slowly adhering cell fraction containing stem cells from murine skeletal muscle by the preplate technique. *Nature Protocols*. 2008;3(9):1501–9.
159. Serban AMC, Tanasie G, Nistor D, Gavriliuc O. Chemotaxis and differentiation promotor factors of stem cells involved in cardiovascular pathology. *Timisoara Medical Journal*. 2008;58(3-4):135–8.
160. Zerwes HG, Risau W. Polarized secretion of a platelet-derived growth factor-like chemotactic factor by endothelial cells in vitro. *The Journal of Cell Biology*. 1987;105(5):2037–41.
161. Zaruba M-M, Theiss HD, Vallaster M, Mehl U, Brunner S, David R, et al. Synergy between CD26/DPP-IV inhibition and G-CSF improves cardiac function after acute myocardial infarction. *Cell Stem Cell*. 2009;4(4):313–23.
162. Arciniegas E, Sutton AB, Allen TD, Schor AM. Transforming growth factor beta 1 promotes the differentiation of endothelial cells into smooth muscle-like cells in vitro. *Journal of Cell Science*. 1992;103(2):521–9.
163. Gabbiani G, Kocher O, Bloom WS, Vandekerckhove J, Weber K. Actin expression in smooth muscle cells of rat aortic intimal thickening, human atheromatous plaque, and cultured rat aortic media. *Journal of Clinical Investigation*. 1984;73:148–52.

164. Graf K, Xi X-P, Yang D, Fleck E, Hsueh WA., Law RE. Mitogen-activated protein kinase activation is involved in platelet-derived growth factor-directed migration by vascular smooth muscle cells. *Hypertension*. 1997;29(1):334–9.
165. Hayashi K, Saga H, Chimori Y, Kimura K, Yamanaka Y, Sobue K. Differentiated phenotype of smooth muscle cells depends on signaling pathways through insulin-like growth factors and phosphatidylinositol 3-kinase. *The Journal of Biological Chemistry*. 1998;273(44):28860–7.
166. Klemm DJ, Watson PA, Frid MG, Dempsey EC, Schaack J, Colton LA, Nesterova A, Stenmark KR, Reusch JE-B. cAMP response element-binding protein content is a molecular determinant of smooth muscle cell proliferation and migration. *The Journal of Biological Chemistry*. 2001;276(49):46132–41.
167. Ota S, Uehara K, Nozaki M, Kobayashi T, Terada S, Tobita K, Fu FH, Huard J. Intramuscular transplantation of muscle-derived stem cells accelerates skeletal muscle healing after contusion injury via enhancement of angiogenesis. *The American Journal of Sports Medicine*. 2011;39(9):1912–22.
168. Nurden AT. Platelets, inflammation and tissue regeneration. *Thrombosis and Haemostasis*. 2011;105 Suppl (6):S13–33.
169. Williams GM, Lin JW, Sah RL. Cartilage Reshaping via In Vitro Mechanical Loading. *Tissue Engineering*. 2007;13(12):2903–11.
170. Tanaka H, Manske PR, Pruitt DL, Larson BJ. Effect of cyclic tension on lacerated flexor tendons in vitro. *The Journal of Hand Surgery*. 1995;20(A):467–73.
171. Merryman WD, Bieniek PD, Guilak F, Sacks MS. Viscoelastic properties of the aortic valve interstitial cell. *Journal of Biomechanical Engineering*. 2009;131(4):041005.
172. Sucusky P, Balachandran K, Elhammali A, Jo H, Yoganathan AP. Altered shear stress stimulates upregulation of endothelial VCAM-1 and ICAM-1 in a BMP-4- and TGF-beta1-dependent pathway. *Arteriosclerosis, Thrombosis, and Vascular Biology*. 2009;29(2):254–60.
173. Gorman RC, Jackson BM, Burdick JA, Gorman JH. Infarct restraint to limit adverse ventricular remodeling. *Journal of Cardiovascular Translational Research*. 2011;4(1):73–81.
174. Stella JA, Wagner WR, Sacks MS. Scale-dependent fiber kinematics of elastomeric electrospun scaffolds for soft tissue engineering. *Journal of Biomedical Materials Research Part A*. 2010;93(3):1032–42.

175. Mikos AG, Herring SW, Ochareon P, Elisseeff J, Lu HH, Kandel R, Schoen FR, Toner M, Mooney D, Atala A, van Dyke ME, Kaplan D, Vunjak-Novakovic G. Engineering complex tissues. *Tissue Engineering*. 2006;12(12):3307–39.
176. Johnson J, Ghosh A, Lannutti J. Microstructure-Property Relationships in a Tissue-Engineering Scaffold. *Journal of Applied Polymer Science*. 2007;104(5):2919–27.
177. Shi Q, Wong S-C, Ye W, Hou J, Zhao J, Yin J. Mechanism of adhesion between polymer fibers at nanoscale contacts. *Langmuir*. 2012;28(10):4663–71.
178. Cardwell RD, Dahlgren LA, Goldstein AS. Electrospun fibre diameter , not alignment , affects mesenchymal stem cell differentiation into the tendon / ligament lineage. *Journal of Tissue Engineering and Regenerative Medicine*. 2012;In Press:DOI: 10.1002/term.1589.
179. Neal RA, Tholpady SS, Foley PL, Swami N, Ogle RC, Botchwey EA. Alignment and composition of laminin-polycaprolactone nanofiber blends enhance peripheral nerve regeneration. *Journal of Biomedical Materials Research. Part A*. 2011;100A(2):406–23.
180. Milleret V, Hefti T, Hall H, Vogel V, Eberli D. Influence of the fiber diameter and surface roughness of electrospun vascular grafts on blood activation. *Acta Biomaterialia*. 2012;8(12):4349–56.
181. Beason DP, Connizzo BK, Dourte LM, Mauck RL, Soslowsky LJ, Steinberg DR, Bernstein J. Fiber-aligned polymer scaffolds for rotator cuff repair in a rat model. *Journal of Shoulder and Elbow Surgery*. 2012;21(2):245–50.
182. Vaquette C, Fan W, Xiao Y, Hamlet S, Hutmacher DW, Ivanovski S. A biphasic scaffold design combined with cell sheet technology for simultaneous regeneration of alveolar bone/periodontal ligament complex. *Biomaterials*. 2012;33(22):5560–73.
183. Yin Z, Chen X, Chen JL, Shen WL, Nguyen TMH, Gao L, Ouyang HW. The regulation of tendon stem cell differentiation by the alignment of nanofibers. *Biomaterials*. 2010;31(8):2163–75.
184. Sutton MA, Ke X, Lessner SM, Goldbach M, Yost M, Zhao F, Schreier HW. Strain field measurements on mouse carotid arteries using microscopic three-dimensional digital image correlation. *Journal of Biomedical Materials Research Part A*. 2008;84(1):178–90.
185. Park S, Park K, Yoon H, Son J, Min T, Kim G. Apparatus for preparing electrospun nanofibers : designing an electrospinning process for nanofiber fabrication. *Polymer International*. 2007;56:1361–6.
186. Martins A, Pinho ED, Correlo VM, Faria S, Marques AP, Reis RL, Neves NM. Biodegradable nanofibers-reinforced microfibrillar composite scaffolds for bone tissue engineering. *Tissue Engineering. Part A*. 2010;16(12):3599–609.

187. Shin M, Yoshimoto H, Vacanti JP. In vivo bone tissue engineering using mesenchymal stem cells on a novel electrospun nanofibrous scaffold. *Tissue Engineering*. 2004;10(1-2):33-41.